

# Processes $\gamma\gamma \rightarrow \phi_i\phi_j$ in Higgs Extensions of the Standard Models, II: Inert Higgs Doublet Models, Two Higgs Doublet Models

Khiem Hong Phan<sup>a,b</sup>, Dzung Tri Tran<sup>a,b</sup>, Thanh Huy Nguyen<sup>c,d</sup>

<sup>a</sup>*Institute of Fundamental and Applied Sciences, Duy Tan University, Ho Chi Minh City 70000, Vietnam*

<sup>b</sup>*Faculty of Natural Sciences, Duy Tan University, Da Nang City 50000, Vietnam*

<sup>c</sup>*Department of Theoretical Physics, University of Science, Ho Chi Minh City 700000, Vietnam*

<sup>d</sup>*Vietnam National University, Ho Chi Minh City 700000, Vietnam*

---

## Abstract

In this paper, we study one-loop contributions to the processes  $\gamma\gamma \rightarrow \phi_i\phi_j$  with CP-even Higgses  $\phi_{i,j} \equiv h, H$  at high energy photon-photon collision, within the Higgs Extensions of the Standard Models, considering Inert Higgs Doublet Models and Two Higgs Doublet Models. Analytic results for one-loop form factors of the processes under investigations are written in terms of the scalar Passarino-Veltman functions in following the standard notations of the packages `LoopTools` and `Collier`. As a result, the physical results can be generated by using one of the above-mentioned packages. In phenomenological studies, the enhancement factors defined as the ratio of cross-sections of  $\gamma\gamma \rightarrow \phi_i\phi_j$  in the Higgs Extensions of the Standard Models over the corresponding ones for  $\gamma\gamma \rightarrow hh$  in the SM, are examined in parameter space of the models under consideration.

*Keywords:* Higgs phenomenology, one-loop corrections, analytic methods for quantum field theory, dimensional regularization.

---

## 1. Introduction

Precise measurements for the properties of the discovered SM-like Higgs boson at the Large Hadron Colliders (LHC), are one of the top-priority purposes at future colliders, e.g. the High-luminosity LHC (HL-LHC) [1, 2], future lepton colliders (LC) [3, 4]. Since the measurable data will provide an profound information for verifying the scalar Higgs sector and it, consequently, will be answered for the nature of the electroweak symmetry breaking (EWSB). In this scheme, probing for scalar Higgs self-couplings including SM-like Higgs trilinear- (and quadratic-) couplings as well as the couplings between scalar Higgses in many physics beyond the Standard Models (BSM) plays important roles for determining the shape of the scalar Higgs potential. It means that Higgs boson pair productions and multi-scalar Higgs productions should be measured as precise as possible at future colliders. Recently, search for Higgs boson pair productions in the two bottom quarks plus two photons, four bottom quarks, etc in the final states in  $pp$  collisions have been performed at the LHC as in [5, 6, 7, 8, 9, 10, 11, 12, 13, 14, 15, 16].

It is well-known that the measurements for Higgs self-couplings are rather challenging at the LHC. The results from the study of Refs. [17, 18] show that the expected accuracy in the measurement of trilinear Higgs self-coupling would be about 20% – 30% at the high luminosity of  $3000 \text{ fb}^{-1}$ . We know that physics the future lepton colliders will be complementary to the

---

*Email address:* phanhongkhiem@duytan.edu.vn (Khiem Hong Phan)

LHC in many aspects, as studied in Ref. [19]. Furthermore, the LC can significantly improve the LHC measurements in many cases and more important photon-photon collision is an option of the LC [3, 4] which the scalar Higgs pair productions ( $\phi_i\phi_j$ ) can be measured via the channels  $f\bar{f} \rightarrow f\bar{f}\gamma^*\gamma^* \rightarrow f\bar{f}\phi_i\phi_j$  for  $f \equiv e, \mu$ . In this aspect, the LC also open a window for probing new physics signals through multi-scalar Higgs productions.

From theoretical calculation side, one-loop corrections to Higgs boson pair productions at the LHC have calculated within the SM, the Higgs Extensions of the Standard Models (HESM), as well as other BSM frameworks by many groups. For examples, it is worth to mention typical works as in Refs. [20, 21, 22, 23, 24, 25, 26, 27, 28, 29, 30, 31, 32, 33, 34, 35, 36, 37, 38, 39, 40, 41, 42, 43, 44, 45, 46, 47, 48, 49, 50, 51, 52, 53, 54, 55, 56, 57, 58, 59, 60, 61, 62, 63, 64, 65, 66, 67, 68, 69, 70, 71, 72, 73, 74, 75, 76, 77, 78, 79, 80], for further reviews in Ref. [81] and the related-references therein. Additionally, one-loop induced for Higgs boson pair production in the high-energy photon-photon collisions in the SM, the HESM and other BSMs have computed in Refs. [82, 83, 84, 85, 86, 87, 88, 89, 90, 91, 92, 93, 94, 95, 96]. Other computations for one-loop induced for Higgs boson pair productions in the linear lepton colliders including future multi-TeV muon colliders, have performed in Refs. [97, 98, 99, 100] and the additional references therein. Furthermore, pseudo-scalar Higgs boson pair production at a photon-photon collision in the two Higgs doublet model have reported in Ref. [101].

Due to the most important of the scalar Higgs pair productions at future colliders, we revisited the evaluations for one-loop corrections to the processes  $\gamma\gamma \rightarrow \phi_i\phi_j$  with CP-even Higgses  $\phi_{i,j} \equiv h, H$  at the high-energy photon-photon collisions within the Higgs Extensions of the Standard Models, considering the Inert Higgs Doublet Models the Two Higgs Doublet Models and the Triplet Higgs Models. In comparison with all previous papers, our works have further advantages as follows. (i) A general analytic formulas derived in 't Hooft-Feynman gauge, are given in the works, which are valid for a class of the HESM. (ii) Analytic results for one-loop form factors of the calculated processes are written in terms of the scalar Passarino-Veltman functions following the standard conventions of the packages `LoopTools` [102] and `Collier` [103]. The analytical expressions are tested by several numerical checks such as the ultraviolet finiteness, infrared finiteness of the one-loop amplitudes. Furthermore, the amplitudes also obey the so-called ward identity. This identity is also verified numerically in the works. Additionally, both the packages `LoopTools` and `Collier` are used for cross-checking for the final results before generating physical results. Last but not least, we present the physical results for the processes under investigations with the most precise input parameters from the updated experimental data and take the updated constraints in parameter space of the HESM. This paper arrive at the part II of the works in which we focus on the phenomenological studies for the concerned processes in the Inert Higgs Doublet Models and the Two Higgs Doublet Models. For phenomenological studies, the enhancement factors defined as the ratio of cross-sections of  $\gamma\gamma \rightarrow \phi_i\phi_j$  in the HESM over the corresponding cross-sections of  $\gamma\gamma \rightarrow hh$  in the SM, are examined in parameter space of the HESM.

Overview of the paper is as follows. We first review briefly the HESM in the section 2. We then present in detail the evaluations for one-loop corrections to  $\gamma\gamma \rightarrow \phi_i\phi_j$  with CP-even Higgses  $\phi_{i,j} \equiv h, H$  in the HESM. Phenomenological results for the HESM are shown in section 4. Conclusion and outlook are devoted in section 5. In appendices *A*, *B* we derive all the related couplings to the processes under consideration in the above-mentioned models.

## 2. Higgs Extensions of the Standard Model

The Higgs Extensions of the Standard Models are reviewed in the following subsections. Two typical the HESMs are examined in the current work. The first one is to the Inert Higgs Doublet

Models reviewed in next subsection. We then discuss the second HESMs is to the Two Higgs Doublet Models in subsection 2.2.

### 2.1. Inert Higgs Doublet Models

We first arrive at reviewing the Inert Doublet Higgs Model (IHDM), one of the HESM mentioned in this paper, which an inert scalar  $SU(2)_L$  doublet is added into the scalar sector of the SM. In this model, the inert scalar particles will respond for dark matter candidates. For reviewing the model in further detail, we refer the following papers [106, 107, 108, 109, 110, 111, 112, 113, 114, 115, 116, 117, 118]. The scalar potential of the IHDM obeying the renormalizable conditions and relying on the gauge invariant form, read the general expression as follows:

$$\begin{aligned} \mathcal{V}_{\text{IHDM}}(\Phi_1, \Phi_2) = & \mu_1^2 |\Phi_1|^2 + \mu_2^2 |\Phi_2|^2 + \lambda_1 |\Phi_1|^4 + \lambda_2 |\Phi_2|^4 + \lambda_3 |\Phi_1|^2 |\Phi_2|^2 \\ & + \lambda_4 |\Phi_1^\dagger \Phi_2|^2 + \frac{\lambda_5}{2} \left\{ (\Phi_1^\dagger \Phi_2)^2 + \text{h.c.} \right\}. \end{aligned} \quad (1)$$

In the IHDM, the scalar sector is conserved with respect to the so-called the global  $Z_2$ -symmetry, e.g.  $\Phi_1 \leftrightarrow +\Phi_1$ ,  $\Phi_2 \leftrightarrow -\Phi_2$ . In this case, the scalar  $\Phi_2$  is odd and  $\Phi_1$  as well as all SM particles are considered to be even under the  $Z_2$ -symmetry. Since the  $Z_2$ -symmetry is unbroken after the electroweak symmetry breaking (EWSB) in the model, the field  $\Phi_2$  has the zero of vacuum expectation values (VEV). Instead of the zero of VEV in the field  $\Phi_2$ , the field  $\Phi_1$  develops non-zero VEV. Subsequently, two scalar fields are then parameterized around VEV for the EWSB as follows:

$$\Phi_1 = \begin{pmatrix} G^\pm \\ \frac{1}{\sqrt{2}}(v + h + iG^0) \end{pmatrix}, \quad \Phi_2 = \begin{pmatrix} H^\pm \\ \frac{1}{\sqrt{2}}(H + iA^0) \end{pmatrix}. \quad (2)$$

Where the vacuum expectation value is fixed at  $v \sim 246$  GeV as the electroweak scale for coinciding with the SM case. The Nambu-Goldstone bosons  $G^0$ ,  $G^\pm$  are giving the masses for gauge bosons  $Z$  and  $W^\pm$ , respectively. It is found that there are no mixing between two neutral CP-even Higgses  $h$  and  $H$ . After the EWSB, the physical spectrum of the IHDM is consisted of three neutral scalar physical states such as two CP-even Higgses  $h, H$  and a CP-odd Higgs  $A_0$ . In further, we have pair of singly charged Higgs bosons  $H^\pm$  in this model. In the physical spectrum, neutral scalar Higgs  $h$  is identical to the SM-like Higgs boson discovered at the LHC. All masses of scalar bosons are expressed in terms of the pare parameters  $\mu_1, \mu_2, \lambda_1, \dots, \lambda_5$ , namely:

$$M_h^2 = -2\mu_1^2 = 2\lambda_1 v^2, \quad (3)$$

$$M_H^2 = \mu_2^2 + \frac{v^2}{2} (\lambda_3 + \lambda_4 + \lambda_5), \quad (4)$$

$$M_{A^0}^2 = \mu_2^2 + \frac{v^2}{2} (\lambda_3 + \lambda_4 - \lambda_5), \quad (5)$$

$$M_{H^\pm}^2 = \mu_2^2 + \frac{v^2}{2} \lambda_3. \quad (6)$$

As we mentioned in the above paragraphs, the global  $Z_2$ -symmetry is unbroken after the EWSB, all "inert" Higgs bosons  $H$ ,  $A^0$  and  $H^\pm$  having odd number under the  $Z_2$ -transformation. Subsequently, the "inert" Higgs bosons don't couple to the SM particles. As the result, the lightest neutral Higgs bosons ( $H$  or  $A^0$ ) may be considered as dark matter candidates.

As a consequent of the unbroken of the  $Z_2$ -symmetry, the Yukawa Lagrangian of the IHDM must be the same as that of the SM. In detail, the Yukawa Lagrangian is expressed as follows:

$$\mathcal{L}_{\text{Yukawa}} = - \sum_{f=u,d,\ell} g_{hff} \cdot h \bar{f} f + \dots, \quad (7)$$

where  $g_{hff} = g_{hff}^{\text{SM}} = m_f/v$ , and  $f$  is a SM fermion with mass  $m_f$ . All the related-couplings to the processes  $\gamma\gamma \rightarrow hh$ ,  $HH$  in the IDHM are listed in Table 1 (for all physical couplings) and Table 2 (for all couplings relating to unphysical particles). The detailed derivations of all the concerned-couplings are shown in the appendix A. It is important to note that the processes  $\gamma\gamma \rightarrow hH$  are forbidden in the IHDM due to the  $Z_2$ -symmetry.

Vertices	Notations	Coupling
$hW_\mu W_\nu$	$g_{hWW} \cdot g_{\mu\nu}$	$i \left( \frac{2M_W^2}{v} \right) \cdot g_{\mu\nu}$
$hZ_\mu Z_\nu$	$g_{hZZ} \cdot g_{\mu\nu}$	$i \left( \frac{M_Z^2}{v} \right) \cdot g_{\mu\nu}$
$hH^\pm H^\mp$	$g_{hH^\pm H^\mp}$	$i \frac{2(\mu_2^2 - M_{H^\pm}^2)}{v}$
$Z_\mu H^\pm H^\mp$	$g_{ZH^\pm H^\mp} \cdot (p_{H^\pm} - p_{H^\mp})_\mu$	$i \left( \frac{M_Z c_{2W}}{v} \right) \cdot (p_{H^\pm} - p_{H^\mp})_\mu$
$A_\mu H^\pm H^\mp$	$g_{AH^\pm H^\mp} \cdot (p_{H^\pm} - p_{H^\mp})_\mu$	$i \left( \frac{M_Z s_{2W}}{v} \right) \cdot (p_{H^\pm} - p_{H^\mp})_\mu$
$hhh$	$g_{hhh}$	$-i \left( \frac{3M_h^2}{v} \right)$
$hHH$	$g_{hHH}$	$i \frac{2(\mu_2^2 - M_H^2)}{v}$
$HH^\pm W^\mp$	$g_{HH^\pm W} \cdot (p_{H^\pm} - p_H)_\mu$	$\pm i \left( \frac{M_W}{v} \right) \cdot (p_{H^\pm} - p_H)_\mu$
$H^\pm H^\mp A_\mu A_\nu$	$g_{AAH^\pm H^\mp} \cdot g_{\mu\nu}$	$i \left( \frac{M_Z^2 s_{2W}^2}{v^2} \right) \cdot g_{\mu\nu}$
$HH^\pm W_\nu^\mp A_\mu$	$g_{HH^\pm W A} \cdot g_{\mu\nu}$	$i \left( \frac{2M_Z^2 c_W^2 s_W}{v^2} \right) \cdot g_{\mu\nu}$
$hhH^\pm H^\mp$	$g_{hhH^\pm H^\mp}$	$i \frac{2(\mu_2^2 - M_{H^\pm}^2)}{v^2}$
$HHH^\pm H^\mp$	$g_{HHH^\pm H^\mp}$	$-2i\lambda_2$
$hhW_\mu^\pm W_\nu^\mp$	$g_{hhWW} \cdot g_{\mu\nu}$	$i \left( \frac{2M_Z^2 c_W^2}{v^2} \right) \cdot g_{\mu\nu}$
$HHW_\mu^\pm W_\nu^\mp$	$g_{HHWW} \cdot g_{\mu\nu}$	$i \left( \frac{2M_Z^2 c_W^2}{v^2} \right) \cdot g_{\mu\nu}$

Table 1: All couplings contributing to the process amplitudes  $\gamma\gamma \rightarrow hh$ ,  $\gamma\gamma \rightarrow HH$  in the IHDM are shown in the Table (physical couplings are presented). Here,  $A_\mu$  is the photon field,  $p^\pm$  is the incoming momentum of  $H^\pm$ ,  $s_W(c_W)$  is sine (and cosine) of the Weinberg's angle, respectively.

Vertices	Notations	Coupling
$A_\mu W_\nu^\pm G^\mp$	$g_{AW^\pm G^\mp} \cdot g_{\mu\nu}$	$i \left( \frac{2M_Z^2 c_W^2 s_W}{v} \right) \cdot g_{\mu\nu}$
$HH^\pm G^\mp$	$g_{HH^\pm G^\mp}$	$i \frac{M_{H^\pm}^2 - M_H^2}{v}$
$hhG^\pm G^\mp$	$g_{hhG^\pm G^\mp}$	$-i \frac{M_h^2}{v^2}$
$HHG^\pm G^\mp$	$g_{HHG^\pm G^\mp}$	$i \frac{2(\mu_2^2 - M_{H^\pm}^2)}{v^2}$
$A_\mu A_\nu G^\pm G^\mp$	$g_{AAG^\pm G^\mp} \cdot g_{\mu\nu}$	$i \left( \frac{M_Z^2 s_W^2}{v^2} \right) \cdot g_{\mu\nu}$
$A_\mu G^\pm G^\mp$	$g_{AG^\pm G^\mp} \cdot (p_{G^\pm} - p_{G^\mp})_\mu$	$\pm i \left( \frac{M_Z s_W}{v} \right) \cdot (p_{G^\pm} - p_{G^\mp})_\mu$

Table 2: All couplings relating to one-loop contribution for the calculated processes  $\gamma\gamma \rightarrow hh, \gamma\gamma \rightarrow HH$  in the IHDM are shown in the Table (unphysical couplings are concerned). Here,  $A_\mu$  is the photon field,  $p^\pm$  is the incoming momentum of  $H^\pm$ ,  $s_W(c_W)$  is sine (and cosine) of the Weinberg's angle, respectively.

We confirm the following relations

$$g_{HH^\pm G^\mp} = \frac{M_H^2 - M_{H^\pm}^2}{M_W} g_{HH^\pm W^\mp}, \quad (8)$$

$$g_{HH^\pm W A} = \frac{-2M_W s_W}{v} g_{HH^\pm W^\mp}. \quad (9)$$

The set of scanning parameters in the IHDM is chosen in our analysis as follows:

$$\mathcal{P}_{\text{IHDM}} = \{\mu_2^2, \lambda_2^2, M_h^2 \sim 125.\text{GeV}, M_H^2, M_{A^0}^2, M_{H^\pm}^2\}. \quad (10)$$

## 2.2. Two Higgs Doublet Models

We next to consider the second kind of the Higgs extension of the SM which is to the Two Higgs Doublet Models (THDM) in this paper. For reviewing the theory and the phenomenological studies for the THDM, we refer the paper Ref. [119] for further information. The model is summarized briefly in this section. An additional complex Higgs doublet with the hypercharge  $Y = 1/2$  is taken into account in the scalar sector of the SM. Following the renormalizable conditions as well as the gauge invariance requirements for gauge theories, the scalar Higgs potential in the THDM reads the general form as follows:

$$\begin{aligned} \mathcal{V}_{\text{THDM}}(\Phi_1, \Phi_2) &= m_{11}^2 \Phi_1^\dagger \Phi_1 + m_{22}^2 \Phi_2^\dagger \Phi_2 - \left[ m_{12}^2 \Phi_1^\dagger \Phi_2 + \text{h.c.} \right] \\ &+ \frac{\lambda_1}{2} (\Phi_1^\dagger \Phi_1)^2 + \frac{\lambda_2}{2} (\Phi_2^\dagger \Phi_2)^2 + \lambda_3 (\Phi_1^\dagger \Phi_1) (\Phi_2^\dagger \Phi_2) \\ &+ \lambda_4 (\Phi_1^\dagger \Phi_2) (\Phi_2^\dagger \Phi_1) + \frac{1}{2} [\lambda_5 (\Phi_1^\dagger \Phi_2)^2 + \text{h.c.}] \end{aligned} \quad (11)$$

In the scope of the present work, we only consider the CP-conserving version of the THDM. Subsequently, all pare parameters in the scalar potential are considered to be real parameters in this case. Additionally, the scalar potential of the THDM follows the  $Z_2$ -symmetry, e.g.  $\Phi_1 \leftrightarrow \Phi_1$  and  $\Phi_2 \leftrightarrow -\Phi_2$ , up to the soft breaking terms as  $m_{12}^2 \Phi_1^\dagger \Phi_2 + \text{h.c.}$  are added into the potential. Where the parameter  $m_{12}^2$  plays a key role for soft-breaking scale of the  $Z_2$ -symmetry.

For the EWSB, two scalar doublets can be parameterized into the form of

$$\Phi_1 = \begin{bmatrix} \phi_1^+ \\ (v_1 + \rho_1 + i\eta_1)/\sqrt{2} \end{bmatrix}, \quad (12)$$

$$\Phi_2 = \begin{bmatrix} \phi_2^+ \\ (v_2 + \rho_2 + i\eta_2)/\sqrt{2} \end{bmatrix}. \quad (13)$$

With the above parameterizations, the vacuum expectation value is then fixed at  $v = \sqrt{v_1^2 + v_2^2} \sim 246$  GeV for coinciding with the SM case. The physical spectrum of the THDM after the EWSB contains of two CP-even Higgs bosons  $h$  and  $H$  in which  $h$  is identified as the SM-like Higgs boson discovered at LHC, a CP-odd Higgs  $A^0$ , and a pair of singly charged Higgses  $H^\pm$ . In order to find the physical masses for the above-mentioned scalar particles, we first diagonalize the mass matrices in their flavor bases. The rotation matrices of the flavor bases to the masses bases for all scalar Higgs bosons are given explicitly as follows:

$$\begin{pmatrix} \rho_1 \\ \rho_2 \end{pmatrix} = \mathcal{R}(\alpha) \begin{pmatrix} H \\ h \end{pmatrix}, \quad (14)$$

$$\begin{pmatrix} \phi_1^\pm \\ \phi_2^\pm \end{pmatrix} = \mathcal{R}(\beta) \begin{pmatrix} G^\pm \\ H^\pm \end{pmatrix}, \quad (15)$$

$$\begin{pmatrix} \eta_1 \\ \eta_2 \end{pmatrix} = \mathcal{R}(\beta) \begin{pmatrix} G^0 \\ A^0 \end{pmatrix}. \quad (16)$$

Where  $\alpha$  is the mixing angle between two neutral Higgses and  $\beta$  is corresponding to the mixing angle between charged scalar particles with charged Goldstone bosons  $G^\pm$  (and CP-odd Higgs with neutral Goldstone boson  $G^0$  as well). The mixing angle  $\beta$  is given by  $t_\beta \equiv \tan \beta = v_2/v_1$ . While  $\alpha$  is considered as a free parameter which will be constrained by experimental data. All rotation matrices are taken the form of

$$\mathcal{R}(\theta) = \begin{pmatrix} c_\theta & -s_\theta \\ s_\theta & c_\theta \end{pmatrix} \quad (17)$$

where  $\theta$  stands for  $\alpha$  and  $\beta$  in this case. The masses of Higgs bosons are written in terms of the pare parameters as follows:

$$M_{H^\pm}^2 = M^2 - \frac{1}{2}(\lambda_4 + \lambda_5)v^2, \quad (18)$$

$$M_{A^0}^2 = M^2 - \lambda_5 v^2, \quad (19)$$

$$M_h^2 = M_{11}^2 s_{\beta-\alpha}^2 + M_{22}^2 c_{\beta-\alpha}^2 + M_{12}^2 s_{2(\beta-\alpha)}, \quad (20)$$

$$M_H^2 = M_{11}^2 c_{\beta-\alpha}^2 + M_{22}^2 s_{\beta-\alpha}^2 - M_{12}^2 s_{2(\beta-\alpha)} \quad (21)$$

where the parameter  $M^2$  is used as  $M^2 = m_{12}^2/(s_\beta c_\beta)$ . The matrix elements  $M_{ij}$  for  $i, j = 1, 2$  are shown explicitly as follows:

$$M_{11}^2 = (\lambda_1 c_\beta^4 + \lambda_2 s_\beta^4)v^2 + \frac{v^2}{2} \lambda_{345} s_{2\beta}^2, \quad (22)$$

$$M_{22}^2 = M^2 + \frac{v^2}{4} [\lambda_1 + \lambda_2 - 2\lambda_{345}] s_{2\beta}^2, \quad (23)$$

$$M_{12}^2 = -\frac{v^2}{2} [\lambda_1 c_\beta^2 - \lambda_2 s_\beta^2 - \lambda_{345} c_{2\beta}] s_{2\beta}. \quad (24)$$

Here, we have used the shorten notation as  $\lambda_{345} = \lambda_3 + \lambda_4 + \lambda_5$ .

All couplings relating to the calculations for one-loop contributions to the scattering amplitudes  $\gamma\gamma \rightarrow hh, hH, HH$  in the THDM are shown in Tables 3, 5. Here  $A_\mu$  is the photon field,  $p^\pm$  is the incoming momentum of  $H^\pm$ ,  $s_W(c_W)$  is sine (and cosine) of the Weinberg's angle, respectively. Deriving all couplings in Tables 3, 5 for the THDM are shown in further detail in the appendix B.

Vertices	Notations	Couplings
$hW_\mu W_\nu$	$g_{hWW} \cdot g_{\mu\nu}$	$i \left( \frac{2M_W^2}{v} s_{\beta-\alpha} \right) \cdot g_{\mu\nu}$
$HW_\mu W_\nu$	$g_{HWW} \cdot g_{\mu\nu}$	$i \left( \frac{2M_W^2}{v} c_{\beta-\alpha} \right) \cdot g_{\mu\nu}$
$hZ_\mu Z_\nu$	$g_{hZZ} \cdot g_{\mu\nu}$	$i \left( \frac{2M_Z^2}{v} s_{\beta-\alpha} \right) \cdot g_{\mu\nu}$
$HZ_\mu Z_\nu$	$g_{HZZ} \cdot g_{\mu\nu}$	$i \left( \frac{2M_Z^2}{v} c_{\beta-\alpha} \right) \cdot g_{\mu\nu}$
$hH^\pm H^\mp$	$g_{hH^\pm H^\mp}$	$i \left[ \frac{c_{\alpha+\beta}(4M^2 - 3M_h^2 - 2M_{H^\pm}^2)}{2vs_{2\beta}} + \frac{(2M_{H^\pm}^2 - M_h^2)c_{(\alpha-3\beta)}}{2vs_{2\beta}} \right]$
$Z_\mu H^\pm(p^+) H^\mp(p^-)$	$g_{ZH^\pm H^\mp} \cdot (p^+ - p^-)_\mu$	$i \left( \frac{M_Z c_{2W}}{v} \right) \cdot (p^+ - p^-)_\mu$
$A_\mu H^\pm(p^+) H^\mp(p^-)$	$g_{AH^\pm H^\mp} \cdot (p^+ - p^-)_\mu$	$i \left( \frac{M_Z s_{2W}}{v} \right) \cdot (p^+ - p^-)_\mu$
$hhh$	$g_{hhh}$	$i \frac{3e}{4M_W s_W s_{2\beta}} \left[ M^2 c_{\alpha-3\beta} + (M^2 - M_h^2) c_{3\alpha-\beta} + (2M^2 - 3M_h^2) c_{\alpha+\beta} \right]$
$HHH$	$g_{HHH}$	$i \frac{3e}{4M_W s_W s_{2\beta}} \left[ M^2 s_{\alpha-3\beta} + (M_H^2 - M^2) s_{3\alpha-\beta} + (2M^2 - 3M_H^2) s_{\alpha+\beta} \right]$
$hHH$	$g_{hHH}$	$i \frac{s_{\alpha-\beta} [s_{2\alpha}(3M^2 - M_h^2 - 2M_H^2) + M^2 s_{2\beta}]}{v s_{2\beta}}$
$Hhh$	$g_{Hhh}$	$i \frac{c_{\alpha-\beta} [s_{2\alpha}(3M^2 - M_H^2 - 2m_h^2) - M^2 s_{2\beta}]}{2vs_{2\beta}}$

Table 3: All couplings contributing to the considered processes  $\gamma\gamma \rightarrow hh, hH, HH$  in the THDM are shown in the Table. Here,  $A_\mu$  is for the photon field,  $p^\pm$  is the incoming momentum of  $H^\pm$ ,  $s_W(c_W)$  is sine (and cosine) of the Weinberg's angle, respectively.

Vertices	Notations	Couplings
$HH^\pm H^\mp$	$g_{HH^\pm H^\mp}$	$i \left[ \frac{s_{\alpha+\beta}(4M^2 - 3M_H^2 - 2M_{H^\pm}^2)}{2v s_{2\beta}} + \frac{(2M_{H^\pm}^2 - M_H^2)s_{\alpha-3\beta}}{2v s_{2\beta}} \right]$
$H(p_H)H^\pm(p_{H^\pm})W_\mu^\mp$	$g_{HH^\pm W} \cdot (p_H - p_{H^\pm})_\mu$	$\pm i \left( \frac{M_W s_{\beta-\alpha}}{v} \right) \cdot (p_H - p_{H^\pm})_\mu$
$h(p_h)H^\pm(p_{H^\pm})W_\mu^\mp$	$g_{hH^\pm W} \cdot (p_h - p_{H^\pm})_\mu$	$\mp i \left( \frac{M_W c_{\alpha-\beta}}{v} \right) \cdot (p_h - p_{H^\pm})_\mu$
$H^\pm H^\mp A_\mu A_\nu$	$g_{H^\pm H^\mp AA} \cdot g_{\mu\nu}$	$i \left( \frac{4M_W^2 s_W^2}{v^2} \right) \cdot g_{\mu\nu}$
$HH^\pm W_\mu^\mp A_\nu$	$g_{HH^\pm WA} \cdot g_{\mu\nu}$	$i \left( \frac{2M_W^2 s_W s_{\alpha-\beta}}{v^2} \right) \cdot g_{\mu\nu}$
$hH^\pm W_\mu^\mp A_\nu$	$g_{hH^\pm WA} \cdot g_{\mu\nu}$	$i \left( \frac{2M_W^2 s_W c_{\alpha-\beta}}{v^2} \right) \cdot g_{\mu\nu}$
$hHH^\pm H^\mp$	$g_{HhH^\pm H^\mp}$	$i\lambda_{HhH^\pm H^\mp}$ [in Eq. (71)]
$HHH^\pm H^\mp$	$g_{HHH^\pm H^\mp}$	$i\lambda_{HHH^\pm H^\mp}$ [in Eq. (75)]
$hhH^\pm H^\mp$	$g_{hhH^\pm H^\mp}$	$i\lambda_{hhH^\pm H^\mp}$ [in Eq. (76)]
$hhW_\mu^\pm W_\nu^\mp$	$g_{hhWW} \cdot g_{\mu\nu}$	$i \left( \frac{4M_W^2}{v^2} \right) \cdot g_{\mu\nu}$
$HHW_\mu^\pm W_\nu^\mp$	$g_{HHWW} \cdot g_{\mu\nu}$	$i \left( \frac{4M_W^2}{v^2} \right) \cdot g_{\mu\nu}$

Table 4: Additional couplings relating to the computed processes  $\gamma\gamma \rightarrow hh, hH, HH$  in the THDM are shown in the Table. Here,  $A_\mu$  is for the photon field,  $p^\pm$  is the incoming momentum of  $H^\pm$ ,  $s_W(c_W)$  is sine (and cosine) of the Weinberg's angle, respectively.

Vertices	Notations	Couplings
$A_\mu W_\nu^\pm G^\mp$	$g_{AW^\pm G^\mp} \cdot g_{\mu\nu}$	$i \left( \frac{2M_W^2 s_W}{v} \right) \cdot g_{\mu\nu}$
$HH^\pm G^\mp$	$g_{HH^\pm G^\mp}$	$i \frac{e s_{\alpha-\beta}}{2M_W s_W} (M_{H^\pm}^2 - M_H^2)$
$A_\mu A_\nu G^\pm G^\mp$	$g_{AAG^\pm G^\mp} \cdot g_{\mu\nu}$	$i \left( \frac{4M_W^2 s_W^2}{v^2} \right) \cdot g_{\mu\nu}$
$A_\mu G^\pm G^\mp$	$g_{AG^\pm G^\mp} \cdot (p_{G^\pm} - p_{G^\mp})_\mu$	$i \left( \frac{2M_W s_W}{v} \right) \cdot (p_{G^\pm} - p_{G^\mp})_\mu$
$hHG^\pm G^\mp$	$g_{hHG^\pm G^\mp}$	$i\lambda_{hHG^\pm G^\mp}$ [in Eq. (72)]
$hhG^\pm G^\mp$	$g_{hhG^\pm G^\mp}$	$i\lambda_{hhG^\pm G^\mp}$ [in Eq. (77)]
$HHG^\pm G^\mp$	$g_{HHG^\pm G^\mp}$	$i\lambda_{HHG^\pm G^\mp}$ [Eq. (78)]

Table 5: All couplings involving to the calculated processes  $\gamma\gamma \rightarrow hh, hH, HH$  in the THDM are presented in the Table (unphysical couplings are shown). Here,  $A_\mu$  is the photon field,  $p^\pm$  is the incoming momentum of  $H^\pm$ ,  $s_W(c_W)$  is sine (and cosine) of the Weinberg's angle, respectively.

We confirm the following relations

$$g_{HH^\pm G^\mp} = \frac{M_H^2 - M_{H^\pm}^2}{M_W} g_{HH^\pm W^\mp}, \quad (25)$$

$$g_{HH^\pm W A} = \frac{-2M_W s_W}{v} g_{HH^\pm W^\mp}. \quad (26)$$

Finally, we consider the Yukawa sector in the THDM. The discrete  $Z_2$ -symmetry may be imposed in the THDM for avoiding Tree-level Flavor-Changing Neutral Currents (FCNCs). The  $Z_2$ -parity assignments for all fermions [120], e.g. for quark doublets  $Q$ , lepton doublet  $L$  and for up-type (down-type) quark singlet  $u_R$  ( $d_R$ ), respectively as well as lepton singlet  $\ell_R$ , are shown in three right columns in Table 6. In the three left columns, the four Yukawa types of the  $Z_2$ -symmetry for the THDM are defined in which these Yukawa types are defined by the couplings of scalar Higgs doublet with different kind of fermions.

	$u$ -type	$d$ -type	leptons	$Q$	$u_R$	$d_R$	$L$	$\ell_R$
Type I	$\Phi_2$	$\Phi_2$	$\Phi_2$	+	-	-	+	-
Type II	$\Phi_2$	$\Phi_1$	$\Phi_1$	+	-	+	+	+
Type X	$\Phi_2$	$\Phi_2$	$\Phi_1$	+	-	-	+	+
Type Y	$\Phi_2$	$\Phi_1$	$\Phi_2$	+	-	+	+	-

Table 6: The  $Z_2$ -parity assignments for all fermions, e.g. for quark doublets  $Q$ , lepton doublet  $L$  and for all up-type (down-type) quark singlet  $u_R$  ( $d_R$ ), respectively as well as all lepton singlet  $\ell_R$ , are shown.

Subsequently, the four independent types of Yukawa Lagrangian are presented as follows:

$$\text{Type I: } \mathcal{L}_Y^{(I)} = -y_{\ell_i} \bar{L}_{iL} \ell_{iR} \Phi_2 - \tilde{y}_d^{ij} \bar{Q}_{iL} d'_{jR} \Phi_2 - \tilde{y}_u^{ij} \bar{Q}_{iL} u'_{jR} \tilde{\Phi}_2 + \text{h.c.} \quad (27)$$

$$\text{Type II: } \mathcal{L}_Y^{(II)} = -y_{\ell_i} \bar{L}_{iL} \ell_{iR} \Phi_1 - \tilde{y}_d^{ij} \bar{Q}_{iL} d'_{jR} \Phi_1 - \tilde{y}_u^{ij} \bar{Q}_{iL} u'_{jR} \tilde{\Phi}_2 + \text{h.c.} \quad (28)$$

$$\text{Type X: } \mathcal{L}_Y^{(X)} = -y_{\ell_i} \bar{L}_{iL} \ell_{iR} \Phi_1 - \tilde{y}_d^{ij} \bar{Q}_{iL} d'_{jR} \Phi_2 - \tilde{y}_u^{ij} \bar{Q}_{iL} u'_{jR} \tilde{\Phi}_2 + \text{h.c.} \quad (29)$$

$$\text{Type Y: } \mathcal{L}_Y^{(Y)} = -y_{\ell_i} \bar{L}_{iL} \ell_{iR} \Phi_2 - \tilde{y}_d^{ij} \bar{Q}_{iL} d'_{jR} \Phi_1 - \tilde{y}_u^{ij} \bar{Q}_{iL} u'_{jR} \tilde{\Phi}_2 + \text{h.c.} \quad (30)$$

Here the doublet  $\tilde{\Phi}_2 = i\sigma^2 \Phi_2^*$ , lepton doublet  $L_{iL} = (\nu_{iL}, \ell_{iL})^T$  and quark doublet  $Q_{iL} = (u'_{iL}, d'_{iL})^T$  for generation index  $i = 1, 2, 3$ . The mixing matrices  $\tilde{y}_d^{ij}$  ( $\tilde{y}_u^{ij}$ ) for down-quarks (for up-quarks) respectively, can be diagonalized by using the rotation matrix  $(U_d)_{ij}$ . In concrete, the relations are shown explicitly as

$$(U_d)_{ij}^\dagger \tilde{y}_d^{jk} (U_d)_{kl} = y_{d_i} \delta_{il}, \quad (31)$$

$$(U_u)_{ij}^\dagger \tilde{y}_u^{jk} (U_u)_{kl} = y_{u_i} \delta_{il}. \quad (32)$$

The quarks basis  $u'_i$  and  $d'_i$  are related to their mass basis  $u_i$  and  $d_i$  through

$$d'_i = (U_d)_{ij} d_j, \quad u'_i = (U_u)_{ij} u_j. \quad (33)$$

The Cabibbo-Kobayashi-Maskawa matrix is then identified as

$$\text{CKM}_{ij} = (U_u)_{ik}^\dagger (U_d)_{kj}. \quad (34)$$

The Yukawa Lagrangian is then expressed in terms of the mass eigenstates is as in [119]

$$\mathcal{L}_{\text{Yukawa}} = - \sum_{f=u,d,\ell} (g_{hff} \cdot \bar{f} f h + g_{Hff} \cdot \bar{f} f H - i g_{A_0 ff} \cdot \bar{f} \gamma_5 f A^0) + \dots, \quad (35)$$

The Yukawa couplings for four different types of the THDM are then given in Table 8, see [119] for further detail.

Type	$g_{huu}$	$g_{hdd}$	$g_{h\ell\ell}$
I	$\frac{m_u c_\alpha}{\sqrt{2} v s_\beta}$	$\frac{m_d c_\alpha}{\sqrt{2} v s_\beta}$	$\frac{m_\ell c_\alpha}{\sqrt{2} v s_\beta}$
II	$\frac{m_u c_\alpha}{\sqrt{2} v s_\beta}$	$-\frac{m_d s_\alpha}{\sqrt{2} v c_\beta}$	$-\frac{m_\ell s_\alpha}{\sqrt{2} v c_\beta}$
X	$\frac{m_u c_\alpha}{\sqrt{2} v s_\beta}$	$\frac{m_d c_\alpha}{\sqrt{2} v s_\beta}$	$-\frac{m_\ell s_\alpha}{\sqrt{2} v c_\beta}$
Y	$\frac{m_u c_\alpha}{\sqrt{2} v s_\beta}$	$-\frac{m_d s_\alpha}{\sqrt{2} v c_\beta}$	$\frac{m_\ell c_\alpha}{\sqrt{2} v s_\beta}$

Table 7: The Yukawa couplings in THDMs with type I,II, X, and Y respectively.

Type	$g_{Huu}$	$g_{Hdd}$	$g_{H\ell\ell}$
I	$\frac{m_u c_\alpha}{\sqrt{2} v s_\beta}$	$\frac{m_d c_\alpha}{\sqrt{2} v s_\beta}$	$\frac{m_\ell c_\alpha}{\sqrt{2} v s_\beta}$
II	$\frac{m_u c_\alpha}{\sqrt{2} v s_\beta}$	$-\frac{m_d s_\alpha}{\sqrt{2} v c_\beta}$	$-\frac{m_\ell s_\alpha}{\sqrt{2} v c_\beta}$
X	$\frac{m_u c_\alpha}{\sqrt{2} v s_\beta}$	$\frac{m_d c_\alpha}{\sqrt{2} v s_\beta}$	$-\frac{m_\ell s_\alpha}{\sqrt{2} v c_\beta}$
Y	$\frac{m_u c_\alpha}{\sqrt{2} v s_\beta}$	$-\frac{m_d s_\alpha}{\sqrt{2} v c_\beta}$	$\frac{m_\ell c_\alpha}{\sqrt{2} v s_\beta}$

Table 8: The Yukawa couplings in THDMs with type I,II, X, and Y respectively.

The physical parameter space  $\mathcal{P}_{\text{THDM}}$  for THDM is set as follows

$$\mathcal{P}_{\text{THDM}} = \{M_h^2 \sim 125.\text{GeV}, M_H^2, M_{A_0}^2, M_{H^\pm}^2, m_{12}^2, t_\beta, s_{\beta-\alpha}\}. \quad (36)$$

We are interested in the alignment limit of the SM. Thus, we are going to take  $s_{\beta-\alpha} \rightarrow 1$  in this work. Moreover, the role of CP-odd Higgs  $A_0$  is not related to the calculated processes. All physical results presenting in the next sections will be independent of  $M_{A_0}$ . The parameter  $m_{12}^2$  as mentioned, play a role of the soft-breaking scale of the  $Z_2$ -symmetry. In the numerical

results, we will fix the value  $m_{12}^2$  (or  $M^2$ ) appropriately. As a result, the production cross-sections for the processes under consideration are scanned over the parameter space, e.g.  $M_{H^\pm}^2$ ,  $t_\beta$  and  $M_{H^\pm}^2$ ,  $M^2$ , etc.

### 3. One-loop corrections to $\gamma\gamma \rightarrow \phi_i\phi_j$ with CP-even Higgses $\phi_{i,j} \equiv h, H$ in HESM

In the frameworks of the above-mentioned Higgs Extensions of the Standard Models, all one-loop induced Feynman diagrams for the production processes  $\gamma\gamma \rightarrow \phi_i\phi_j$  with CP-even Higgses  $\phi_{i,j} \equiv h, H$  are listed in the following paragraphs. We are working in the 't Hooft-Feynman gauge (HF), all one-loop induced Feynman diagrams can be categorized into the following groups. We first mention group 1, as plotted in Fig. 1, all one-loop diagrams with fermions exchanging in the loop with  $\phi_k^*$ -poles for  $\phi_k^* = h^*, H^*$  or with connecting the sub-processes  $\phi_k^* \rightarrow \phi_i\phi_j$ . These kinds of diagrams appear in this group can be considered as one-loop contributions for off-shell decay of CP-even Higgs  $\phi_k^* \rightarrow \gamma\gamma$  with fermions propagating in the loop.

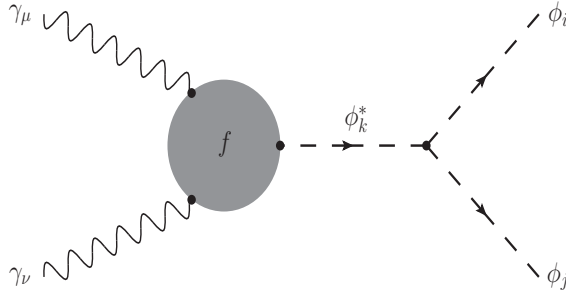


Figure 1: All one-loop diagrams with fermions exchanging in the loop of  $\phi_k^*$ -poles with  $\phi_k^* = h^*, H^*$  contributing to the processes under investigations in the HESM.

We next show all one-loop Feynman diagrams with vector  $W$ -boson propagating in the loop. It is well-known that in the HF gauge, this group also takes into account all charged Goldstone  $G^\pm$  as well as Ghost particles exchanging in the loop with connecting to  $\phi_k^*$ -poles, or  $\phi_k^* \rightarrow \phi_i\phi_j$ . (called as group 2 hereafter). As same as group 1, these kinds of diagrams belong to off-shell decay  $\phi_k^* \rightarrow \gamma\gamma$  with  $W$  boson in the loop, as described in Fig. 2.

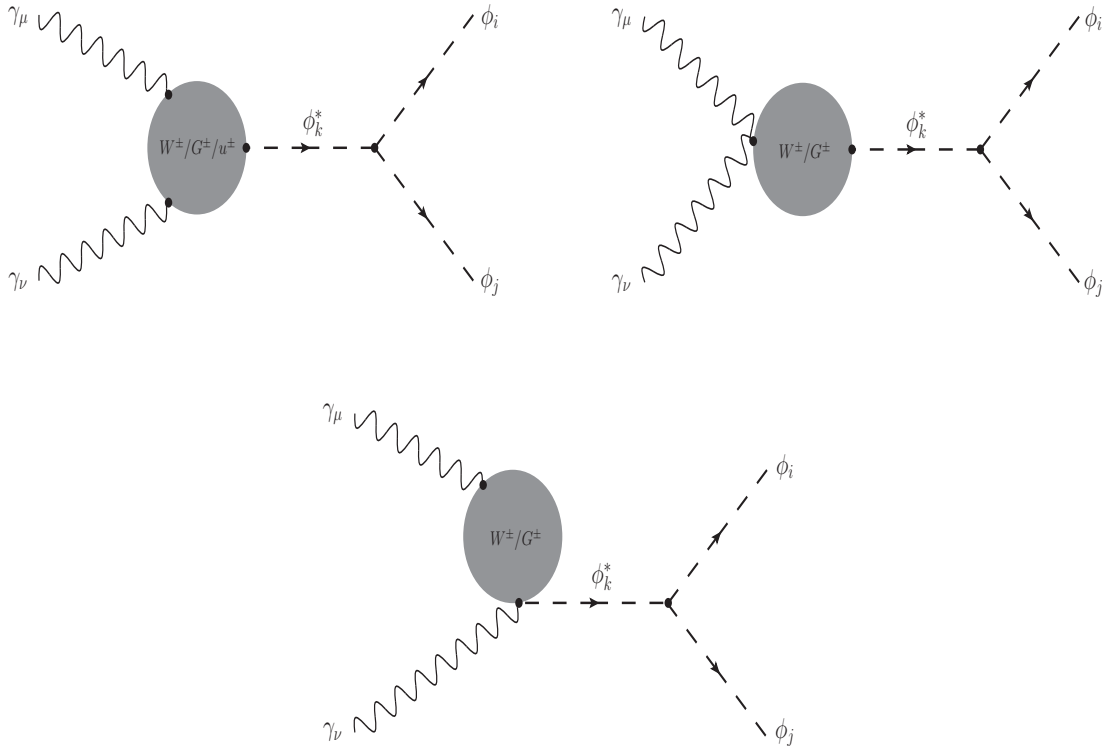


Figure 2: All one loop Feynman diagrams with vector W-boson, charged Goldstone, Ghost particles in the loop with connecting to  $\phi_k^*$ -poles, for  $\phi_k^* = h^*, H^*$  contributing to the processes under consideration in the HESM.

We also have singly charged Higgs appear in the mentioned HESMs which can also be exchanged in the loop of diagrams in the processes under investigations. As plotted in Fig. 3, one-loop triangle diagrams with the singly charged Higgs propagating in the loop in connecting with  $\phi_k^*$ -poles are concerned. As same previous groups 1, 2, all one-loop diagrams in group 3 can be considered as one-loop charged Higgs contributing for off-shell decay  $\phi_k^* \rightarrow \gamma\gamma$  in many the HESMs.

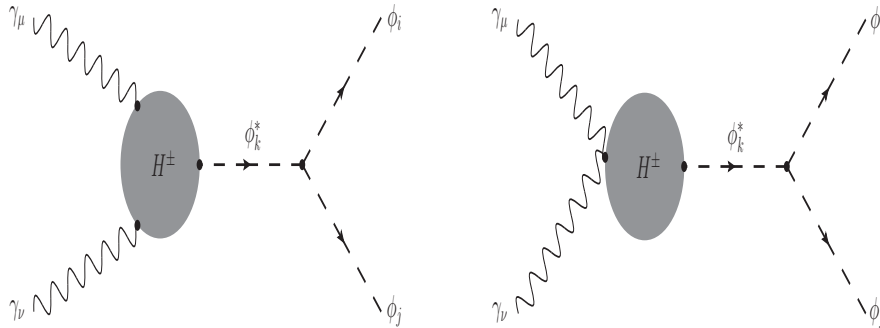


Figure 3: All Feynman diagrams with charged Higgs exchanging in the loop attributing to the processes under consideration in the HESM. These diagrams belong to one-loop charged Higgs contributing to the off-shell decay  $\phi_k^* \rightarrow \gamma\gamma$ .

One-loop box diagrams contributing to the computed processes are next mentioned. The group 4, as plotted in Fig. 4, we take into account all fermions exchanging in the loop box diagrams.

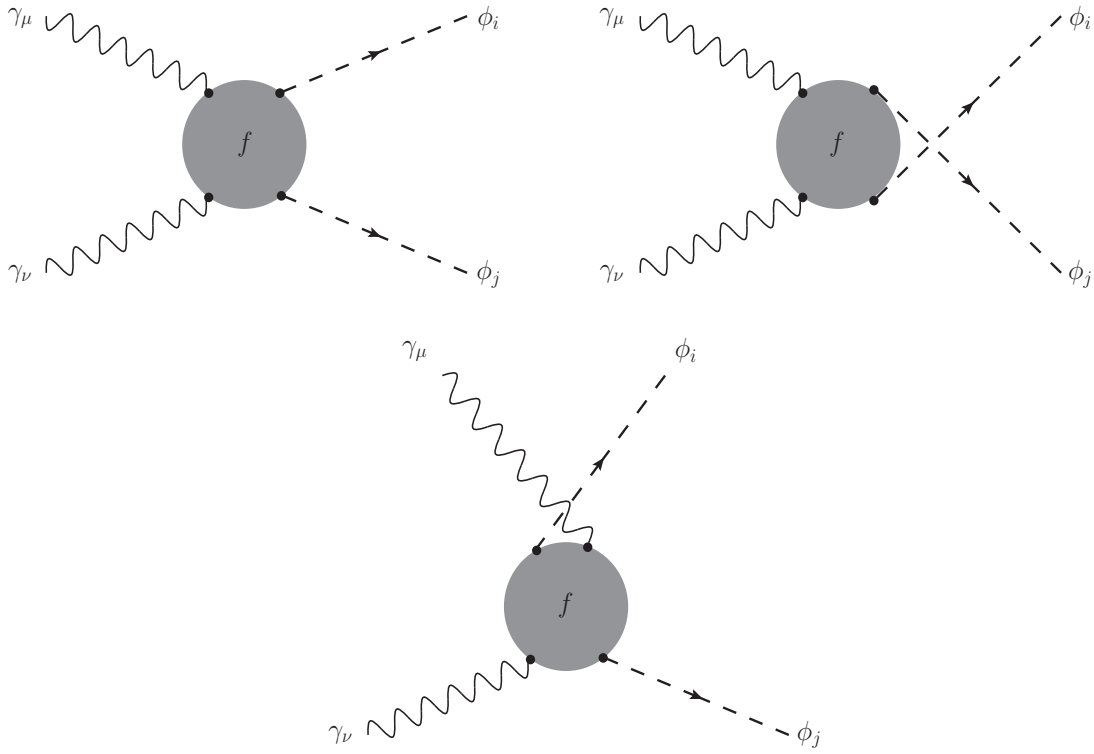


Figure 4: All one-loop box diagrams contributing to the computed processes with fermions in the loop attributing to the processes under consideration in the HESM.

Additionally, one-loop box diagrams with vector  $W$ -boson as well as the charged Goldstone bosons and Ghost particles (appear in the HF gauge) propagating in the loop, are contributed to the processes under consideration. We classify these diagrams into group 5 as shown in Figs. 5, 6).

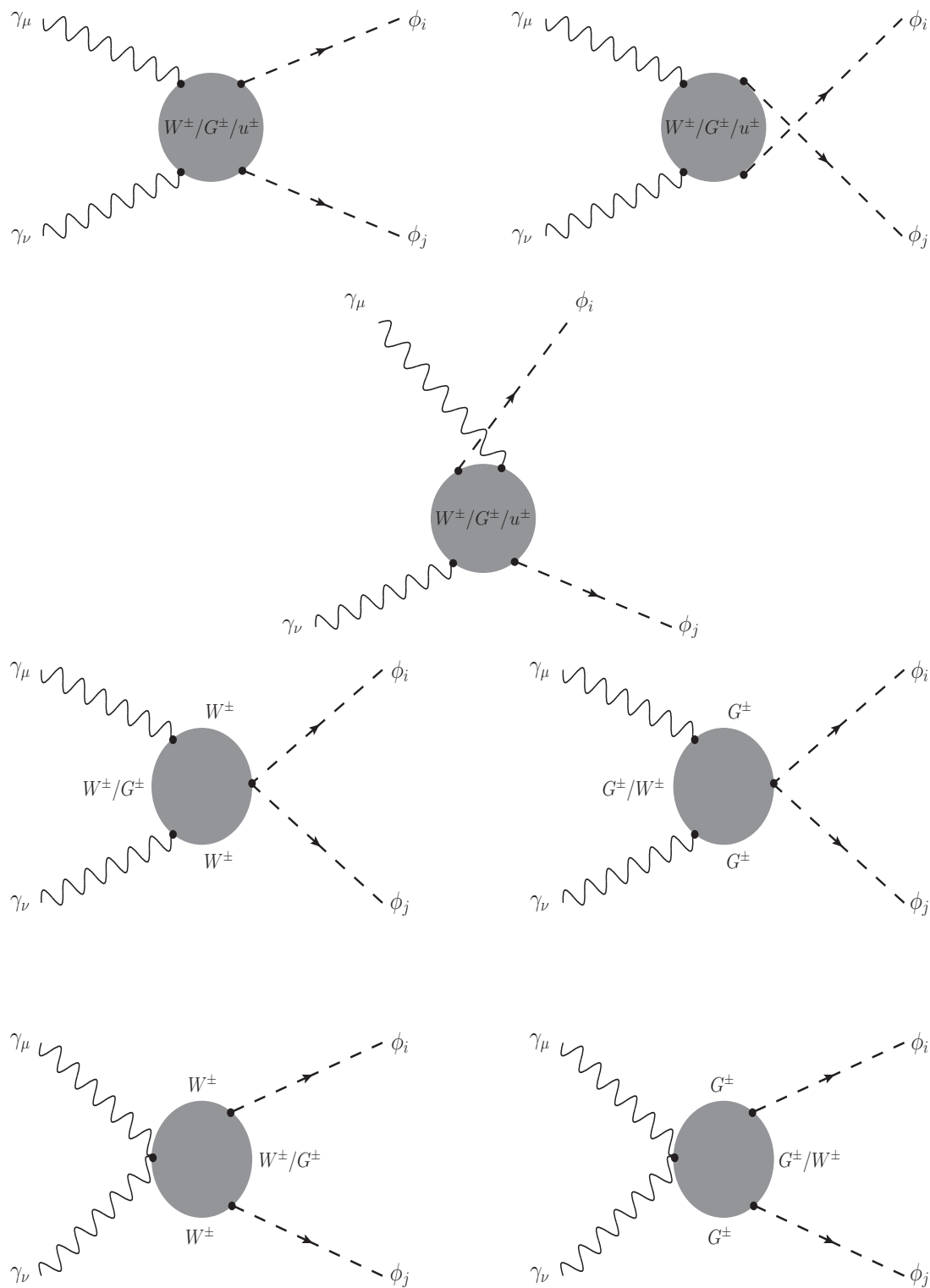


Figure 5: All one-loop box diagrams contributing to the processes with  $W$ -boson, charged Goldstone bosons and Ghost particles propagating in the loop relating to the processes under consideration in the HESM.

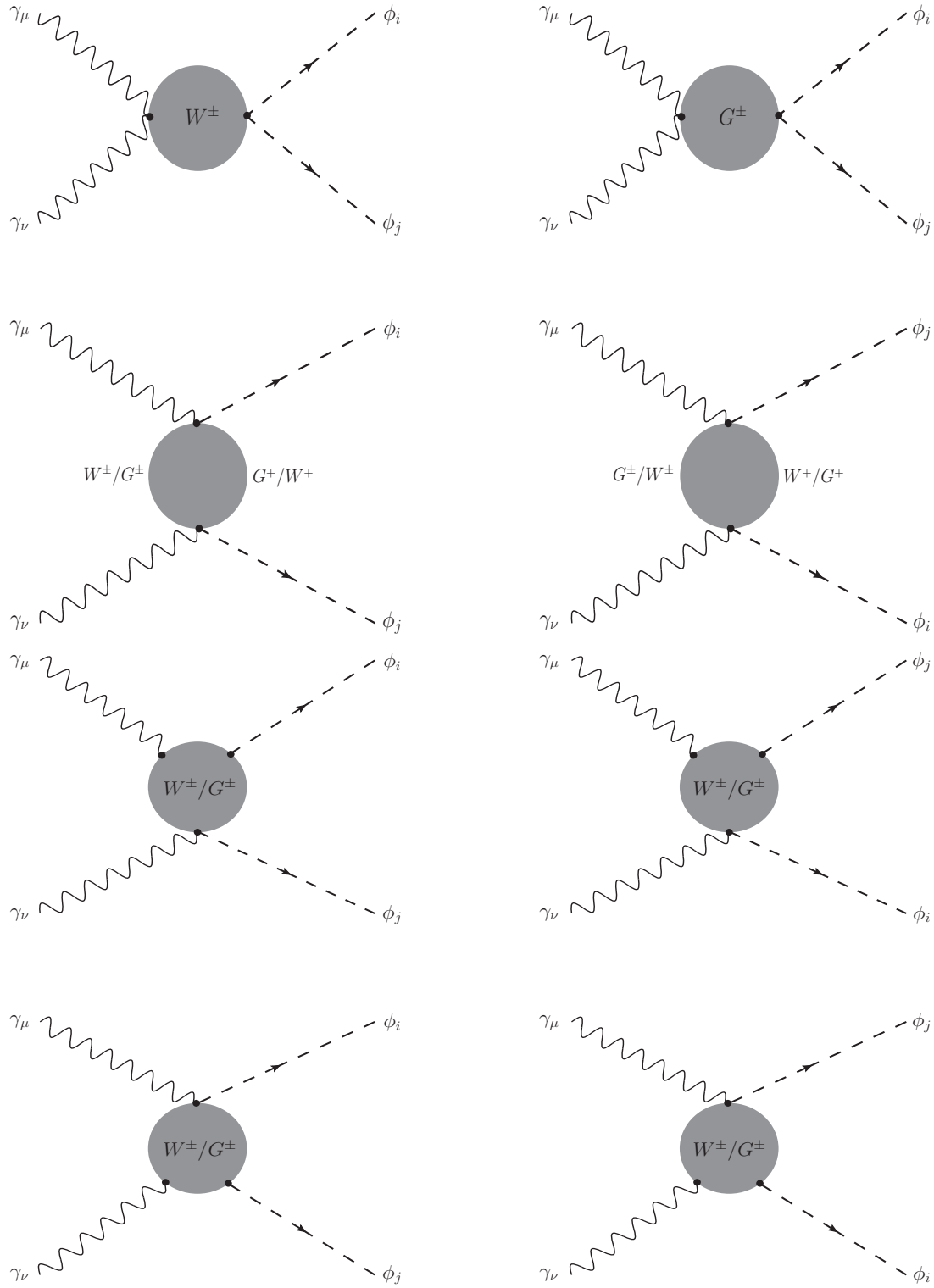


Figure 6: All one-loop box diagrams contributing to the processes with  $W$ -boson propagating in the loop relating to the processes under consideration in the HESM.

Within the frameworks of the HESMs under investigations in the paper, we also have one-loop box diagrams with both vector  $W$ -boson and singly charged Higgs propagating in the loop, seen Figs. 7, 8. We classify these diagrams into group 6. Working in the HF gauge, the charged Goldstone bosons and Ghost particles in the internal lines are also contributed in this group.

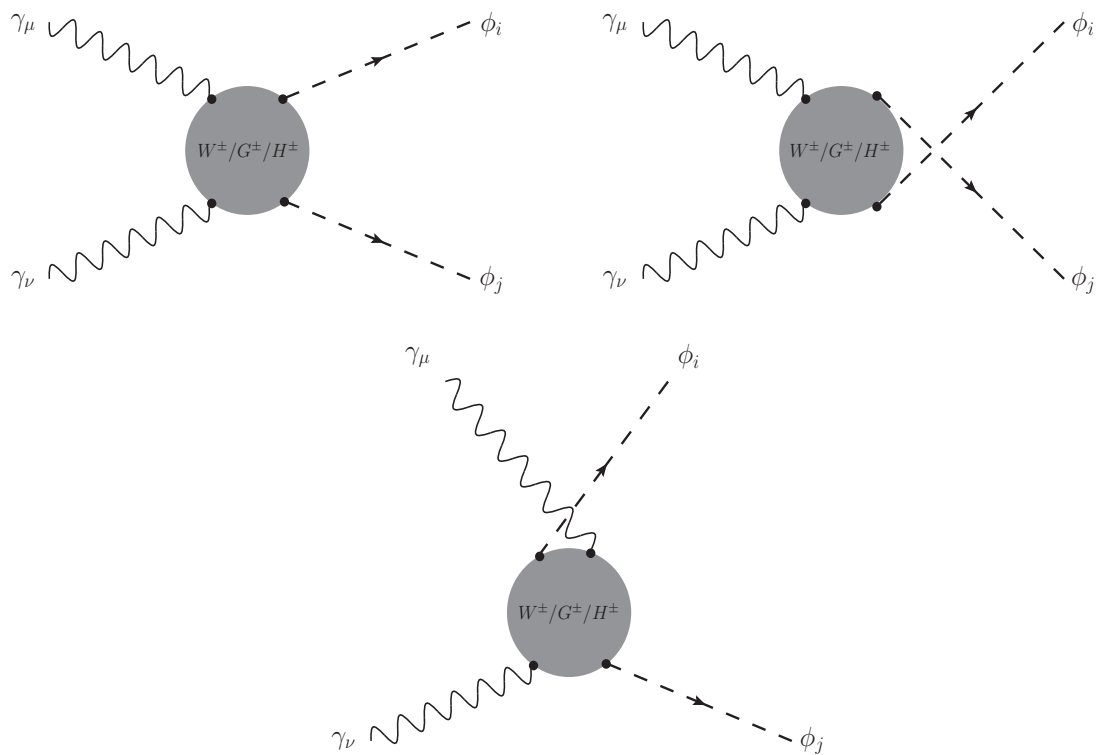


Figure 7: One-loop box diagrams with both vector  $W$ -boson, charged Goldstone bosons, Ghost particles and charged Higgs propagating in the loop contributing to the processes under consideration in the HESM.

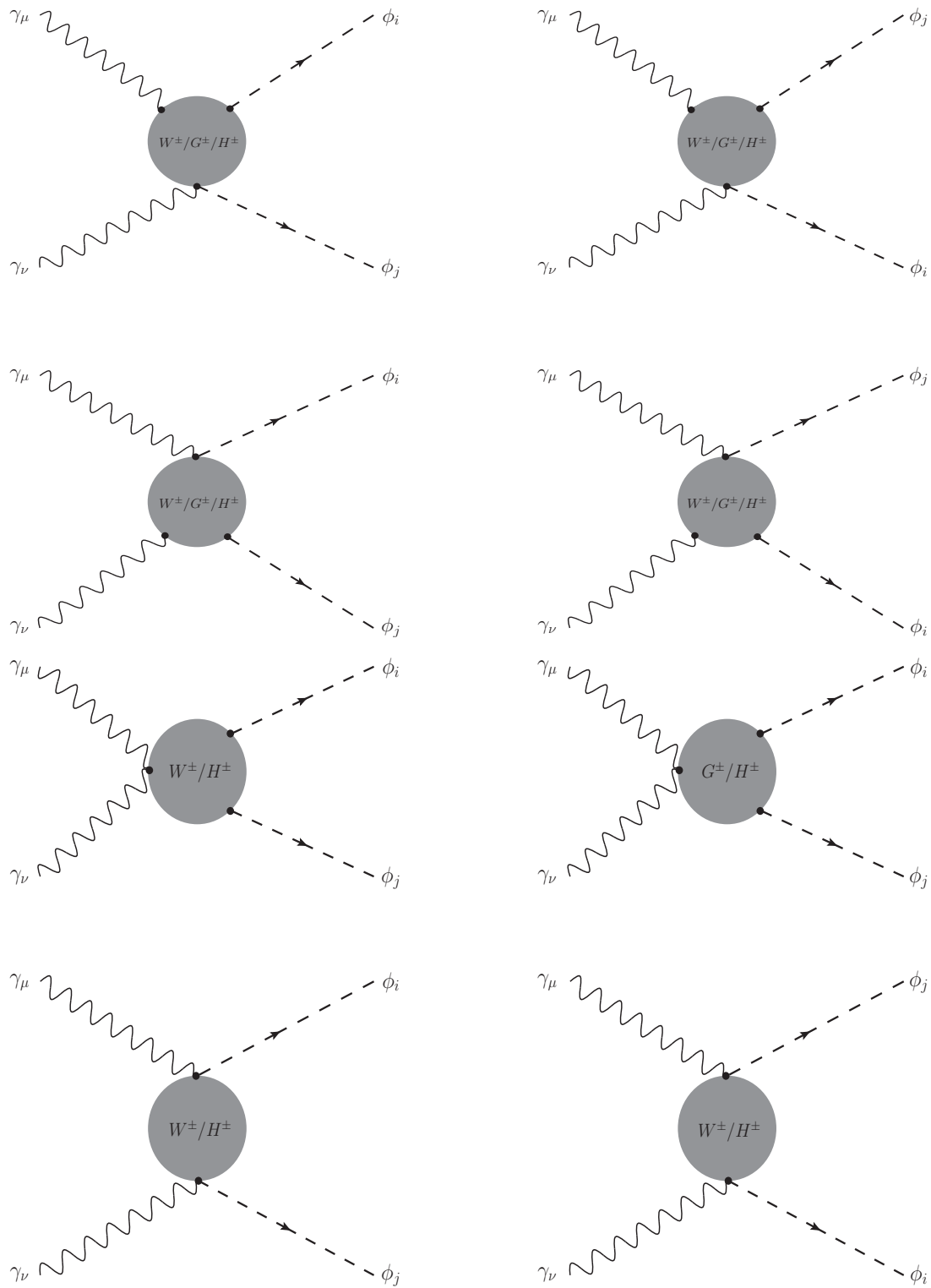


Figure 8: One-loop box diagrams with both vector  $W$ -boson, charged Goldstone bosons, Ghost particles and charged Higgs propagating in the loop contributing to the processes under consideration in the HESM.

Finally, we consider all one-loop box diagrams with singly charged Higgs in the loop, as shown in Fig. 9. These diagrams are then putted into group 7.

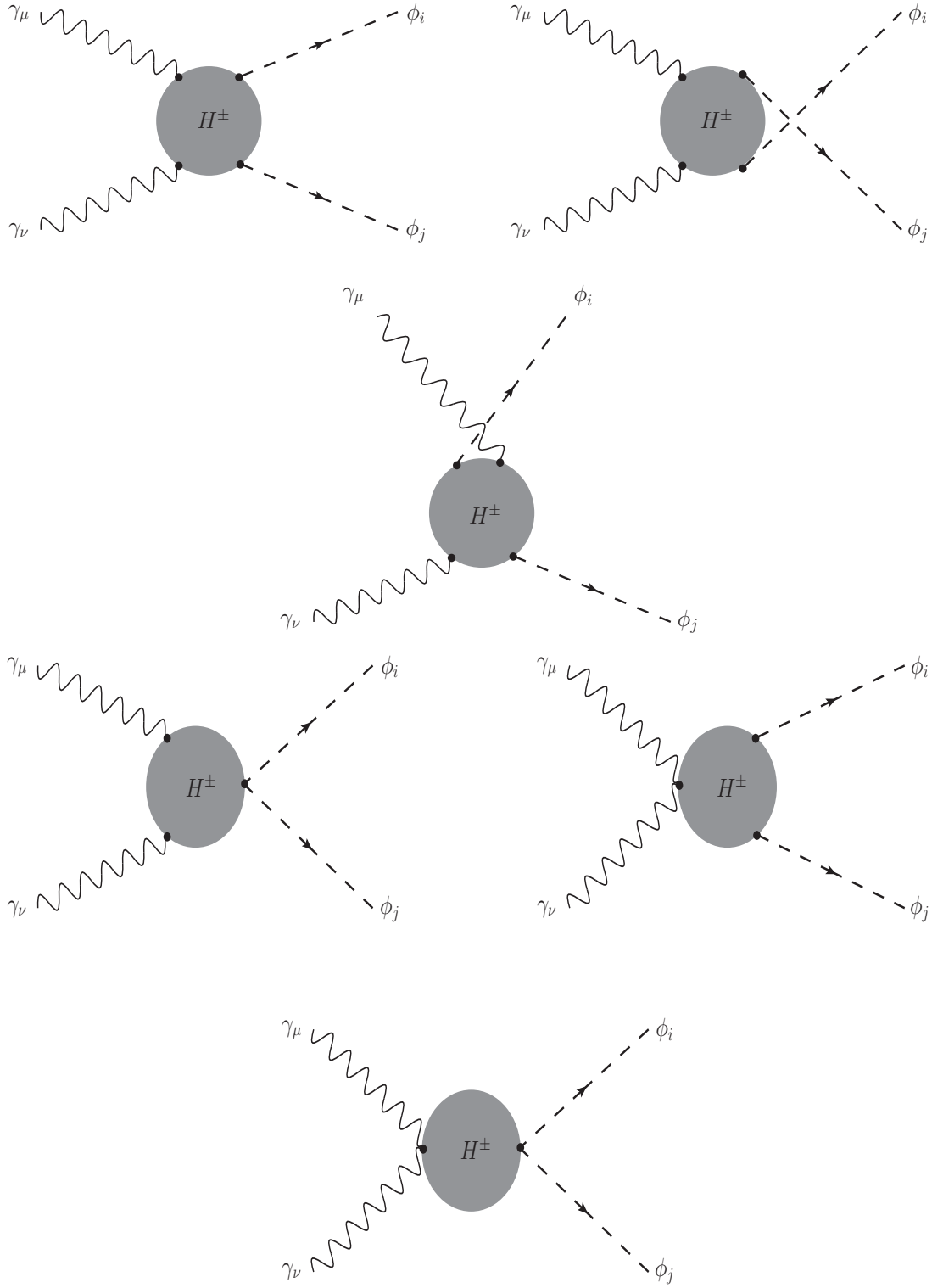


Figure 9: One-loop box diagrams with charged Higgs in the loop propagating in the loop contributing to the concerned processes in the HESM.

We turn our attention to discuss on analytic results. In general, one-loop amplitude for scattering processes  $\gamma_\mu(q_1) \gamma_\nu(q_2) \rightarrow \phi_i(q_3) \phi_j(q_4)$  is expressed in terms of Lorentz structure as follows:

$$\mathcal{A}_{\gamma\gamma \rightarrow \phi_i \phi_j} = \left[ F_{00} g^{\mu\nu} + F_{12} q_1^\nu q_2^\mu + F_{13} q_1^\nu q_3^\mu + F_{23} q_2^\mu q_3^\nu + F_{33} q_3^\mu q_3^\nu \right] \varepsilon_\mu(q_1) \varepsilon_\nu(q_2). \quad (37)$$

In this formulas, the vector  $\varepsilon_\mu(q)$  is polarization vector of external photon with the 4-dimension momentum  $q$ . The scalar coefficients  $F_{ij}$  for  $i, j = 1, 2, 3$  are called as one-loop form factors which are presented as functions of the following kinematic invariant variables:

$$s = (q_1 + q_2)^2 = q_1^2 + 2q_1 \cdot q_2 + q_2^2 = 2q_1 \cdot q_2, \quad (38)$$

$$t = (q_1 - q_3)^2 = q_1^2 - 2q_1 \cdot q_3 + q_3^2 = M_{\phi_i}^2 - 2q_1 \cdot q_3, \quad (39)$$

$$u = (q_2 - q_3)^2 = q_2^2 - 2q_2 \cdot q_3 + q_3^2 = M_{\phi_i}^2 - 2q_2 \cdot q_3. \quad (40)$$

The invariant masses for external particles are given by

$$q_1^2 = q_2^2 = 0, \quad q_3^2 = M_{\phi_i}^2, \quad q_4^2 = M_{\phi_j}^2 \quad (41)$$

and they obey the following relation

$$s + t + u = M_{\phi_i}^2 + M_{\phi_j}^2. \quad (42)$$

With on-shell photons in initial states, the amplitude follows the so-called ward identity. As a result, we derive the following relations between the form factors as:

$$F_{00} = \frac{t - M_{\phi_i}^2}{2} F_{13} - \frac{s}{2} F_{12}, \quad (43)$$

$$F_{00} = \frac{u - M_{\phi_i}^2}{2} F_{23} - \frac{s}{2} F_{12}, \quad (44)$$

$$F_{13} = \frac{u - M_{\phi_i}^2}{s} F_{33}, \quad (45)$$

$$F_{23} = \frac{t - M_{\phi_i}^2}{s} F_{33}. \quad (46)$$

Using the above relations, one-loop amplitude is expressed via two independent one-loop form factors, e.g. taking  $F_{12}$  and  $F_{33}$  as an example. Finally, the one-loop amplitude can be rewritten as follows:

$$\begin{aligned} \mathcal{A}_{\gamma\gamma \rightarrow \phi_i \phi_j} = & \left\{ \left[ \frac{(M_{\phi_i}^2 - t)(M_{\phi_i}^2 - u)}{2s} \cdot g^{\mu\nu} + q_3^\mu q_3^\nu + \frac{(t - M_{\phi_i}^2)}{s} \cdot q_2^\mu q_3^\nu \right. \right. \\ & \left. \left. + \frac{(u - M_{\phi_i}^2)}{s} \cdot q_3^\mu q_1^\nu \right] \cdot F_{33} + \left[ q_2^\mu q_1^\nu - \frac{s}{2} \cdot g^{\mu\nu} \right] \cdot F_{12} \right\} \varepsilon_\mu(q_1) \varepsilon_\nu(q_2). \end{aligned} \quad (47)$$

In this paper, we implement the HESM into **FeynArts** program [104]. All one-loop diagrams are then generated automatically by using the program. From **FeynArts** program, we can generate the calculated amplitude which is expressed in term of one-loop tensor integrals. The mentioned tensor integrals appear in the production amplitude can be reduced into the scalar PV-functions by **FormCalc** package [105]. Finally, we collect all one-loop form factors  $F_{12}$  and  $F_{33}$  for the calculated processes in the HESM. Analytic results are expressed in terms of the scalar one-loop PV-functions following the standard conventions of the packages **LoopTools** [102] and **Collier** [103].

The form factors  $F_{ab}$  for  $ab = 12, 33$  are divided into triangle and box ones which are corresponding to the contributions from one-loop triangle and one-loop box diagrams given in the above-paragraphs. The form factors are expressed as follows:

$$F_{12} = \sum_{\phi_k^* = h^*, H^*} \frac{g_{\phi_k^* \phi_i \phi_j}}{\left[ s - M_{\phi_k}^2 + i\Gamma_{\phi_k} M_{\phi_k} \right]} \times \quad (48)$$

$$\begin{aligned}
& \times \left\{ \sum_f g_{\phi_k^* ff} \cdot F_{12,f}^{\text{Trig}} + g_{\phi_k^* WW} \cdot F_{12,W}^{\text{Trig}} + g_{\phi_k^* SS} \cdot F_{12,S}^{\text{Trig}} \right\} \\
& + \sum_f g_{\phi_i ff} \cdot g_{\phi_j ff} \cdot F_{12,f}^{\text{Box}} \\
& + \left\{ g_{\phi_i WW} \cdot g_{\phi_j WW} \cdot F_{12,W}^{\text{Box},1} + g_{\phi_i \phi_j WW} \cdot F_{12,W}^{\text{Box},2} + g_{\phi_i \phi_j GG} \cdot F_{12,W}^{\text{Box},3} \right\} \\
& + \left\{ g_{\phi_i SS} \cdot g_{\phi_j SS} \cdot F_{12,S}^{\text{Box},1} + g_{\phi_i \phi_j SS} \cdot F_{12,S}^{\text{Box},2} \right\} \\
& + g_{\phi_i SW} \cdot g_{\phi_j SW} \cdot F_{12,WS}^{\text{Box}}, \\
F_{33} = & \sum_f g_{\phi_i ff} \cdot g_{\phi_j ff} \cdot F_{33,f}^{\text{Box}} + g_{\phi_i WW} \cdot g_{\phi_j WW} \cdot F_{33,W}^{\text{Box}} \\
& + g_{\phi_i SS} \cdot g_{\phi_j SS} \cdot F_{33,S}^{\text{Box}} + g_{\phi_i SW} \cdot g_{\phi_j SW} \cdot F_{33,WS}^{\text{Box}}, \tag{49}
\end{aligned}$$

where  $S \equiv H^\pm$  in this case. In further detail, the first part of form factors  $F_{12}$  are calculated from one-loop diagrams with  $\phi_k^*$ -poles in connecting to the off-shell  $\phi_k^* \rightarrow \gamma\gamma$ . One-loop form factors for the off-shell decay are presented in terms of each factor in the bracket, e.g.  $F_{12,f}^{\text{Trig}}$  (contributed from diagrams in Fig. 1),  $F_{12,W}^{\text{Trig}}$  (evaluated from diagrams in Fig. 2),  $F_{12,S}^{\text{Trig}}$  (attributed from diagrams in Fig. 3). While the factors  $F_{12,f}^{\text{Box}}$  are calculated from the one-loop box diagrams in Fig. 4. Other form factors computed from one-loop box diagrams with  $W$  propagating in the loop as in Fig. 5, are divided into the following parts, e.g.  $F_{12,W}^{\text{Box},k}$  for  $k = 1, 2, 3$  are corresponding to the factors factorized out by general trilinear-couplings of  $\phi_i WW$ ,  $\phi_j WW$ , quadratic-couplings of  $\phi_i \phi_j WW$  and  $\phi_i \phi_j GG$  as in Eq. 48. We have also expressed the factors attributing from one-loop box diagrams with charged Higgs in the loop into two sub-factors  $F_{12,S}^{\text{Box},k}$  for  $k = 1, 2$  which are factorized out by general trilinear-couplings of  $\phi_i SS$ ,  $\phi_j SS$ , quadratic-couplings of  $\phi_i \phi_j WW$  and  $\phi_i \phi_j SS$  as in Eq. 48. Lastly, from diagrams with mixing  $W$  boson and charged Higgs exchanging in the loop, we have the last factors  $F_{12,WS}^{\text{Box}}$  which can be factorized out in term of the trilinear-couplings  $\phi_i SW$ ,  $\phi_j SW$ . This can be done by applying the above relations Eqs. 8, 9 for the IDHM and Eqs. 25, 26 for the THDM. Otherwise, the form factors  $F_{33}$  are only contributed from one-loop box diagrams. They can be factorized out in term of general couplings as in Eq. 49. Analytic results for all factors appear in the above equations are shown in [130].

All one-loop form factors  $F_{12}$  and  $F_{33}$  for the processes  $\gamma\gamma \rightarrow hh$  in the HESM can be reduced to the corresponding ones in the SM. For this case, we set all general couplings related to the HESM  $\phi_k SS$ ,  $\phi_k WS$ ,  $\phi_i \phi_j SS$  being zero and all other couplings back to the corresponding ones in the SM. Due to the  $Z_2$ -symmetry, the processes  $\gamma\gamma \rightarrow hH$  in the IDHM are forbidden in this case. Reduction for one-loop form factors  $\gamma\gamma \rightarrow hh$ ,  $HH$  in the IHDM can be performed by setting appropriately the general couplings. We can apply the same strategies for getting all one-loop form factors in the THDM. Having all the necessary form factors, we are going to perform numerical checks for the calculation. The checks rely on the ultraviolet finiteness, infrared finiteness of the one-loop amplitudes. Furthermore, the amplitudes also obey the so-called ward identity. This identity is also verified numerically in the works. Additionally, both the packages `LoopTools` and `Collier` are used for cross-checking for the final results. The numerical tests for the calculations are referred to part I of our paper [130] for further detail.

Having all the correctness one-loop amplitudes, the cross-sections are then evaluated as fol-

lows

$$\hat{\sigma}_{\gamma\gamma\rightarrow\phi_i\phi_j} = \frac{1}{n} \frac{1}{16\pi s^2} \int_{t_{\min}}^{t_{\max}} dt \frac{1}{4} \sum_{\text{unpol.}} |\mathcal{A}_{\gamma\gamma\rightarrow\phi_i\phi_j}|^2 \quad (50)$$

with  $n = 2$  if the final particles are identical such as  $\gamma\gamma \rightarrow hh$ ,  $HH$ , and 1 otherwise like  $\gamma\gamma \rightarrow hH$ . The integration limits are

$$t_{\min(\max)} = -\frac{s}{2} \left\{ 1 - \frac{M_{\phi_i}^2 + M_{\phi_j}^2}{s} \pm \left[ 1 - 2 \left( \frac{M_{\phi_i}^2 + M_{\phi_j}^2}{s} \right) + \left( \frac{M_{\phi_i}^2 - M_{\phi_j}^2}{s} \right)^2 \right]^{1/2} \right\}. \quad (51)$$

The unpolarized amplitude is given

$$\begin{aligned} \frac{1}{4} \sum_{\text{unpol.}} |\mathcal{A}_{\gamma\gamma\rightarrow\phi_i\phi_j}|^2 &= \frac{M_{\phi_i}^4 s^2 + (M_{\phi_i}^2 M_{\phi_j}^2 - tu)^2}{8s^2} |F_{33}|^2 \\ &\quad - \frac{M_{\phi_i}^2 s}{4} \mathcal{R}e \left[ F_{33} \cdot (F_{12})^* \right] \\ &\quad + \frac{s^2}{8} |F_{12}|^2. \end{aligned} \quad (52)$$

In phenomenological analyses, we are interested in examining the enhancement factors  $\mu_{\phi_i\phi_j}^{\text{NP}}$  with NP standing for the THDM and the IDHM, accordingly, defined as the ratio of cross-sections of  $\gamma\gamma \rightarrow \phi_i\phi_j$  in the HESM over the corresponding ones for  $\gamma\gamma \rightarrow hh$  in the SM. The factors are given explicitly by

$$\mu_{\phi_i\phi_j}^{\text{NP}} = \frac{\hat{\sigma}_{\gamma\gamma\rightarrow\phi_i\phi_j}^{\text{NP}}}{\hat{\sigma}_{\gamma\gamma\rightarrow hh}^{\text{SM}}} (\mathcal{P}_{\text{NP}}). \quad (53)$$

In this work, the enhancement factors are scanned over the parameter space of the THDM and the IDHM.

#### 4. Phenomenological results

We turn our attention to the phenomenological studies for the processes under investigations in both the IHDM and the THDM in this section. For generating physical results, we use the following input parameters. In gauge sector, we take the masses and the decay widths for gauge bosons as follows:  $M_Z = 91.1876$  GeV,  $\Gamma_Z = 2.4952$  GeV,  $M_W = 80.379$  GeV,  $\Gamma_W = 2.085$  GeV. Moreover, we use  $M_{h^0} = 125.1$  GeV,  $\Gamma_{h^0} = 4.07 \cdot 10^{-3}$  GeV for the SM-like Higgs boson. The masses of all fermions are used as  $m_e = 0.00052$  GeV,  $m_\mu = 0.10566$  GeV and  $m_\tau = 1.77686$  GeV. In the quark sector, their masses are taken like  $m_u = 0.00216$  GeV,  $m_d = 0.0048$  GeV,  $m_c = 1.27$  GeV,  $m_s = 0.93$  GeV,  $m_t = 173.0$  GeV, and  $m_b = 4.18$  GeV. The  $G_\mu$ -scheme is applied in this work in which the Fermi constant is considered as an the input parameter, taking  $G_\mu = 1.16638 \cdot 10^{-5}$  GeV<sup>-2</sup>. The electroweak constant is then obtained subsequently:

$$\alpha = \sqrt{2}/\pi G_\mu M_W^2 (1 - M_W^2/M_Z^2) = 1/132.184. \quad (54)$$

In each model under investigations, we are going to present the corresponding parameter space for phenomenological studies in next subsections.

#### 4.1. IHDM

Phenomenological studies for the processes  $\gamma\gamma \rightarrow \phi_i\phi_j$  in the IHDM are presented in this subsection. As usual procedure, we first review the current constraints on the physical parameter space in the IDHM given in Eq. (10). The limitations for the physical parameter space rely on theoretical and experimental constraints. In the perspective of the experimental constraints, we take into account the Electroweak Precision Tests (EWPT) of the IHDM, Dark matter search at the LHC, as well as including the LEP data. These topics have implicated in Refs. [106, 107, 108, 109]. Additionally, one loop-induced decays of the SM-like Higgs ( $h$ ) to  $V\gamma$  with  $V \equiv Z, \gamma$  have also studied in the IHDM framework, e.g. decay process  $h \rightarrow \gamma\gamma$  [110, 117, 118], and decay channels  $h \rightarrow Z\gamma$  [117, 118]. Furthermore, in Refs. [111, 112, 113, 114, 115, 116], searching signals of the IHDM at future colliders have performed. In the theoretical aspect, the most important theoretical constraints are from that the models follow the tree-level unitarity, the vacuum stability, the perturbative regime. These requirements give the limitations on the Higgs self-couplings  $\lambda_i$  for  $i = 1, 2, \dots, 5$  and  $\mu_2$ . By combining all theoretical and experimental constraints in the above-mentioned papers, there is reasonable to select the parameter space for the IDHM as follows: one can take logically  $5 \text{ GeV} \leq M_H \leq 150 \text{ GeV}$ ,  $70 \text{ GeV} \leq M_{H^\pm}, M_{A^0} \leq 1000 \text{ GeV}$ ,  $|\mu_2| \leq 500 \text{ GeV}$ , and  $0 \leq \lambda_2 \leq 8\pi$ .

##### 4.1.1. Production cross-sections

In the IDHM, the process  $\gamma\gamma \rightarrow hH$  is forbidden by the  $Z_2$ -symmetry. For this reason, we only concern the production cross-sections for the processes  $\gamma\gamma \rightarrow hh, HH$  in the IDHM. In Fig. 10, we show total cross-sections for  $\gamma\gamma \rightarrow hh, HH$  in the IHDM, together with the ones for  $hh$  production in the SM, as functions of center-of-mass (CoM) energy  $\sqrt{\hat{s}_{\gamma\gamma}}$  (or  $E_{\gamma\gamma}$ ). For the below generated data, we select the following parameter space in the IDHM as  $M_{H^\pm} = 200 \text{ GeV}$ ,  $M_H = 150 \text{ GeV}$  in this case. Consequently, in the plots we vary  $350 \text{ GeV} \leq \sqrt{\hat{s}_{\gamma\gamma}} \leq 1500 \text{ GeV}$ . We present the cross-sections for  $\mu_2^2 = 0 \text{ GeV}^2$  on the left pannel and for  $200^2 \text{ GeV}^2$  on the right panel, respectively. Furthermore, we fix  $\lambda_2 = 0.8$  for all cases. In the plots, the black line shows for total cross-sections for  $\gamma\gamma \rightarrow hh$  in the SM and the blue (green) line presents for  $\gamma\gamma \rightarrow hh$  ( $HH$ ) in THDM, respectively.

We comment on the data for the case of  $\mu_2^2 = 0 \text{ GeV}^2$ . We find that the cross-sections for  $hh, HH$  in the IHDM have peaks at  $\sqrt{\hat{s}_{\gamma\gamma}} \sim 2M_{H^\pm} = 400 \text{ GeV}$ . The cross-sections develop to the peaks and they are decreased rapidly beyond the peaks. In the regions  $\sqrt{\hat{s}_{\gamma\gamma}} \leq 750 \text{ GeV}$ , the cross-sections for the productions  $hh, HH$  in the IHDM are larger than the corresponding ones for  $hh$  production in the SM. Beyond the regions of  $\sqrt{\hat{s}_{\gamma\gamma}} \geq 750 \text{ GeV}$ , the cross-sections for  $HH$  in the IHDM are suppressed in comparison with  $hh$  productions in both the SM and the IHDM. It is interested in finding that the production cross-sections for  $\gamma\gamma \rightarrow hh, HH$  in the IDHM are dominant around the peaks compared with the corresponding ones for  $hh$  production in the SM. It indicates that the contributions from singly charged Higgs exchanging in the loop of the processes  $\gamma\gamma \rightarrow hh, HH$  are massive attributions in the regions

In the case of  $\mu_2^2 = 200^2 \text{ GeV}^2$ , we only observe a peak of the cross-sections for  $HH$  production in the IHDM around  $\sqrt{\hat{s}_{\gamma\gamma}} \sim 2M_{H^\pm} = 400 \text{ GeV}$ . In further, the data shows that the cross-sections for  $HH$  production are dominant in the regions  $\sqrt{\hat{s}_{\gamma\gamma}} \leq 750 \text{ GeV}$  in contrast with the corresponding ones for  $hh$  productions in both the SM and the IDHM. Beyond the regions  $\sqrt{\hat{s}_{\gamma\gamma}} \geq 750 \text{ GeV}$ , the cross-sections for  $HH$  production are suppressed. It is inspired in finding that the cross-sections for  $hh$  production in the IHDM are smaller than the corresponding one in the SM when  $\sqrt{\hat{s}_{\gamma\gamma}} \leq 550 \text{ GeV}$ . Beyond the regions  $\sqrt{\hat{s}_{\gamma\gamma}} \geq 550 \text{ GeV}$ , they tend to the cross-sections for  $hh$  production in the SM. This can be explained as follows. Since the  $hh$  productions in the IHDM are different from the ones in the SM by the contributions of charged

Higgs in the loop of triangle  $h^*$ -pole and box diagrams. These contributions depend on  $M_{H^\pm}$  and the couplings of  $hH^\pm H^\mp$ ,  $hhH^\pm H^\mp$  expressing in terms of  $\mu_2^2$ . At the large value of  $\mu_2^2$  these contributions may be cancelled out. As a result, cross-sections for  $hh$  productions in the IDHM tend to the corresponding ones in the SM. Another case of  $HH$  production, we have no couplings of  $HH^\pm H^\mp$  due to the  $Z_2$ -symmetry and the vertex  $HHH^\pm H^\mp$  depend on  $\lambda_2$ . Therefore, we have no the cancellations among the contributions of singly charged propagating in the loop. It is reasonable that the cross-sections for  $HH$  production in the IHDM are dominant in the regions  $\sqrt{\hat{s}_{\gamma\gamma}} \leq 550$  GeV and they also have peak at  $\sqrt{\hat{s}_{\gamma\gamma}} \sim 2M_{H^\pm} = 400$  GeV.

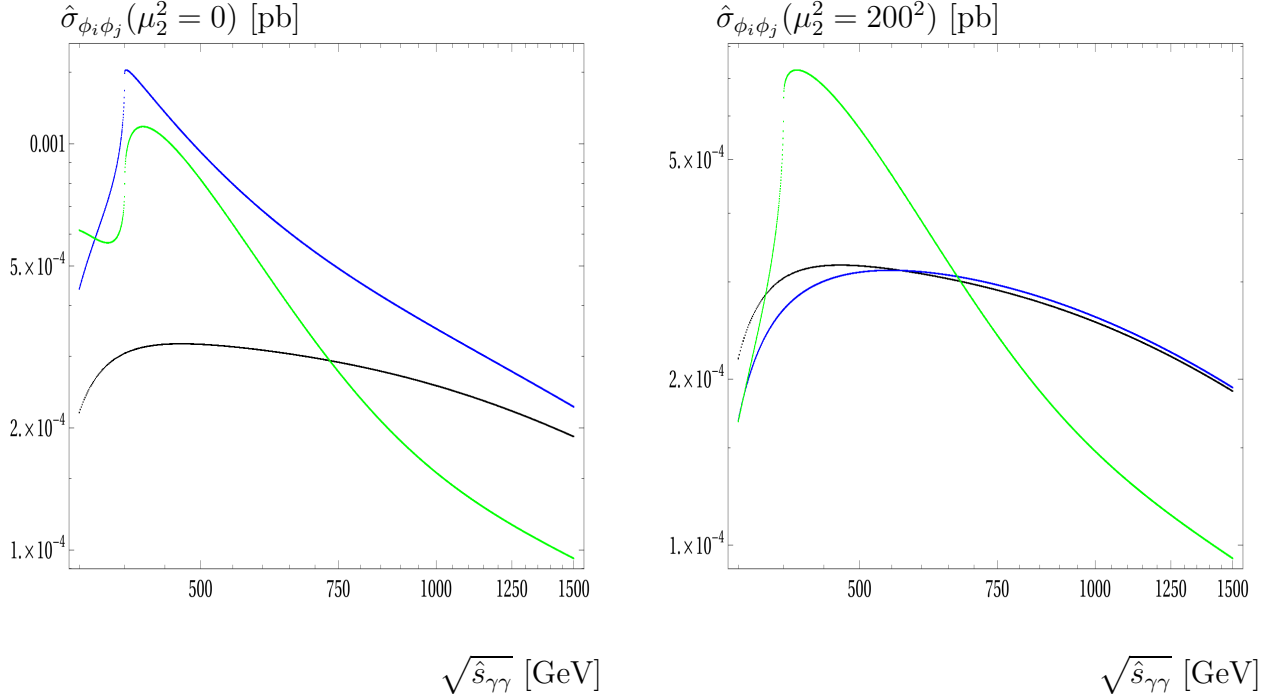


Figure 10: Total cross-sections for  $\gamma\gamma \rightarrow hh$ ,  $HH$  in the SM and IHDM are presented as functions of center-of-mass energy  $\sqrt{\hat{s}_{\gamma\gamma}}$ . For the generated data, we select  $M_{H^\pm} = 200$  GeV,  $M_H = 150$  GeV in this case. We vary  $350 \text{ GeV} \leq \sqrt{\hat{s}_{\gamma\gamma}} \leq 1500$  GeV. In the below plots, we fix  $\mu_2^2 = 0, 200^2$  GeV<sup>2</sup> and  $\lambda_2 = 0.8$  for all cases. In the plots, the black line shows for cross section of  $\gamma\gamma \rightarrow hh$  in the SM. Additionally, the blue (green) line presents for  $\gamma\gamma \rightarrow hh$  ( $HH$ ) in THDM.

#### 4.1.2. Enhancement factors

The enhancement factors given in Eq. 53 are examined in the IDHM in the following subsections. In Fig. 11, the factors for  $\gamma\gamma \rightarrow hh$ ,  $HH$  are presented in terms of parameter space of  $M_{H^\pm}$ ,  $\mu_2^2$ . In the following scatter plots, singly charged Higgs masses are varied from  $70 \text{ GeV} \leq M_{H^\pm} \leq 600$  GeV and  $-200 \text{ GeV} \leq \mu_2 \leq 200$  GeV. Furthermore, we fix  $\lambda_2 = 0.8$  and  $M_H = 150$  GeV for all cases. The data is generated at center-of-mass energy  $\sqrt{\hat{s}_{\gamma\gamma}} = 500$  (all left panel scatter plots) GeV and at  $\sqrt{\hat{s}_{\gamma\gamma}} = 1000$  GeV (all right panel scatter plots).

The factors for  $hh$  productions in the IHDM are first analyzed. Since the cross-sections for  $hh$  productions are enhanced around the peaks at  $\sqrt{\hat{s}_{\gamma\gamma}} \sim 2M_{H^\pm}$ . Therefore, it is not surprised in finding that  $\mu_{hh}^{\text{IHDM}}$  becomes largest at  $\sqrt{\hat{s}_{\gamma\gamma}} \sim 2M_{H^\pm} = 250$  GeV (for the left plots) and at  $\sqrt{\hat{s}_{\gamma\gamma}} \sim 2M_{H^\pm} = 500$  GeV (for the right plots). Around these peaks, it is inspired that the enhancement factors will tend to about  $\sim 1.5$  in the limit of  $\mu_2^2 \rightarrow M_{H^\pm}^2$ . This is because of the

contributions of charged Higgs exchanging in the loop of triangle diagrams and the box diagrams being small (due to couplings of  $hH^\pm H^\mp$ ,  $hhH^\pm H^\mp$  tend to zero in this limit). It is found that the enhancement factors can reach to factor of 6 (for 500 GeV of CoM) and factor of 13 (for 1000 GeV of CoM) around the peaks. Beyond the peaks, we observe that  $1 \leq \mu_{hh}^{\text{IHD M}} \leq 2$ .

For the enhancement factors of  $HH$  productions in the IDHM, we also find  $\mu_{HH}^{\text{IHD M}}$  becomes largest contributions at  $\sqrt{\hat{s}_{\gamma\gamma}} \sim 2M_{H^\pm} = 250$  GeV (for the left plots) and at  $\sqrt{\hat{s}_{\gamma\gamma}} \sim 2M_{H^\pm} = 500$  GeV (for the right plots). It is attentive to realize that  $\mu_{HH}^{\text{IHD M}}$  have different behavior in comparison with  $\mu_{hh}^{\text{IHD M}}$ . At the 500 GeV of CoM, the factors develop to the peak and then are decreased rapidly beyond the peak. However, they grow up with the charged Higgs masses in the above regions of  $M_{H^\pm} \geq \sim 300$  GeV. Because there aren't couplings  $HH^\pm H^\mp$  due to the  $Z_2$ -symmetry and the vertex  $HHH^\pm H^\mp$  only depends on  $\lambda_2$ . Therefore, in the high regions of charged Higgs masses, the factors  $\mu_{HH}^{\text{IHD M}}$  are increased with  $M_{H^\pm}$ .

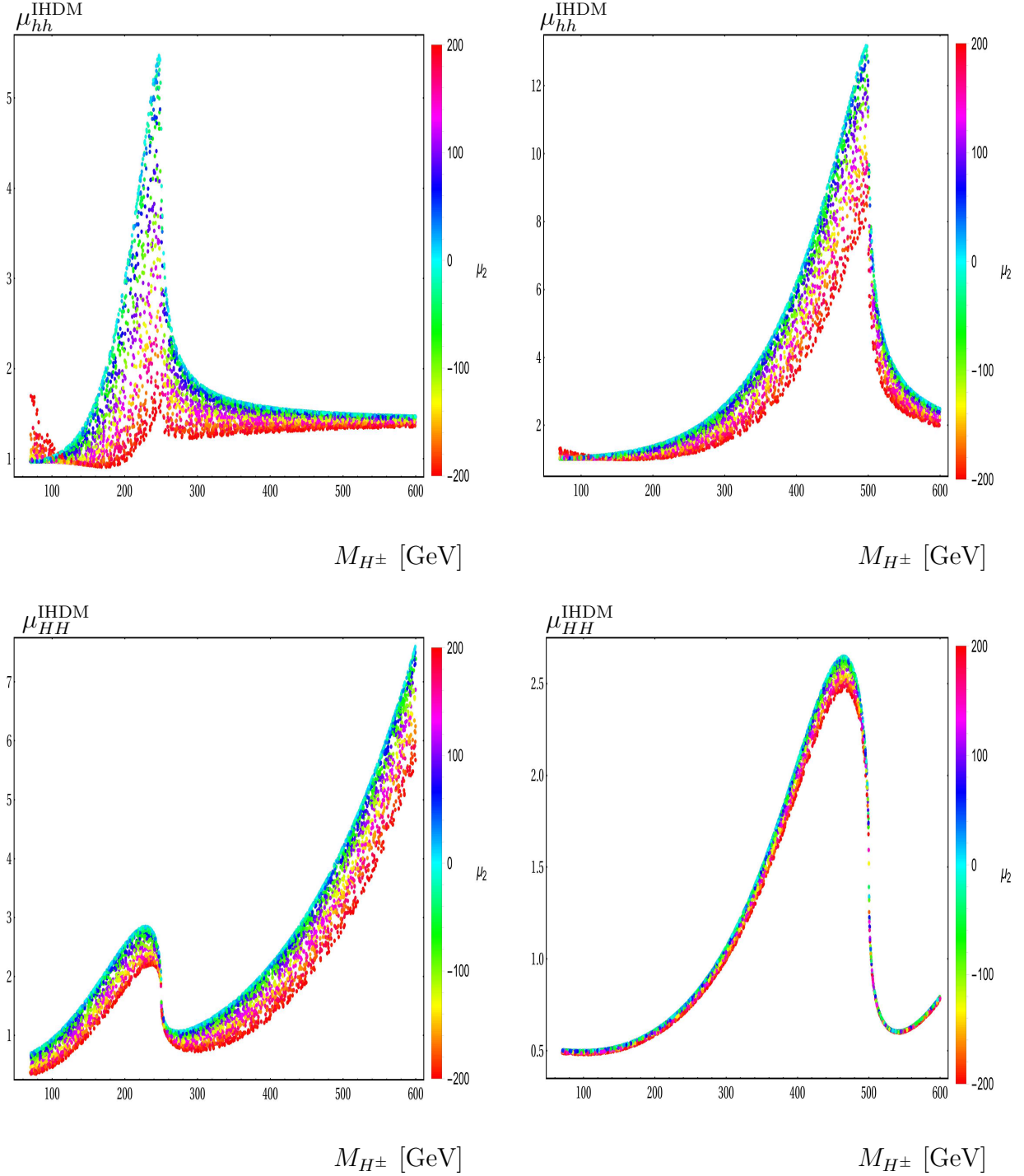


Figure 11: The enhancement factors are presented in the parameter space of  $M_{H^\pm}$ ,  $\mu_2^2$ . We vary  $70 \text{ GeV} \leq M_{H^\pm} \leq 1000 \text{ GeV}$  and  $-200 \text{ GeV} \leq \mu_2 \leq 200 \text{ GeV}$ . We fix  $\lambda_2 = 0.8$  and  $M_H = 150 \text{ GeV}$  for all cases. In the plots, we set  $\sqrt{\hat{s}_{\gamma\gamma}} = 500 \text{ GeV}$  (for the left panel plots) and  $\sqrt{\hat{s}_{\gamma\gamma}} = 1000 \text{ GeV}$  (for the right panel plots).

In Fig. 12, the enhancement factors for  $\gamma\gamma \rightarrow hh$ ,  $HH$  are generated in the space of  $M_{H^\pm}$ ,  $\lambda_2$ . The charged Higgs masses are varied as  $70 \text{ GeV} \leq M_{H^\pm} \leq 600 \text{ GeV}$  and  $0 \leq \lambda_2 \leq 4$ . We fix  $\mu_2^2 = 200^2 \text{ GeV}^2$  and  $M_H = 150 \text{ GeV}$  for all cases. In the scatter plots, we set  $\sqrt{\hat{s}_{\gamma\gamma}} = 500$  (for all left panel plots) GeV and  $\sqrt{\hat{s}_{\gamma\gamma}} = 1000$  GeV (for all right panel plots). For the factors  $\mu_{hh}^{IHDM}$  (as shown in all the above scatter plots), both the couplings  $hH^\pm H^\mp$  and  $hhH^\pm H^\mp$  are independent of  $\lambda_2$ . As a result, the factors only depend on  $M_{H^\pm}$ . For the factors  $\mu_{HH}^{IHDM}$  (as

shown in all the below scatter plots), it is found that the quadratic-coupling  $HHH^\pm H^\mp$  depend on  $\lambda_2$ . As a result, the factors depend strongly on  $\lambda_2$  and  $M_{H^\pm}$ . These massive contributions are mainly from the charged Higgs exchanging in the box diagrams.

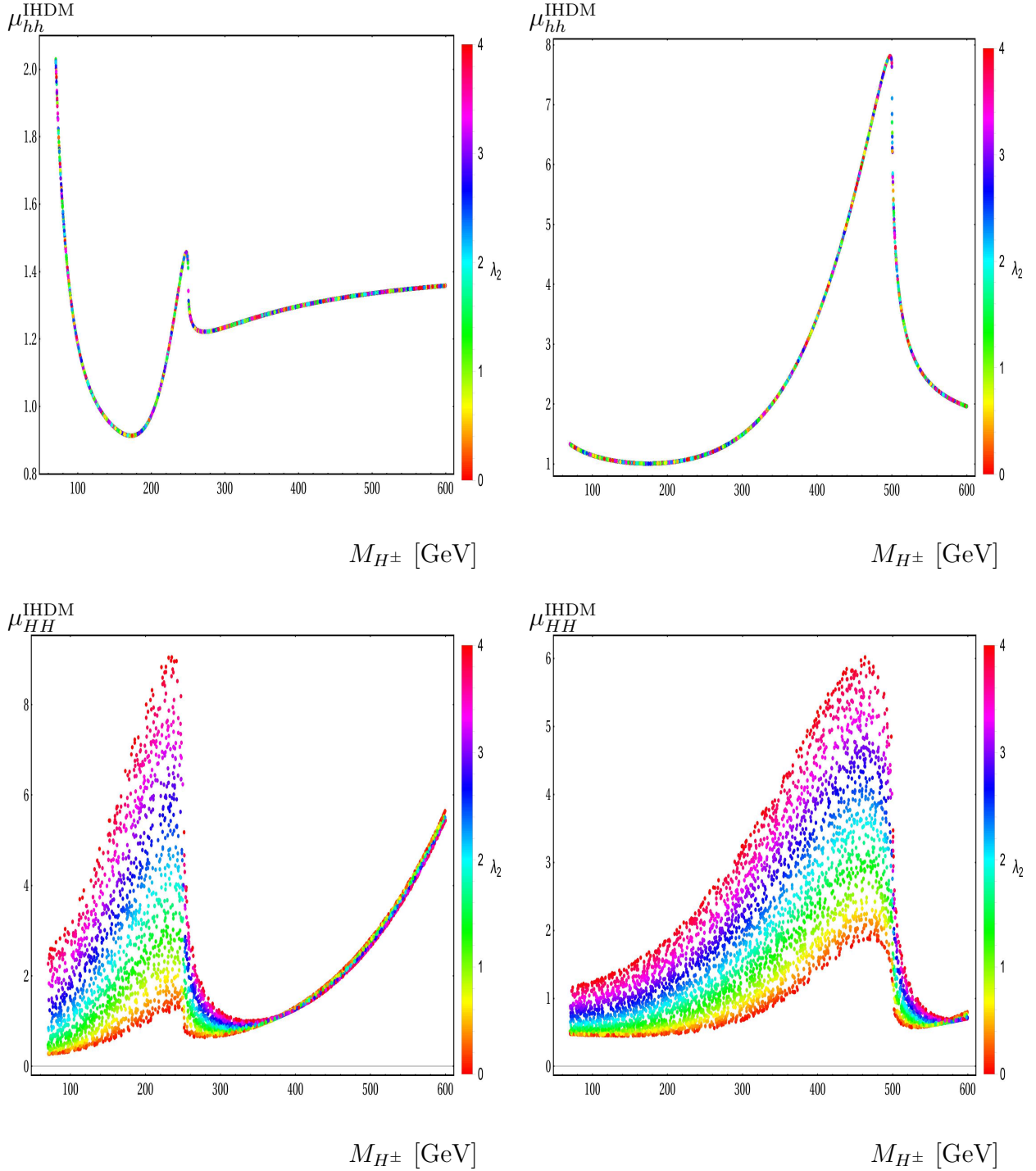


Figure 12: The enhancement factors are scanned over the parameter space of  $M_{H^\pm}, \lambda_2$ . We vary  $70 \text{ GeV} \leq M_{H^\pm} \leq 1000 \text{ GeV}$  and  $0 \leq \lambda_2 \leq 4$ . We fix  $\mu_2^2 = 200^2 \text{ GeV}^2$  and  $M_H = 150 \text{ GeV}$  for all cases. In the plots, we set  $\sqrt{\hat{s}_{\gamma\gamma}} = 500 \text{ GeV}$  (for the above Figures) and  $\sqrt{\hat{s}_{\gamma\gamma}} = 1000 \text{ GeV}$  (for the below Figures), correspondingly.

## 4.2. THDM

The phenomenological results for the production processes  $\gamma\gamma \rightarrow \phi_i\phi_j$  with CP-even Higgses  $\phi_{i,j} \equiv h, H$  in the THDM are analysed in the following subsection. As same as the IDHM, we first summarize the current constraints the parameter space of the THDM. The theoretical and experimental constraints for the THDM taking into consideration, we arrive at the current regions for the parameter space for the mentioned model. Theoretical constraints reply on the subjects of the requirements for perturbative regime, tree-level unitarity of gauge theories and for vacuum stability conditions of the scalar Higgs potential. These topics have studied in the following papers [121, 122, 123, 124, 126] and references therein. In further, we take into consideration the electroweak precision tests (EWPT) for the THDM in aspect of experimental constraints. Implicating for these topics at LEP are reported in Refs. [127, 128]. Searching for the masses range of scalar particles for the THDM have performed at the LEP, the Tevaron as well as at the LHC as reviewed in the paper [125]. Moreover, one-loop induced for the SM-like Higgs decay channels like  $h \rightarrow \gamma\gamma$  and  $h \rightarrow Z\gamma$  in the THDM have implicated in Refs. [117, 118] and references therein. Combining all the above constraints, we select reasonably the physical parameters as follows:  $126 \text{ GeV} \leq M_H \leq 1000 \text{ GeV}$ ,  $60 \text{ GeV} \leq M_{A^0} \leq 1000 \text{ GeV}$  and  $80 \text{ GeV} \leq M_{H^\pm} \leq 1000 \text{ GeV}$  in the type I and type X of the THDM. For the Type-II and Y of the THDM, the physical parameters can be scanned consistently as follows:  $500 \text{ GeV} \leq M_H \leq 1000 \text{ GeV}$ ,  $500 \text{ GeV} \leq M_{A^0} \leq 1000 \text{ GeV}$  and  $580 \text{ GeV} \leq M_{H^\pm} \leq 1500 \text{ GeV}$ . Additionally, we take  $2 \leq t_\beta \leq 20$ ,  $0.95 \leq s_{\beta-\alpha} \leq 1$  for the alignment limit of the SM (we take  $s_{\beta-\alpha} \sim 0.98$  for below physical results) in both types of the THDM. The  $Z_2$ -breaking parameter can be selected as  $m_{12}^2 = M_H^2 s_\beta c_\beta$ . Last but not least, further limitations on  $t_\beta$ ,  $M_{H^\pm}$  have also studied for the THDM with the softly broken  $Z_2$ -symmetry from implying the flavor experimental data in Ref. [129]. Following the results in Ref. [129], it is interested in finding that the small values of  $t_\beta$  are favoured for matching the flavor experimental data. As a result, for complemental discussions we are also interested in considering the small values of  $t_\beta$  (scan this parameter reasonably over the region of  $2 \leq t_\beta \leq 10$  in some cases, for examples) in our work.

### 4.2.1. Production cross-sections

We are going to present physical results for the processes in the THMD in detail. The total cross-sections for  $\gamma\gamma \rightarrow hh$ ,  $hH$ ,  $HH$  in the THDM are first investigated at several CoM energies. In Fig. 13,  $\hat{\sigma}_{\gamma\gamma \rightarrow \phi_i\phi_j}$  in the THDM together with  $\hat{\sigma}_{\gamma\gamma \rightarrow hh}$  in the SM, are presented as functions of CoM energy  $E_{\gamma\gamma}$ . The following data are generated at  $M_{H^\pm} = 300 \text{ GeV}$ ,  $M_H = 150 \text{ GeV}$ ,  $t_\beta = 5$ . Consequently, in the selected-configurations, we vary CoM energy as  $350 \text{ GeV} \leq E_{\gamma\gamma} \leq 1500 \text{ GeV}$ . In all the below plots, the breaking  $Z_2$ -symmetry scale  $m_{12}^2 = M^2/s_\beta c_\beta$  is selected as follows:  $M^2 = 0, 200^2, 500^2, 700^2 \text{ GeV}^2$ . In further, the mixing angle  $\alpha$  is taken  $c_{\beta-\alpha} = +0.2$  and  $s_{\beta-\alpha} = +\sqrt{1 - c_{\beta-\alpha}^2}$ , accordingly. Our conventions for all the presented plots in below are as follows: the black line shows for cross-sections of  $\gamma\gamma \rightarrow hh$  in the SM. While the blue line presents for  $\gamma\gamma \rightarrow hh$  in THDM. Additionally, the green (red) line presents for  $\gamma\gamma \rightarrow hH$  ( $\gamma\gamma \rightarrow HH$ ) in THDM, respectively.

We find that total cross-sections are enhanced at  $E_{\gamma\gamma} \sim 2M_{H^\pm} = 600 \text{ GeV}$  for all cases. The data confirm that the total cross-sections for  $\gamma\gamma \rightarrow hH$  are suppressed compared with other productions. It is explainable because of the consequences of the soft breaking  $Z_2$ -symmetry. However,  $\hat{\sigma}_{\gamma\gamma \rightarrow hH}$  become more and more significant once  $M^2$  being the large values.

We first inspect the data in the case of  $M^2 = 0$ . One notices that  $\hat{\sigma}_{\gamma\gamma \rightarrow HH}$  become largest in the regions  $E_{\gamma\gamma} \leq \sim 450 \text{ GeV}$  and they are decreased rapidly in the regions  $E_{\gamma\gamma} \geq 450 \text{ GeV}$ . Moreover, in the regions of  $E_{\gamma\gamma} \geq 450 \text{ GeV}$  the cross-sections for  $\gamma\gamma \rightarrow hh$  in the SM and the

THDM are dominant contrasted to the ones for  $\gamma\gamma \rightarrow hH$ ,  $HH$  in the THDM. Among the mentioned cross-sections, the  $hh$  production in the THDM is largest in this case.

When  $M^2 = 200^2 \text{ GeV}^2$ , the cross-sections for  $HH$  productions in THDM become largest in comparison with other ones. These massive contributions are attributed from charged Higgs propagating in the loop of one-loop triangle with  $\phi_k^*$ -poles as well as one-loop box diagrams. Due to the  $Z_2$ -symmetry, the productions of  $hH$  in the THDM are still suppressed in this case. For high regions of  $M^2$ , taking  $M^2 = 500^2, 700^2 \text{ GeV}^2$  as examples, the productions  $\gamma\gamma \rightarrow hH$ ,  $HH$  are more and more dominant in comparison with  $hh$  production in the SM and in the THDM.

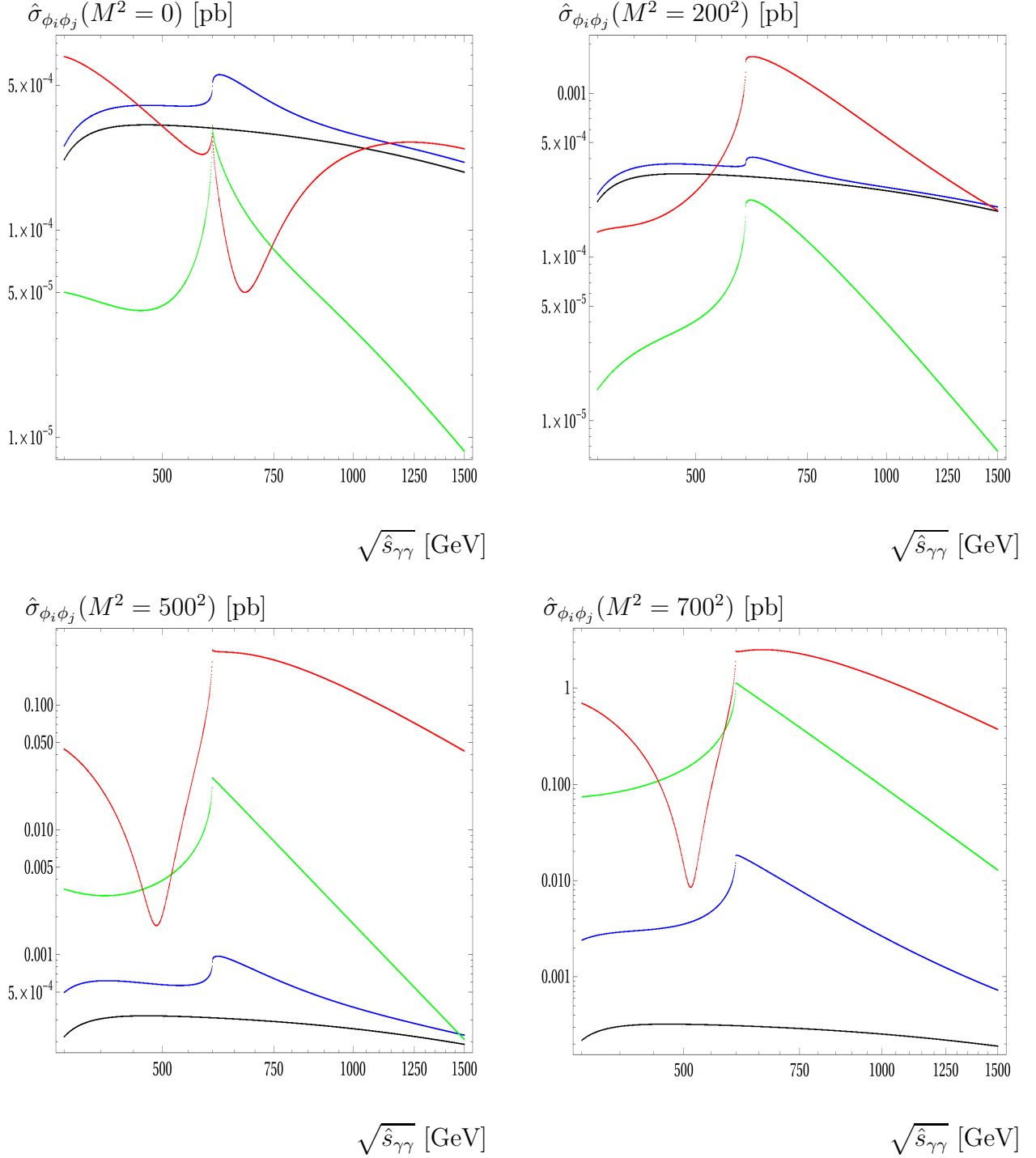


Figure 13: Total cross-sections for  $\gamma\gamma \rightarrow hh, hH, HH$  in the SM and the THDM are shown as functions of  $E_{\gamma\gamma}$ . In the plots, we vary  $350 \text{ GeV} \leq \sqrt{\hat{s}_{\gamma\gamma}} \leq 1500 \text{ GeV}$ . We select  $M_{H\pm} = 300 \text{ GeV}$ ,  $t_\beta = 5$  in this case. Moreover, we fix  $M_H = 150 \text{ GeV}$ ,  $M^2 = 0, 200^2, 500^2, 700^2 \text{ GeV}^2$  and take  $c_{\beta-\alpha} = +0.2$  and  $s_{\beta-\alpha} = +\sqrt{1 - c_{\beta-\alpha}^2}$ , accordingly.

### Fermionphobic limit

The fermionphobic limit in which the mixing angle  $\alpha = \pm\pi/2$  is studied in this case. For a typical example, we take  $\alpha = +\pi/2$  in the following plots. Since, we checked that top quark propagating in the loop is dominant contributions versus other fermions. It is enough to take

top quark in the loop for this calculation. It means that the cross-sections are contributed from  $W$  boson and scalar particles exchanging in the loop once we consider the results in the fermionphobic limit. Subsequently, we can examine the comparative sizes among these contributions. In Fig. 14 (for  $hh$  production), Fig. 15 (for  $hH$  production), Fig. 16 (for  $HH$  production), the corresponding cross-sections for  $\gamma\gamma \rightarrow hh$ ,  $hH$ ,  $HH$  in the THDM together with  $\hat{\sigma}_{\gamma\gamma \rightarrow hh}$  production in the SM as functions of center-of-mass energy  $E_{\gamma\gamma}$ , are studied in the fermionphobic limit. In the plots, we vary  $350 \text{ GeV} \leq E_{\gamma\gamma} \leq 1500 \text{ GeV}$ . We select  $M_{H^\pm} = 300 \text{ GeV}$ ,  $t_\beta = 3$  (blue line),  $t_\beta = 5$  (green line),  $t_\beta = 7$  (red line), respectively for all cases. Moreover, we fix  $M_H = 150 \text{ GeV}$ ,  $M^2 = 0 \text{ GeV}^2$  (for all the left Figures),  $M^2 = +200^2 \text{ GeV}^2$  (for all the right Figures).

The  $hh$  productions in the SM and the THDM at  $M^2 = 0 \text{ GeV}^2$  are first analysed. We notice that the cross-sections depend slightly to  $t_\beta$  in the regions below the peak  $E_{\gamma\gamma} \sim 2M_{H^\pm} = 600 \text{ GeV}$  (they are larger than the ones in the SM in this case). In the regions above the peak, it is found that the cross-sections are more sensitive to  $t_\beta$ . For the case of  $M^2 = 200^2 \text{ GeV}^2$ , the cross-sections are proportional to  $t_\beta$ . They develop to the peak  $\sim 600 \text{ GeV}$  and decreased rapidly beyond the peak. Around the peak region, the cross-sections are enhanced due to the dominant contribution from charged Higgs in the loop.

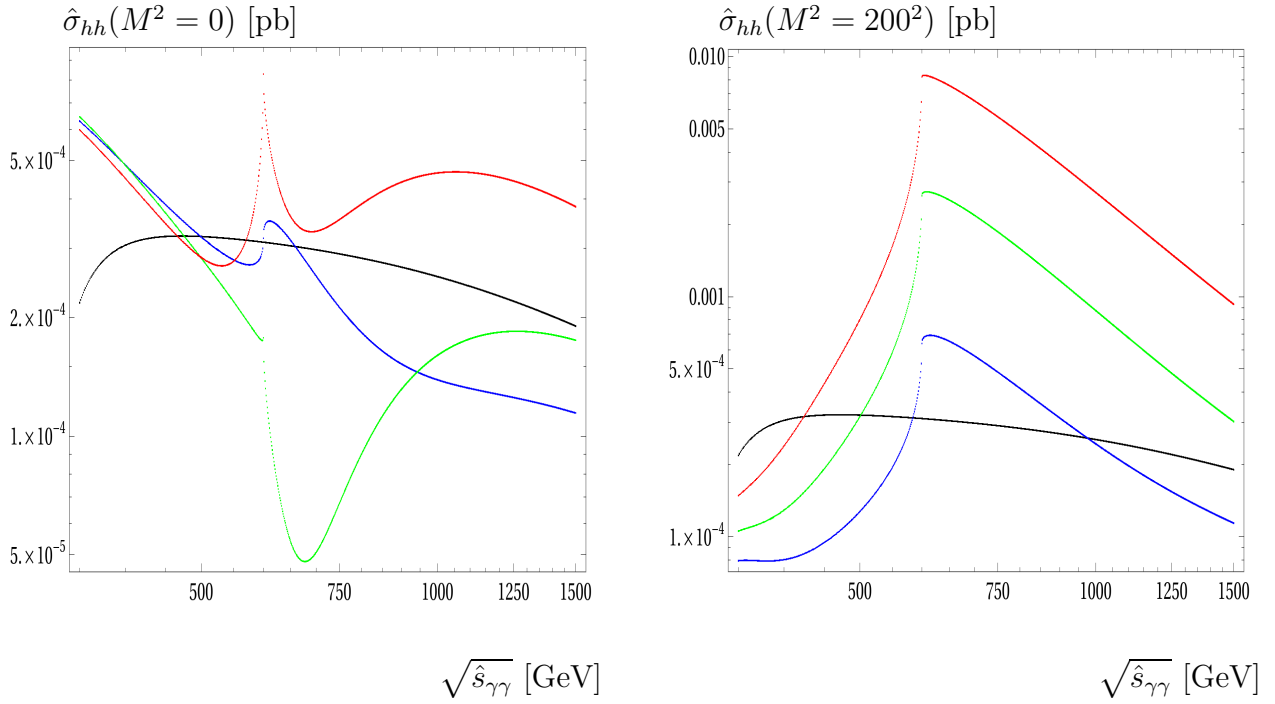


Figure 14: Total cross-sections for  $\gamma\gamma \rightarrow hh$  in the SM and the THDM as functions  $\sqrt{\hat{s}_{\gamma\gamma}}$  are shown in the fermionphobic limit. In the plots, we change  $350 \text{ GeV} \leq \sqrt{\hat{s}_{\gamma\gamma}} \leq 1500 \text{ GeV}$ . We select  $M_{H^\pm} = 300 \text{ GeV}$ ,  $t_\beta = 5$  in this case. Moreover, we fix  $M_H = 150 \text{ GeV}$ ,  $M^2 = 0 \text{ GeV}^2$  (for the left panel),  $M^2 = +200^2 \text{ GeV}^2$  (for the right panel) and take  $\alpha = +\pi/2$  accordingly.

As mentioned in above, the cross-sections for  $hH$  productions in the THDM are suppressed due to the soft symmetry breaking of  $Z_2$ . It is reasonable for cross-sections for  $hH$  productions are much smaller than the corresponding ones for  $hh$  productions in the SM. However, at the peak of  $\sqrt{\hat{s}_{\gamma\gamma}} = 2M_{H^\pm} = 600 \text{ GeV}$ , the cross-sections are enhanced and can reach to the order of the cross sections for  $hh$  production in the SM. At  $M^2 = 0$ ,  $\hat{\sigma}_{\gamma\gamma \rightarrow hH}$  are more sensitive to  $t_\beta$  in

all range of CoM. Another case of  $M^2 = +200^2 \text{ GeV}^2$ , the cross-sections are also more sensitive to  $t_\beta$  in the regions below the peak  $\sim 600 \text{ GeV}$ . But they are nearly proportional to  $t_\beta$  beyond the peak.

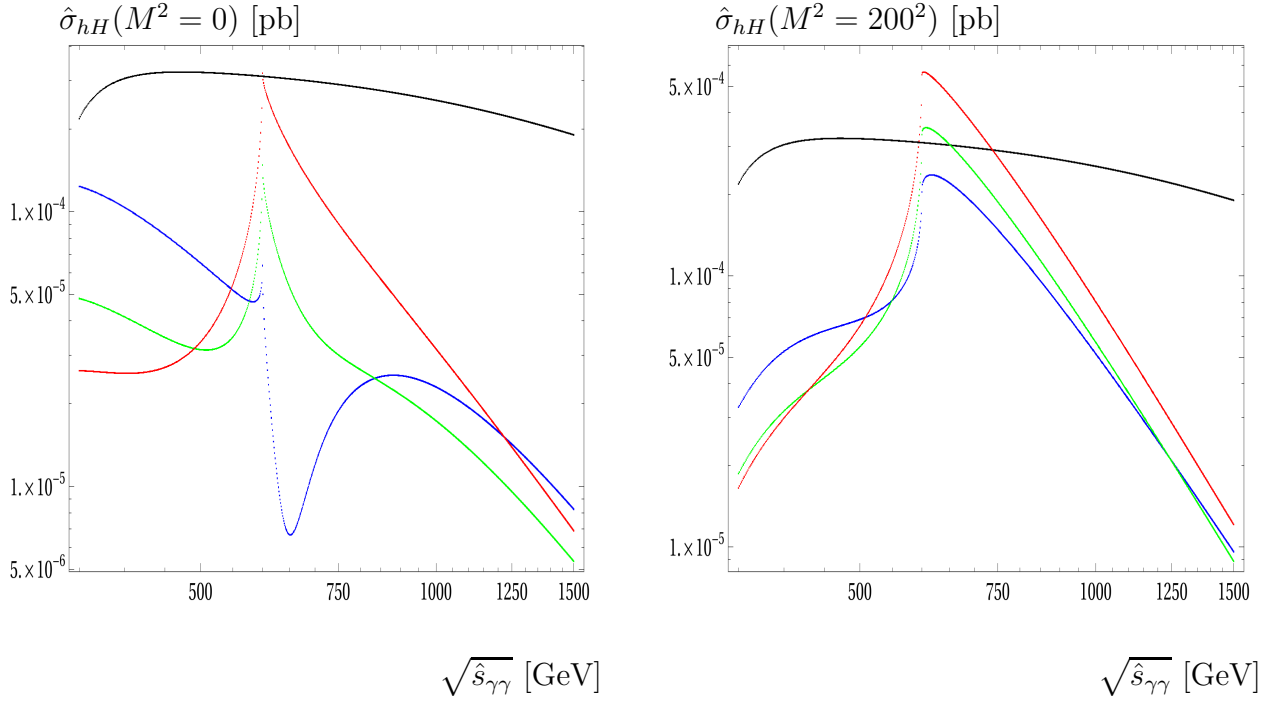


Figure 15: Total cross-sections for  $\gamma\gamma \rightarrow hH$  in the SM and the THDM as functions  $\sqrt{\hat{s}_{\gamma\gamma}}$  in the fermionphobic limit. In the plots, we vary  $350 \text{ GeV} \leq \sqrt{\hat{s}_{\gamma\gamma}} \leq 1500 \text{ GeV}$ . We select  $M_{H^\pm} = 300 \text{ GeV}$ ,  $t_\beta = 5$  in this case. Moreover, we fix  $M_H = 150 \text{ GeV}$ ,  $M^2 = 0 \text{ GeV}^2$  (for the left panel),  $M^2 = +200^2 \text{ GeV}^2$  (for the right panel) and take  $\alpha = +\pi/2$  accordingly.

For all cases of  $M^2$  in  $HH$  productions in the THDM, it is interested in finding that the cross-sections are larger than  $hh$  productions in the SM and they are proportional to  $1/t_\beta$  for all range of CoM. It is stress that the cross-sections are enhanced around the peak  $\sim 2M_{H^\pm} = 600 \text{ GeV}$ . These dominant contributions are from the singly charged Higgs exchanging in the loop.

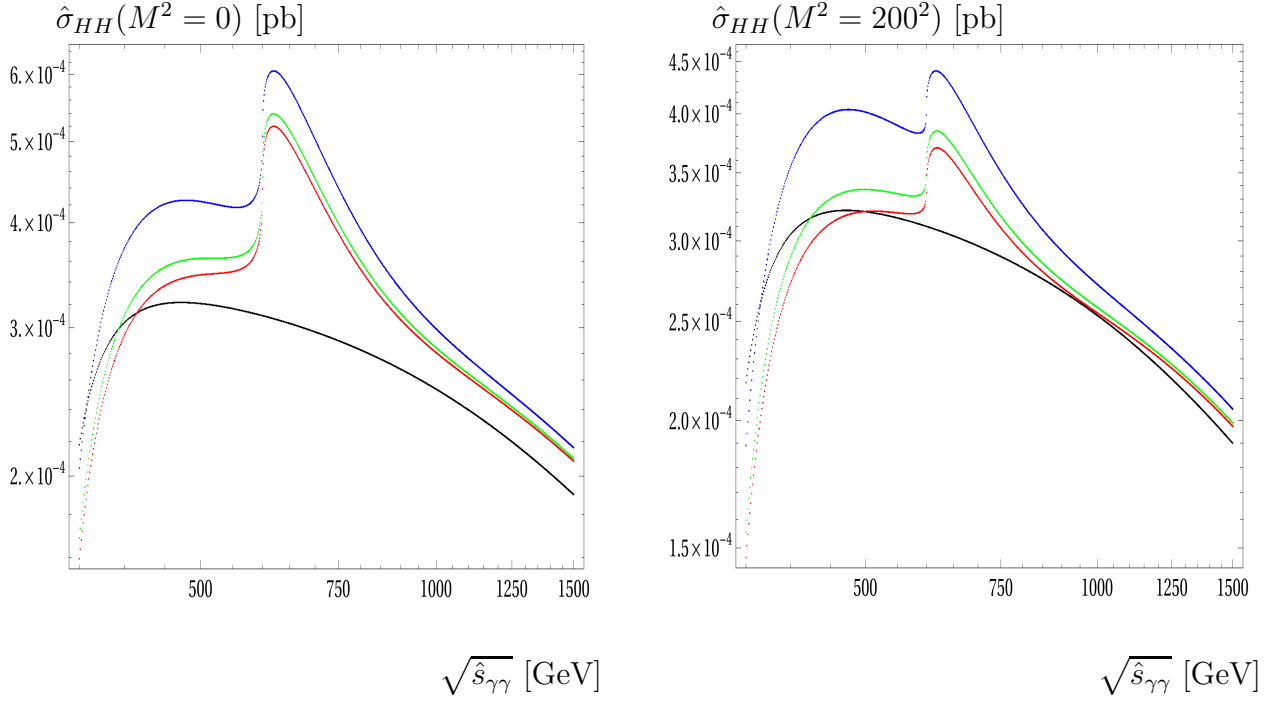


Figure 16: Total cross-sections for  $\gamma\gamma \rightarrow HH$  in the SM and THDM as functions of  $\sqrt{\hat{s}_{\gamma\gamma}}$  in the fermionphobic limit. In the plots, we vary  $350 \text{ GeV} \leq \sqrt{\hat{s}_{\gamma\gamma}} \leq 1500 \text{ GeV}$ . We select  $M_{H^\pm} = 300 \text{ GeV}$ ,  $t_\beta = 5$  in this case. Moreover, we fix  $M_H = 150 \text{ GeV}$ ,  $M^2 = 0 \text{ GeV}^2$  (in the left panel),  $M^2 = +200^2 \text{ GeV}^2$  (in the right panel) and take  $\alpha = +\pi/2$  accordingly.

### Decoupling limit

We next study the decoupling limit in which the mixing angle is taken as  $\beta - \alpha = \pi/2$ . In Fig. 17 ( $hh$  production), Fig. 18 ( $hH$  production), Fig. 19 ( $HH$  production), total cross-sections for  $\gamma\gamma \rightarrow hh$ ,  $hH$ ,  $HH$  for the THDM together with  $\gamma\gamma \rightarrow hh$  in the SM, as functions of CoM energy  $E_{\gamma\gamma}$  are examined in the decoupling limit. In the Figures 17, the cross-sections for  $hh$  productions in the decoupling limit are investigated at  $M^2 = 0 \text{ GeV}^2$  (left panel scatter plots) and at  $M^2 = 200 \text{ GeV}^2$  (right panel scatter plots). The CoM energy is varied as  $350 \text{ GeV} \leq E_{\gamma\gamma} \leq 1500 \text{ GeV}$ . We select  $M_\Phi = M_H = M_{A^0} = M_{H^\pm} = 300 \text{ GeV}$  (blue line),  $400 \text{ GeV}$  (green line),  $500 \text{ GeV}$  (red line) and set  $t_\beta = 5$  in all cases. In both cases, cross-sections  $\hat{\sigma}_{\gamma\gamma \rightarrow hh}$  have the peaks at  $\sqrt{\hat{s}_{\gamma\gamma}} = 2M_{H^\pm} = 600, 800, 1000 \text{ GeV}$ . They develop to the peaks and are decreased rapidly beyond the peaks. Furthermore,  $\hat{\sigma}_{\gamma\gamma \rightarrow hh}$  in the THDM are larger than the corresponding cross-sections in the SM. It is explained that the charged Higgs loop contributions being significant contributions once  $M_\Phi$  being large. At  $M^2 = 0 \text{ GeV}^2$ , it is seen that cross-sections depend on  $1/M_\Phi$  in the regions below the peaks and are proportional to  $M_\Phi$  in the regions above the peak. When  $M^2 = 200 \text{ GeV}^2$ , we find clearly that cross-sections are proportional to  $M_\Phi$ .

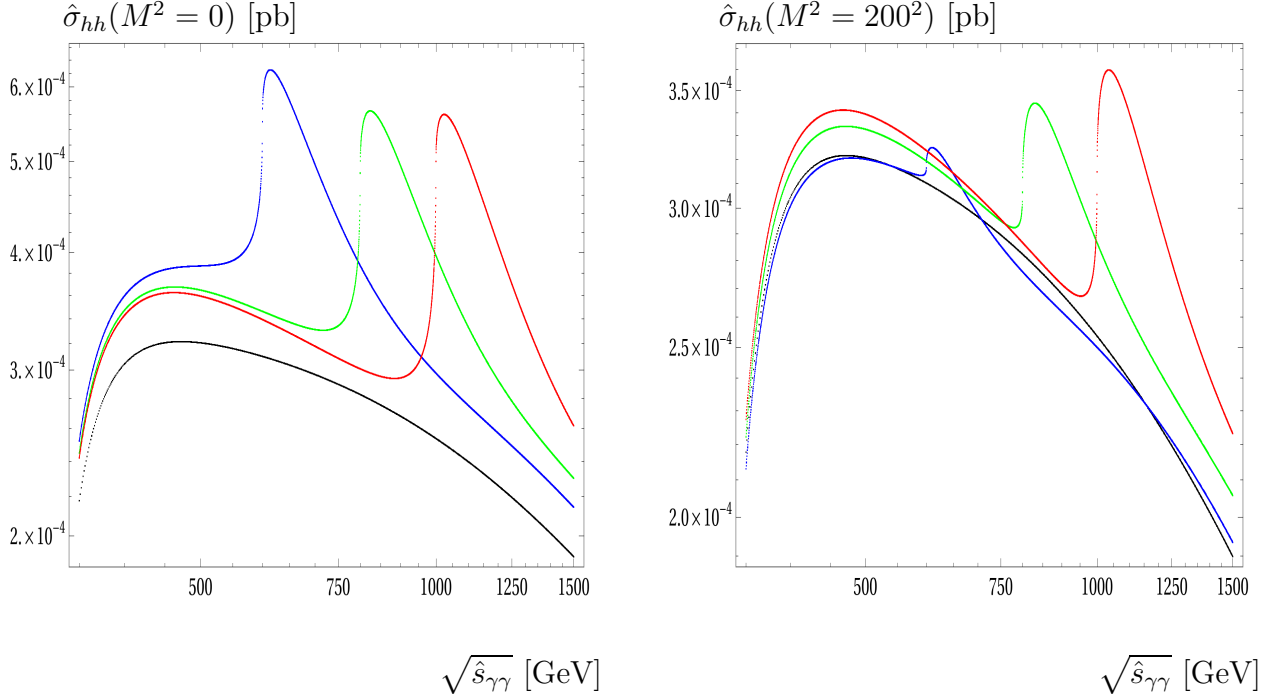


Figure 17: Total cross-sections for  $\gamma\gamma \rightarrow hh$  in the SM and THDM as functions of  $\sqrt{\hat{s}_{\gamma\gamma}}$  are shown in the decoupling limit. In the plots, we vary  $350 \text{ GeV} \leq \sqrt{\hat{s}_{\gamma\gamma}} \leq 1500 \text{ GeV}$ . We select  $M_\Phi = M_H = M_{A^0} = M_{H^\pm} = 300, 400, 500 \text{ GeV}$ ,  $t_\beta = 5$  in this case. In further, we fix  $M^2 = 200^2 \text{ GeV}^2$  and  $\beta - \alpha = \pi/2$ , accordingly.

For the productions of  $hH$ ,  $HH$  in the THDM in the decoupling limit, it is important to note that we take  $M_H = 150 \text{ GeV}$  and  $M_\Phi = M_{H^\pm} = 300, 400, 500 \text{ GeV}$  in these cases. Other parameters are set as in the previous case. It is not surprised that the cross-sections for  $hH$  in the THDM are suppressed because of the soft-breaking of the  $Z_2$ -symmetry. For the  $HH$  productions at  $M^2 = 0$ , the cross-sections are greater than the  $hh$  productions in the SM in the below of the peak regions. But they are decreased rapidly and become smaller than the ones for  $hh$  productions in the SM. For the  $HH$  productions at  $M^2 = 200 \text{ GeV}^2$ , the cross-sections are greater than  $hh$  productions in the SM in the most of the range of CoM.

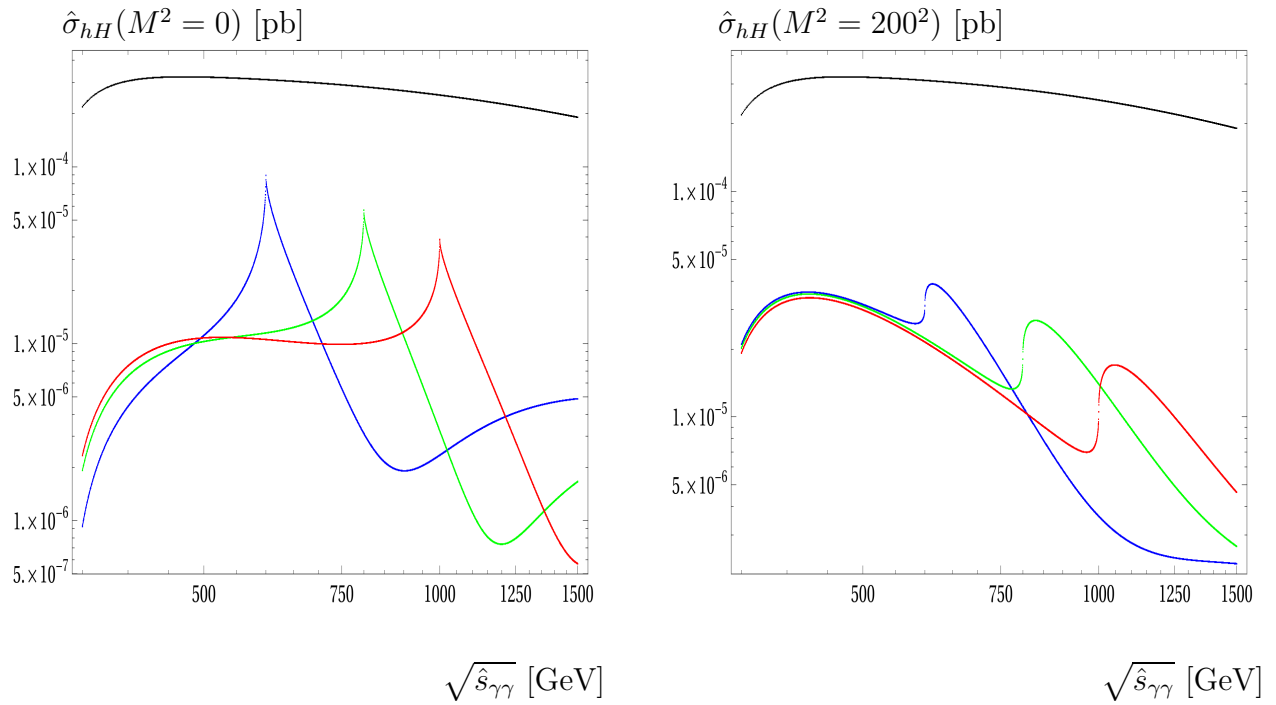


Figure 18: Total cross-sections for  $\gamma\gamma \rightarrow hH$  in the SM and THDM as functions of  $\sqrt{\hat{s}_{\gamma\gamma}}$  are shown in the decoupling limit. In the plots, we vary  $350 \text{ GeV} \leq \sqrt{\hat{s}_{\gamma\gamma}} \leq 1500 \text{ GeV}$ . We note that  $M_\Phi = M_{H^\pm} = 300, 400, 500 \text{ GeV}$  in these cases.

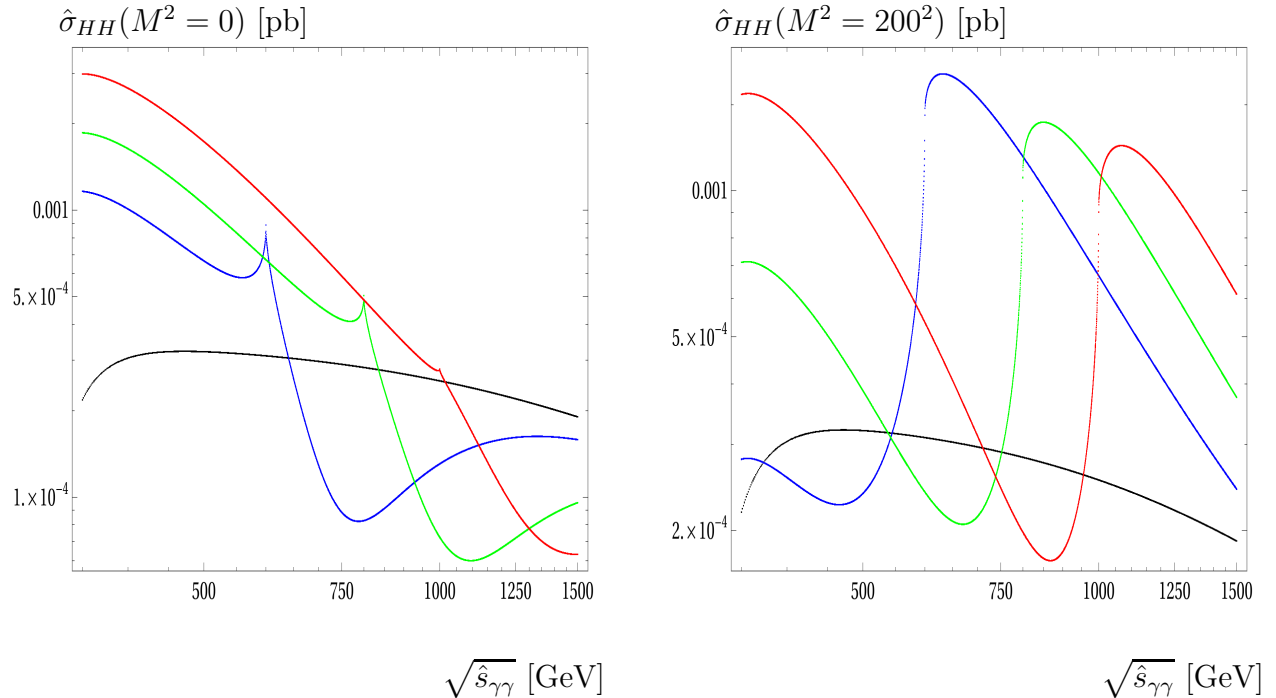


Figure 19: Total cross-sections for  $\gamma\gamma \rightarrow HH$  in the SM and THDM as functions of center-of-mass energy  $\sqrt{\hat{s}_{\gamma\gamma}}$  are shown in the decoupling limit. In the plots, we vary  $350 \text{ GeV} \leq \sqrt{\hat{s}_{\gamma\gamma}} \leq 1500 \text{ GeV}$ . We note that  $M_\Phi = M_{H^\pm} = 300, 400, 500 \text{ GeV}$  in these cases.

#### 4.2.2. Enhancement factors

We pay attention to investigate the enhancement factors defined in Eq. 53 for  $\gamma\gamma \rightarrow \phi_i\phi_j$  with CP-even Higgses  $\phi_{i,j} \equiv h, H$  within the framework of the THDM. The factors scanned over parameter space of  $M_{H^\pm}$ ,  $t_\beta$  are first studied in this subsection. Two scenarios for  $c_{\beta-\alpha} > 0$  and  $c_{\beta-\alpha} < 0$  are examined in detail. In Figs. 20, 21, we fix  $M^2 = M_H^2 = 200^2 \text{ GeV}^2$ . Moreover, we vary  $100 \text{ GeV} \leq M_{H^\pm} \leq 1000 \text{ GeV}$  and set  $2 \leq t_\beta \leq 10$  in the following plots. In all the above-scatter plots,  $\mu_{\phi_i\phi_j}^{\text{THDM}}$  are generated at  $E_{\gamma\gamma} = 500 \text{ GeV}$  (for the above-plots). While in all the below-scatter plots, the factors are examined at  $E_{\gamma\gamma} = 1000 \text{ GeV}$  (for the above-plots). In the left panel, we show for the enhancement factors for  $hh$  productions. In the middle (right) panel, the enhancement factors for  $hH$ , ( $HH$ ) productions are presented, respectively.

In Fig. 20, the first scenario for  $c_{\beta-\alpha} > 0$  is explored. In this scenario, we take  $c_{\beta-\alpha} = +0.2$  for an example and  $s_{\beta-\alpha} = +\sqrt{1 - c_{\beta-\alpha}^2}$ , correspondingly. At  $E_{\gamma\gamma} = 500 \text{ GeV}$ , the factors  $\mu_{hh}^{\text{THDM}}$  change from 1 to 1.5 for all range of charged Higgs mass. The values of  $\mu_{hh}^{\text{THDM}}$  are enhanced around the peak at  $M_H^\pm = E_{\gamma\gamma}/2 = 250 \text{ GeV}$ . Predominantly, the factors are proportional to  $t_\beta^{-1}$  in this case. Interestingly, we observe that the factors  $\mu_{hH}^{\text{THDM}}$  change from 0 to 0.5 for all range of charged Higgs mass. The suppressed values of  $\mu_{hH}^{\text{THDM}}$  are expected as explained in previous paragraphs due to the  $Z_2$ -symmetry. The  $\mu_{hH}^{\text{THDM}}$  are the same behavior as  $\mu_{hh}^{\text{THDM}}$  which they are inversely proportional to  $t_\beta$ . In the other hand, the enhancement factors for  $HH$  productions in the THDM are strongly dependent of the charged Higgs mass but change slightly with  $t_\beta$ . In all range of  $M_H^\pm$ , the factors  $\mu_{HH}^{\text{THDM}}$  are from 0.3 to 1.2.

At  $E_{\gamma\gamma} = 1000 \text{ GeV}$ , the factors  $\mu_{hh}^{\text{THDM}}$  become biggest at the peak at  $M_H^\pm = E_{\gamma\gamma}/2 = 500 \text{ GeV}$ . Around the peak,  $\mu_{hh}^{\text{THDM}}$  change from 1.2 to 1.8. Beyond the peak, the factors vary from 1.0 to 1.2 in all range of charged Higgs mass. It is stress that  $\mu_{hh}^{\text{THDM}}$  slightly change with  $t_\beta$ . For  $HH$  productions,  $\mu_{HH}^{\text{THDM}}$  are vary from 0.4 to 2.5 (around the peak at  $M_{H^\pm} = 500 \text{ GeV}$ ). We also find that  $\mu_{HH}^{\text{THDM}}$  slightly change with  $t_\beta$ . Otherwise,  $\mu_{hH}^{\text{THDM}}$  are much smaller than 1 and are inversely proportional to  $t_\beta$ .

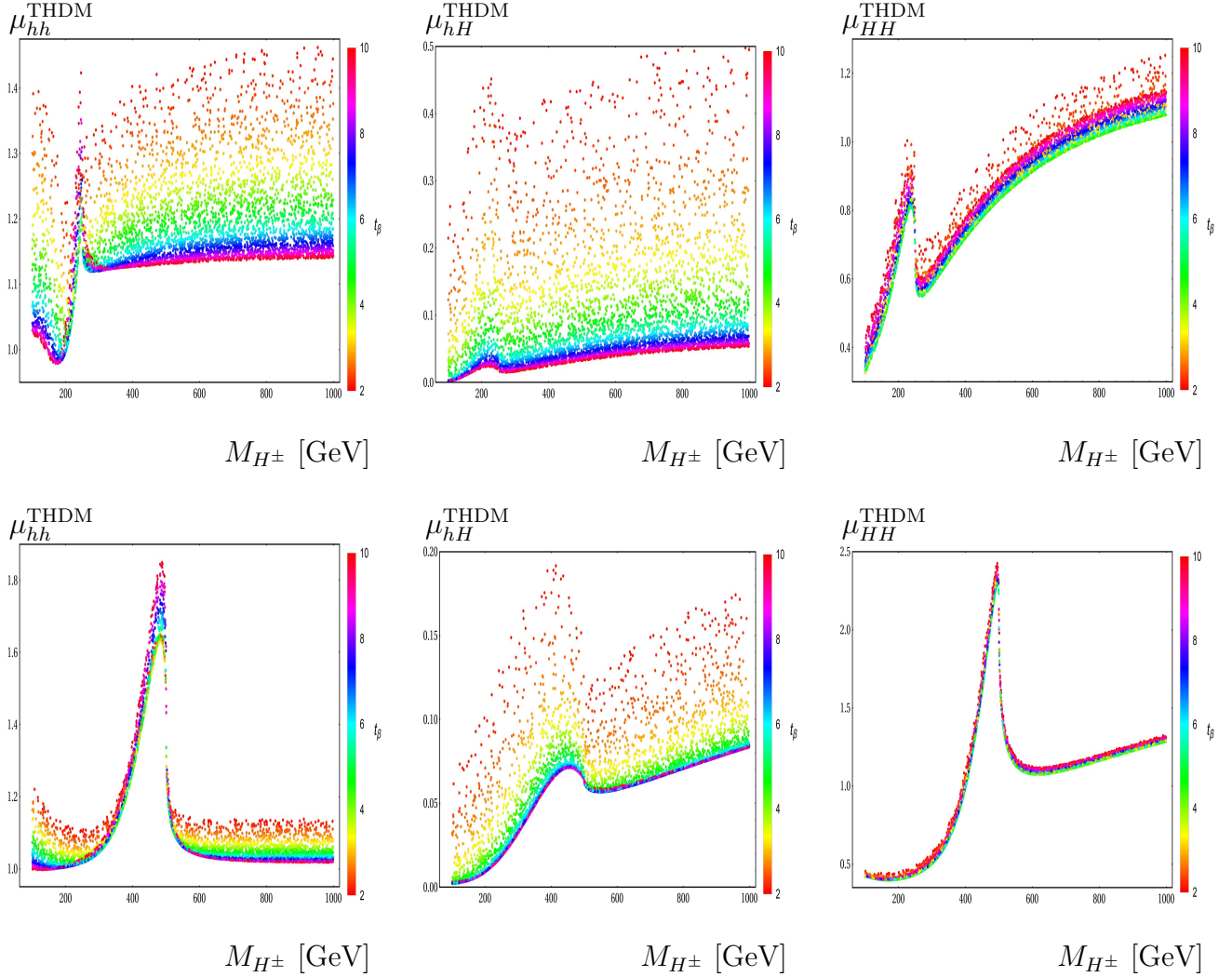


Figure 20: The enhancement factors are presented in the parameter space of  $M_{H^\pm}$ ,  $t_\beta$ . In the plots, we fix  $M^2 = M_H^2 = 200^2$  GeV<sup>2</sup> and we take  $c_{\beta-\alpha} = +0.2$  and  $s_{\beta-\alpha} = +\sqrt{1 - c_{\beta-\alpha}^2}$ , accordingly. In these plots we set  $E_{\gamma\gamma} = 500$  (for the above-plots) GeV and  $E_{\gamma\gamma} = 1000$  GeV (for the below plots), respectively.

Another scenario for  $c_{\beta-\alpha} < 0$  is considered for examining how are the factors effect by setting different sign of  $c_{\beta-\alpha}$  in this work. In Fig. 21, we take  $c_{\beta-\alpha} = -0.2$  for an example and  $s_{\beta-\alpha} = +\sqrt{1 - c_{\beta-\alpha}^2}$ , accordingly. At  $E_{\gamma\gamma} = 500$  GeV, it is excited in observing that  $\mu_{hh}^{THDM}$  are different behavior in comparison with previous scenario. At this CoM energy, the factors  $\mu_{hh}^{THDM}$  can reach to 1.5 in the low region of  $M_{H^\pm} < 200$  GeV. They then are decreased to around 0.9 when  $M_{H^\pm} > 200$  GeV. There isn't peak of the factors observed in this scenario. Because the contributions of singly charged Higgs in triangle diagrams with  $\phi_k^*$ -poles may be cancelled out with the corresponding ones from one-loop charged Higgs box diagrams in this scenario. Surprisingly, we find that the factors  $\mu_{hh}^{THDM}$  are proportional to  $t_\beta$  in this scenario. For the  $hH$  productions, the factors are suppressed and they are in the range of  $[\sim 0.025, \sim 0.3]$ . They are sensitive with  $t_\beta^{-1}$  in all range of charged Higgs mass. In  $HH$  productions, it is found that the factors develop to the peak around  $M_{H^\pm} = 500$  GeV. They reach to factor 2.5 around the peak and the are in the ranges of  $[\sim 0.5, \sim 1.7]$  beyond the peak. In all range of charged Higgs mass, the factors  $\mu_{HH}^{THDM}$  are proportional to  $t_\beta^{-1}$  in this scenario.

The survey for all the enhancement factors at  $E_{\gamma\gamma} = 1000$  GeV are concerned in the next

paragraphs. The factors  $\mu_{hh}^{\text{THDM}}$  are large in the regions ( $M_{H^\pm} \leq 200$  GeV) and they can reach to 1.5. They then are decreased rapidly to  $M_{H^\pm} \sim 300$  GeV and develop to the peak  $M_{H^\pm} = E_{\gamma\gamma}/2 = 500$  GeV. Around the peak, the enhancement factor is about 1.2. In other ranges of charged Higgs mass,  $\mu_{hh}^{\text{THDM}} \sim 0.9$ . One also finds that  $\mu_{hh}^{\text{THDM}}$  is inversely proportional to  $t_\beta$  in this scenario. In  $hH$  productions, the factors are increased to the peak  $M_{H^\pm} = E_{\gamma\gamma}/2 = 500$  GeV and they are about 0.3 around the peak. In all regions of  $M_{H^\pm}$ , the mentioned factors are in the ranges of  $[\sim 0.025, \sim 0.3]$  and they are inversely proportional to  $t_\beta$ . In the last case, it is found that the factors  $\mu_{HH}^{\text{THDM}}$  are same behavior as previous scenario. They are in the ranges of  $[\sim 0.5, \sim 4]$  in all regions of  $M_{H^\pm}$ . However, the factors  $\mu_{HH}^{\text{THDM}}$  depend slightly on  $t_\beta$  in this scenario.

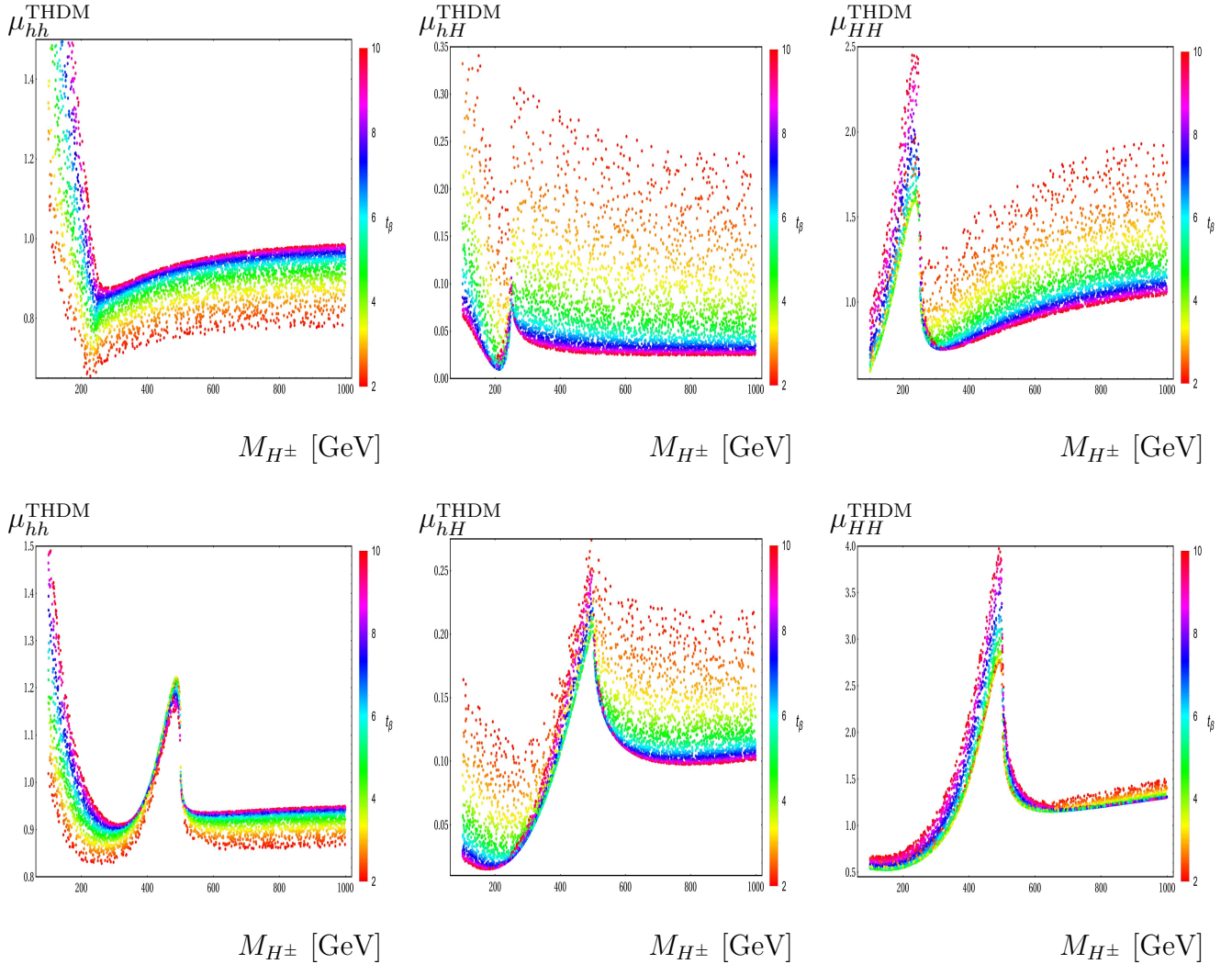


Figure 21: The enhancement factors are presented in the parameter space  $M_{H^\pm}$ ,  $t_\beta$ . In the plots, we consider the scenario for  $c_{\beta-\alpha} = -0.2 < 0$  and  $s_{\beta-\alpha} = +\sqrt{1 - c_{\beta-\alpha}^2}$ , correspondingly. We also fix  $M^2 = M_H^2 = 200^2$  GeV<sup>2</sup> and set  $E_{\gamma\gamma} = 500$  (for all the above-plots) GeV and  $E_{\gamma\gamma} = 1000$  GeV (for all the below-plots).

The enhancement factors scanned over the parameter space of  $M_{H^\pm}$ ,  $M^2$  in the THDM are also interested greatly in this work. Two scenarios for  $c_{\beta-\alpha} > 0$  and  $c_{\beta-\alpha} < 0$  are studied in detail in the following paragraphs. In Fig. 22 (for  $c_{\beta-\alpha} > 0$  scenario), Fig. 23 (for  $c_{\beta-\alpha} < 0$  scenario), we take  $t_\beta = 5$  and  $E_{\gamma\gamma} = 500$  GeV (for all the above scatter plots) and  $E_{\gamma\gamma} = 1000$  GeV (for

all the below scatter plots). Moreover, we vary charged Higgs mass as  $100 \text{ GeV} \leq M_{H^\pm} \leq 1000 \text{ GeV}$  and the soft-breaking parameter as  $0 \text{ GeV}^2 \leq M^2 \leq 200^2 \text{ GeV}^2$ .

In Fig. 22, the first scenario of  $c_{\beta-\alpha} > 0$  is examined. For this case, we take  $c_{\beta-\alpha} = +0.2$  as an example and  $s_{\beta-\alpha} = +\sqrt{1 - c_{\beta-\alpha}^2}$ , accordingly. For  $hh$  production at  $E_{\gamma\gamma} = 500 \text{ GeV}$ , we observe the peak of  $\mu_{hh}^{\text{THDM}}$  at  $M_{H^\pm} = 250 \text{ GeV}$  which is corresponding to the threshold of cross-sections  $hh$  in the THDM at the peak  $E_{\gamma\gamma} = 2M_{H^\pm}$ . Around the peak,  $\mu_{hh}^{\text{THDM}}$  are varied from 1.0 to 1.8. Above the peak, the enhancement factors tend to 1.2 and depend slightly on  $M^2$ . For  $hH$  productions, in below the peak regions,  $\mu_{hH}^{\text{THDM}}$  are more sensitive with  $M^2$ . The factors are in the ranges of  $[0.07, 1.5]$  in above the peak regions. Around the peak,  $\mu_{hH}^{\text{THDM}}$  can reach to 0.3. We also find the same behavior for  $\mu_{HH}^{\text{THDM}}$ . The factors for  $HH$  productions are large in the low regions of  $M_{H^\pm}$  and around the peak  $M_{H^\pm} = 250 \text{ GeV}$ . They are in the ranges of  $[0.7, 2.4]$  in the above the peak regions. Generally, we observe that all factors are proportional to  $1/M$  at this CoM energy.

At  $E_{\gamma\gamma} = 1000 \text{ GeV}$ , we also find that  $\mu_{hh}^{\text{THDM}}$  develop to the peak at  $M_{H^\pm} = 500 \text{ GeV}$  where the factors can reach to 2.2, they are decreased rapidly beyond the peak. The factors depend slightly on  $M^2$  and tend to 1 for above and below the peak regions. For  $hH$  productions, the enhancement factors are sensitive with  $M^2$  in the peak regions. They tend to 0.05 and they are slightly dependent of  $M^2$  in the above the peak regions. For  $HH$  productions, the factors become large in the below the peak regions and they are inversely proportional to  $M^{-1}$ . Around the peak, the factors are enhanced by large values of  $M^2$ . Above the peak regions,  $\mu_{HH}^{\text{THDM}}$  are varied around 1.0.

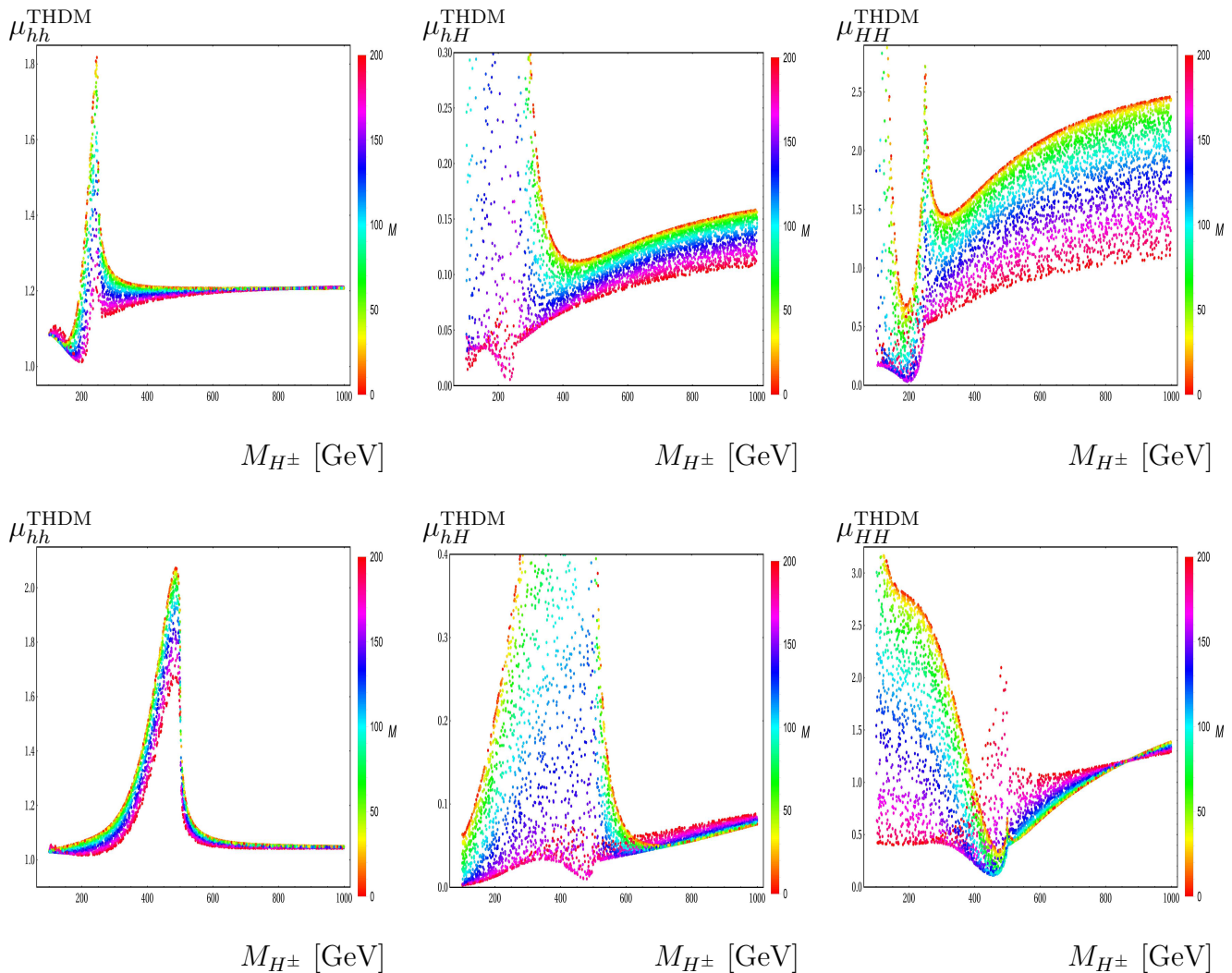


Figure 22: The enhancement factors are presented in the parameter space of  $M_{H^\pm}$ ,  $M^2$ . In the plots, we take  $t_\beta = 5$  and consider the first scenario of  $c_{\beta-\alpha} = +0.2$  and  $s_{\beta-\alpha} = +\sqrt{1 - c_{\beta-\alpha}^2}$ , accordingly. In these plots, we set  $E_{\gamma\gamma} = 500$  GeV (for the above Figures) and  $E_{\gamma\gamma} = 1000$  GeV (for the below Figures).

Another scenario for  $c_{\beta-\alpha} = -0.2 < 0$  is also concerned interestingly in this work. In Fig. 23,  $s_{\beta-\alpha} = +\sqrt{1 - c_{\beta-\alpha}^2}$  is obtained accordingly. We are going to comment on physical results at  $E_{\gamma\gamma} = 500$  GeV. For  $hh$  productions, we observe different behavior of  $\mu_{hh}^{THDM}$  in comparison with the  $c_{\beta-\alpha} > 0$  scenario. In concrete, the factors are large in below the peak regions. Around the peak, they are enhanced by the small value of  $M$  and can reach to 1.6. Above the peak regions, the factors are in the ranges of  $[0.9, 1.1]$ . It is inspired in finding the different behavior for the factors in  $hH$  productions in comparison with the previous scenario. The factors  $\mu_{hH}^{THDM}$  get the large values in the below and around the peak regions and they are enhanced by the large values of  $M$ . They are in the ranges of  $[0.2, 0.6]$  for above the peak regions. In the case of  $HH$  productions,  $\mu_{HH}^{THDM}$  develop to the peak. They are in the range of  $[1.0, 2.4]$  in above the peak regions. In general, the factors  $\mu_{HH}^{THDM}$  depend slightly on charged Higgs mass and are proportional to  $1/M$  in above the peak regions.

We next comment on physical results at  $E_{\gamma\gamma} = 1000$  GeV. The factors  $\mu_{hh}^{THDM}$  are enhanced by the small values of  $M$  in low regions of charged Higgs mass and they can reach 1.2. They tend to 2.5 around the peak. The factors are then varied around  $\sim 0.9$ . In general, the factors depend

on  $M^{-1}$ . In the productions  $hH$ ,  $\mu_{hH}^{\text{THDM}}$  are more sensitive to  $M^{-1}$  around the peak regions. They then tend to 0.2 in the high mass regions of singly charged Higgs. For  $HH$  productions, the factors  $\mu_{HH}^{\text{THDM}}$  strongly depend on  $M^{-1}$ . At the peak, the factors are enhanced by the large value of  $M$ . Above the peak regions,  $\mu_{HH}^{\text{THDM}}$  tend to  $\sim 1$ .

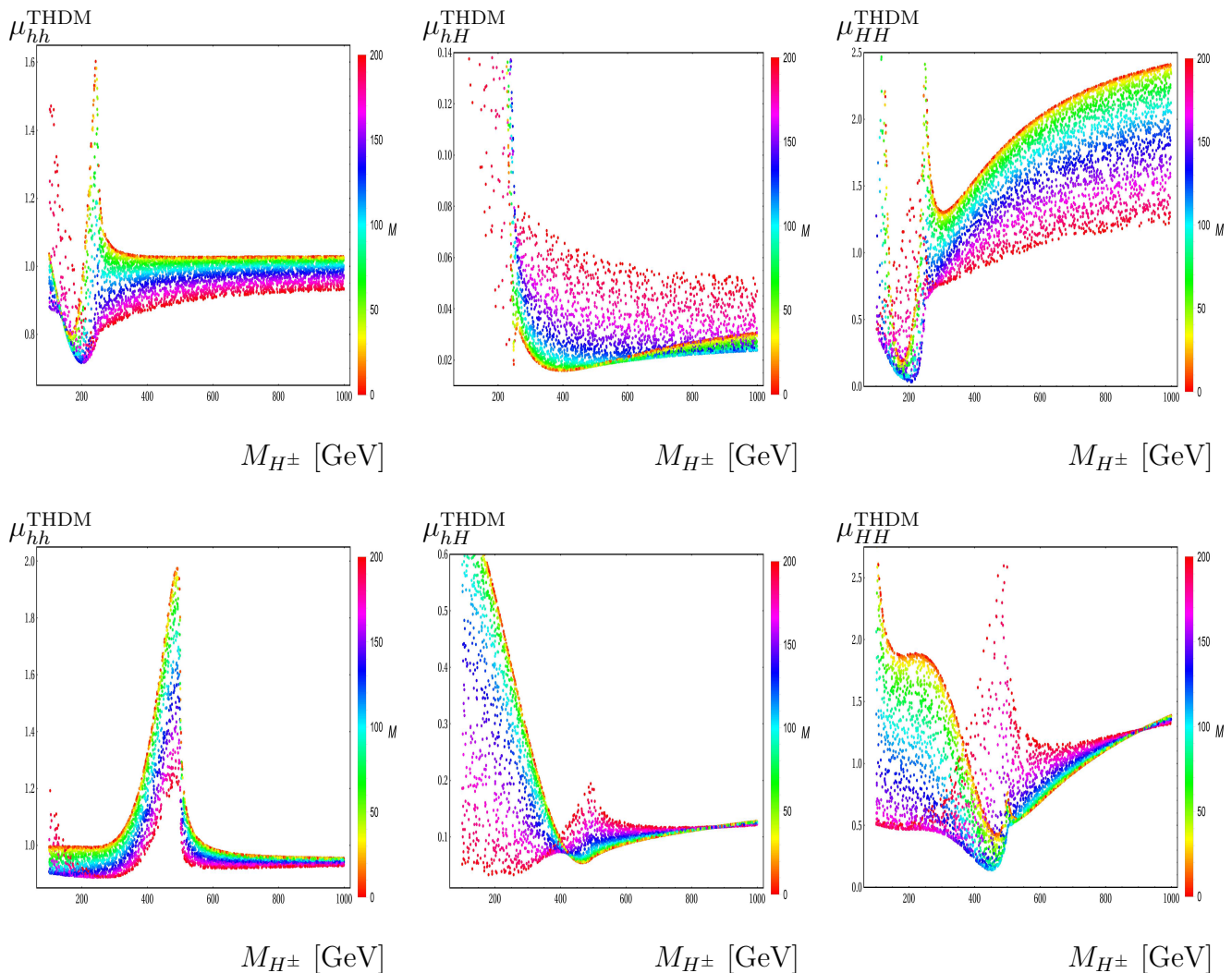


Figure 23: The enhancement factors are presented in the parameter space of  $M_{H^\pm}$ ,  $M^2$ . In the plots, we take  $t_\beta = 5$  and  $c_{\beta-\alpha} = -0.2$  and  $s_{\beta-\alpha} = +\sqrt{1 - c_{\beta-\alpha}^2}$ , accordingly. In these plots, we set  $E_{\gamma\gamma} = 500$  GeV (the above Figures) and  $E_{\gamma\gamma} = 1000$  GeV (the below Figures).

## 5. Conclusions

We have presented one-loop corrections to  $\gamma\gamma \rightarrow \phi_i\phi_j$  with CP-even Higgses  $\phi_{i,j} \equiv h, H$  within the framework of the HESM, considering the Two Higgs Doublet Models and the Inert Higgs Doublet Models in this work. Analytic results are expressed in terms of the scalar PV-functions following the standard conventions of the packages `LoopTools` and `Collier`. In phenomenological results, the enhancement factors  $\mu_{\phi_i\phi_j}^{\text{HESM}}$  are examined in parameter space of the HESM. We found that the enhancement factors  $\mu_{\phi_i\phi_j}^{\text{HESM}}$  are enhanced at the threshold of  $2M_{H^\pm}$  which attributed from charged Higgs in the loop. These effects could be tested at future colliders. Among the  $\phi_i\phi_j$  productions in the HESM, both cross-sections for  $hh$ ,  $HH$  final states

are bigger than the  $hh$  productions in the SM. While cross-sections for  $hH$  in the IDHM are vanished due to the conservation of  $Z_2$ -symmetry. Moreover, cross-sections for  $hH$  in the THDM are suppressed as consequent of the soft symmetry breaking  $Z_2$ .

**Acknowledgment:** This research is funded by Vietnam National Foundation for Science and Technology Development (NAFOSTED) under the grant number 103.01-2023.16. Khiem Hong Phan and Dzung Tri Tran express their gratitude to all the valuable support from Duy Tan University, for the 30th anniversary of establishment (Nov. 11, 1994 - Nov. 11, 2024) towards "Integral, Sustainable and Stable Development.

## Appendix A: Effective Lagrangian in the IDHM

Deriving all couplings for the IHDM are presented in this appendix. From the kinematic terms, one has

$$\begin{aligned}
\mathcal{L}_K &= (D_\mu \Phi_1)^\dagger (D^\mu \Phi_1) + (D_\mu \Phi_2)^\dagger (D^\mu \Phi_2) \\
&\supset \frac{2M_W^2}{v} W_\mu^\pm W^{\mp,\mu} h + \frac{M_Z^2}{v} h Z_\mu Z^\mu + i \frac{M_Z c_{2W}}{v} Z^\mu (H^\mp \partial_\mu H^\pm - H^\pm \partial_\mu H^\mp) \\
&\quad + i \frac{M_Z s_{2W}}{v} A^\mu (H^\mp \partial_\mu H^\pm - H^\pm \partial_\mu H^\mp) + i \frac{2M_Z^2 c_W^2 s_W}{v} A^\mu W_\mu^\pm G^\pm \\
&\quad + i \frac{M_W}{v} (H W^{\mp,\mu} \partial_\mu H^\pm - H^\pm W^{\mp,\mu} \partial_\mu H - H W_\mu^\pm \partial^\mu H^\mp + H^\mp W_\mu^\pm \partial^\mu H) \\
&\quad + \frac{M_Z^2 s_{2W}^2}{v^2} A_\mu A^\mu H^\pm H^\mp + \frac{2M_Z^2 c_W^2 s_W}{v^2} H H^\pm W_\mu^\mp A^\mu + \frac{2M_W^2}{v^2} W_\mu^\pm W^{\mp,\mu} h h \\
&\quad + \frac{2M_W^2}{v^2} W_\mu^\pm W^{\mp,\mu} H H + \frac{M_Z^2 s_{2W}^2}{v^2} A_\mu A^\mu G^\pm G^\mp \\
&\quad + i \frac{M_Z s_{2W}}{v} A^\mu (G^\mp \partial_\mu G^\pm - G^\pm \partial_\mu G^\mp).
\end{aligned} \tag{55}$$

From scalar Higgs potential of the IDHM, we expand and collect the terms relating to Higgs self coupling as follows:

$$\begin{aligned}
-\mathcal{V}(\Phi_1, \Phi_2) &\supset -\frac{3M_h^2}{v} h h h + \frac{2(\mu_2^2 - M_H^2)}{v} h H H + \frac{2(\mu_2^2 - M_{H^\pm}^2)}{v} h H^\pm H^\mp \\
&\quad + i \frac{M_{H^\pm}^2 - M_H^2}{v} H H^\pm G^\mp + \frac{2(\mu_2^2 - M_{H^\pm}^2)}{v^2} h h H^\pm H^\mp - 2\lambda_2 H H H^\pm H^\mp \\
&\quad - \frac{M_h^2}{v^2} h h G^\pm G^\mp + \frac{2(\mu_2^2 - M_{H^\pm}^2)}{v^2} H H G^\pm G^\mp.
\end{aligned} \tag{57}$$

## Appendix B: Effective Lagrangian in the THDM

Deriving all couplings in Tables 3, 5 for the THDM are shown in this appendix. From the kinematic terms, one has

$$\begin{aligned}
\mathcal{L}_K &= (D_\mu \Phi_1)^\dagger (D^\mu \Phi_1) + (D_\mu \Phi_2)^\dagger (D^\mu \Phi_2) \\
&\supset \frac{2M_W^2}{v} s_{\beta-\alpha} h W_\mu^\pm W^{\mp,\mu} + \frac{2M_W^2}{v} c_{\alpha-\beta} H W_\mu^\pm W^{\mp,\mu} + \frac{M_Z^2}{v} s_{\beta-\alpha} h Z_\mu Z^\mu \\
&\quad + \frac{M_Z^2}{v} c_{\alpha-\beta} H Z_\mu Z^\mu + i \frac{M_Z c_{2W}}{v} Z^\mu (H^\mp \partial_\mu H^\pm - H^\pm \partial_\mu H^\mp)
\end{aligned} \tag{58}$$

$$\begin{aligned}
& +i\frac{M_Z s_{2W}}{v} A^\mu (H^\mp \partial_\mu H^\pm - H^\pm \partial_\mu H^\mp) + \frac{4M_W^2 s_W^2}{v^2} H^\pm H^\mp A_\mu A^\mu \\
& -i\frac{M_W s_{\beta-\alpha}}{v} (HW^{\mp,\mu} \partial_\mu H^\pm - HW^{\pm,\mu} \partial_\mu H^\mp + H^\mp W^{\pm,\mu} \partial_\mu H - H^\pm W^{\mp,\mu} \partial_\mu H) \\
& -i\frac{M_W c_{\beta-\alpha}}{v} (-hW^{\mp,\mu} \partial_\mu H^\pm + hW^{\pm,\mu} \partial_\mu H^\mp - H^\mp W^{\pm,\mu} \partial_\mu h + H^\pm W^{\mp,\mu} \partial_\mu h) \\
& + \frac{2M_W^2 s_W c_{\beta-\alpha}}{v^2} hH^\mp W_\mu^\pm A^\mu - \frac{2M_W^2 s_W s_{\beta-\alpha}}{v^2} HH^\mp W_\mu^\pm A^\mu \\
& + \frac{2M_W^2}{v^2} W_\mu^\pm W^{\mp,\mu} HH + \frac{2M_W^2}{v^2} W_\mu^\pm W^{\mp,\mu} hh.
\end{aligned} \tag{59}$$

From scalar potential in the THDM, we have

$$-\mathcal{V}(\Phi_1, \Phi_2) \supset -\frac{\lambda_1}{2}(\Phi_1^\dagger \Phi_1)^2 - \frac{\lambda_2}{2}(\Phi_2^\dagger \Phi_2)^2 - \lambda_3(\Phi_1^\dagger \Phi_1)(\Phi_2^\dagger \Phi_2) \tag{60}$$

$$\begin{aligned}
& -\lambda_4(\Phi_1^\dagger \Phi_2)(\Phi_2^\dagger \Phi_1) - \frac{\lambda_5}{2}[(\Phi_1^\dagger \Phi_2)^2 + (\Phi_2^\dagger \Phi_1)^2] \\
& \supset -\lambda_{hHH} hHH - \lambda_{Hhh} Hhh - \lambda_{hH^\pm H^\mp} hH^\pm H^\mp \\
& -\lambda_{hH^\pm H^\mp} HH^\pm H^\mp - \lambda_{HhH^\pm H^\mp} HhH^\pm H^\mp + \dots,
\end{aligned} \tag{61}$$

where all coefficient couplings are presented explicitly in terms of bare parameters as well as physical parameters as follows:

$$-\lambda_{hHH} = \frac{3\lambda_1 v}{2} s_\alpha c_\alpha^2 c_\beta - \frac{3\lambda_2 v}{2} s_\beta s_\alpha^2 c_\alpha - \frac{\lambda_{345} v}{2} [c_\beta (2s_\alpha c_\alpha^2 - s_\alpha^3) + s_\beta (c_\alpha^3 - 2s_\alpha^2 c_\alpha)] \tag{62}$$

$$= \frac{s_{\alpha-\beta} [s_{2\alpha} (3M^2 - M_h^2 - 2M_H^2) + M^2 s_{2\beta}]}{v s_{2\beta}}, \tag{63}$$

$$-\lambda_{Hhh} = -\frac{3\lambda_1 v}{2} c_\beta c_\alpha s_\alpha^2 - \frac{3\lambda_2 v}{2} s_\beta c_\alpha^2 s_\alpha - \frac{\lambda_{345} v}{2} [s_\beta (s_\alpha^3 - 2c_\alpha^2 s_\alpha) - c_\beta (2c_\alpha s_\alpha^2 - c_\alpha^3)] \tag{64}$$

$$= \frac{c_{\alpha-\beta} [s_{2\alpha} (3M^2 - M_H^2 - 2m_h^2) - M^2 s_{2\beta}]}{v s_{2\beta}}, \tag{65}$$

$$-\lambda_{HH^\pm H^\mp} = -\lambda_1 v c_\beta c_\alpha s_\beta^2 - \lambda_2 v s_\beta s_\alpha c_\beta^2 - \lambda_3 v (s_\beta s_\alpha s_\beta^2 + c_\beta c_\alpha c_\beta^2) + \frac{\lambda_{45}}{2} v s_{(2\beta)} s_{\beta+\alpha} \tag{66}$$

$$= \frac{s_{\alpha+\beta} (4M^2 - 3M_H^2 - 2M_{H^\pm}^2) + (2M_{H^\pm}^2 - M_H^2) s_{\alpha-3\beta}}{2v s_{(2\beta)}}, \tag{67}$$

$$-\lambda_{hH^\pm H^\mp} = \lambda_1 v c_\beta s_\alpha s_\beta^2 - \lambda_2 v s_\beta c_\alpha c_\beta^2 - \lambda_3 v (s_\beta c_\alpha s_\beta^2 - c_\beta s_\alpha c_\beta^2) + \frac{\lambda_{45}}{2} v s_{(2\beta)} c_{(\beta+\alpha)} \tag{68}$$

$$= \frac{c_{\alpha+\beta} (4M^2 - 3M_h^2 - 2M_{H^\pm}^2) + (2M_{H^\pm}^2 - M_h^2) c_{(\alpha-3\beta)}}{2v s_{2\beta}}, \tag{69}$$

and

$$-\lambda_{HhhH^\pm H^\mp} = \lambda_1 s_\beta^2 s_\alpha c_\alpha - \lambda_2 c_\beta^2 s_\alpha c_\alpha + \lambda_3 s_\alpha c_\alpha c_{2\beta} + (\lambda_4 + \lambda_5) s_\beta c_\beta c_{2\alpha} \tag{70}$$

$$\begin{aligned}
& = \frac{s_{2\alpha} (3c_{2\alpha} + c_{2(\alpha-2\beta)} - 4c_{2\beta})}{4v^2 s_{2\beta}^2} M_H^2 - \frac{s_{2\alpha} (3c_{2\alpha} + c_{2(\alpha-2\beta)} + 4c_{2\beta})}{4v^2 s_{2\beta}^2} M_h^2 \\
& + \frac{s_{2(\alpha-\beta)}}{v^2} M_{H^\pm}^2 + \frac{(s_{2(\alpha-3\beta)} + 2s_{2(\alpha-\beta)} + 5s_{2(\alpha+\beta)})}{4v^2 s_{2\beta}^2} M^2,
\end{aligned} \tag{71}$$

$$\begin{aligned}
-\lambda_{HhG^\pm G^\mp} &= \lambda_1 c_\beta^2 s_\alpha c_\alpha - \lambda_2 s_\beta^2 s_\alpha c_\alpha - \lambda_3 s_\alpha c_\alpha c_{2\beta} - (\lambda_4 + \lambda_5) s_\beta c_\beta c_{2\alpha} \\
&= \frac{1}{2v^2 s_{2\beta}} s_{2(\alpha-\beta)} [(M_h^2 - M_H^2) s_{2\alpha} + 2(M^2 - M_{H^\pm}^2) s_{2\beta}].
\end{aligned} \tag{72}$$

Furthermore, we have the following couplings:

$$\begin{aligned}
-\lambda_{hhh} &= 3v \left[ \lambda_1 s_\alpha^3 c_\beta - \lambda_2 c_\alpha^3 s_\beta + (\lambda_3 + \lambda_4 + \lambda_5) (s_\alpha c_\beta c_\alpha^2 - c_\alpha s_\beta s_\alpha^2) \right] \\
&= \frac{3e}{4M_W s_W s_{2\beta}} \left[ M^2 c_{\alpha-3\beta} + (M^2 - M_h^2) c_{3\alpha-\beta} + (2M^2 - 3M_h^2) c_{\alpha+\beta} \right],
\end{aligned} \tag{73}$$

$$\begin{aligned}
-\lambda_{HHH} &= -3v \left[ \lambda_1 c_\alpha^3 c_\beta + \lambda_2 s_\alpha^3 s_\beta + (\lambda_3 + \lambda_4 + \lambda_5) (c_\alpha c_\beta s_\alpha^2 + s_\alpha s_\beta c_\alpha^2) \right] \\
&= \frac{3e}{4M_W s_W s_{2\beta}} \left[ M^2 s_{\alpha-3\beta} + (M_H^2 - M^2) s_{3\alpha-\beta} + (2M^2 - 3M_H^2) s_{\alpha+\beta} \right],
\end{aligned} \tag{74}$$

$$\begin{aligned}
-\lambda_{HHH^\pm H^\mp} &= -\lambda_1 c_\alpha^2 s_\beta^2 - \lambda_2 s_\alpha^2 c_\beta^2 - \lambda_3 (c_\alpha^2 c_\beta^2 + s_\alpha^2 s_\beta^2) + (\lambda_4 + \lambda_5) c_\alpha s_\alpha s_{2\beta} \\
&= -\frac{2c_{\alpha-\beta}^2}{v^2} M_{H^\pm}^2 - \frac{s_{2\alpha} [3s_{2\alpha} + s_{2(\alpha-2\beta)} - 2s_{2\beta}]}{4v^2 s_{2\beta}^2} M_h^2 \\
&\quad - \frac{[c_\alpha^4 + c_\alpha^3 s_\alpha \cot^3 \beta + c_\alpha s_\alpha^3 \cot \beta + s_\alpha^4 \cot^4 \beta] \tan^2 \beta}{v^2} M_H^2 \\
&\quad + \frac{s_\beta [4c_\alpha c_\beta s_\alpha + (1 + \cot^4 \beta) s_\alpha^2 s_\beta + c_\alpha^2 (1 + \cot^4 \beta) s_\beta \tan^2 \beta]}{v^2} M^2,
\end{aligned} \tag{75}$$

$$\begin{aligned}
-\lambda_{hhH^\pm H^\mp} &= -\lambda_1 s_\alpha^2 s_\beta^2 - \lambda_2 c_\alpha^2 c_\beta^2 - \lambda_3 (s_\alpha^2 c_\beta^2 + c_\alpha^2 s_\beta^2) - (\lambda_4 + \lambda_5) c_\alpha s_\alpha s_{2\beta} \\
&= -\frac{2s_{\alpha-\beta}^2}{v^2} M_{H^\pm}^2 - \frac{s_{2\alpha} [3s_{2\alpha} + s_{2(\alpha-2\beta)} + 2s_{2\beta}]}{4v^2 s_{2\beta}^2} M_H^2 \\
&\quad + \frac{(-c_\alpha^4 \cot^2 \beta + c_\alpha s_\alpha^3 \cot \beta + c_\alpha^3 s_\alpha \tan \beta - s_\alpha^4 \tan^2 \beta)}{v^2} M_h^2 \\
&\quad + \frac{s_\beta c_\beta [-4c_\alpha s_\alpha + (1 + \cot^4 \beta) s_\alpha^2 \tan^3 \beta + c_\alpha^2 (\cot^3 \beta + \tan \beta)]}{v^2} M^2,
\end{aligned} \tag{76}$$

$$\begin{aligned}
-\lambda_{hhG^\pm G^\mp} &= -\lambda_1 s_\alpha^2 c_\beta^2 - \lambda_2 c_\alpha^2 s_\beta^2 - \lambda_3 (c_\alpha^2 c_\beta^2 + s_\alpha^2 s_\beta^2) + (\lambda_4 + \lambda_5) c_\alpha s_\alpha s_{2\beta} \\
&= \frac{2c_{\alpha-\beta}^2}{v^2} (M^2 - M_{H^\pm}^2) - \frac{c_{\alpha-\beta}^2 s_{2\alpha}}{v^2 s_{2\beta}} M_H^2 + \frac{-3s_{2\beta} + 2s_{2\alpha} + s_{4\alpha-2\beta}}{4v^2 s_{2\beta}} M_h^2,
\end{aligned} \tag{77}$$

$$\begin{aligned}
-\lambda_{HHG^\pm G^\mp} &= -\lambda_1 c_\alpha^2 c_\beta^2 - \lambda_2 s_\alpha^2 s_\beta^2 - \lambda_3 (s_\alpha^2 c_\beta^2 + c_\alpha^2 s_\beta^2) - (\lambda_4 + \lambda_5) c_\alpha s_\alpha s_{2\beta} \\
&= \frac{2s_{\alpha-\beta}^2}{v^2} (M^2 - M_{H^\pm}^2) + \frac{s_{\alpha-\beta}^2 s_{2\alpha}}{v^2 s_{2\beta}} M_h^2 + \frac{-3s_{2\beta} - 2s_{2\alpha} + s_{4\alpha-2\beta}}{4v^2 s_{2\beta}} M_H^2.
\end{aligned} \tag{78}$$

The relationship between the bare parameters in the Higgs potential and the physical parameters is

$$\lambda_1 = \frac{1}{v^2 c_\beta^2} (c_\alpha^2 M_H^2 + s_\alpha^2 M_h^2 - s_\beta^2 M^2), \tag{79}$$

$$\lambda_2 = \frac{1}{v^2 s_\beta^2} (s_\alpha^2 M_H^2 + c_\alpha^2 M_h^2 - c_\beta^2 M^2), \quad (80)$$

$$\lambda_3 = \frac{s_{2\alpha}}{v^2 s_{2\beta}} (M_H^2 - M_h^2) - \frac{1}{v^2} (M^2 - 2M_{H^\pm}^2), \quad (81)$$

$$\lambda_4 = \frac{1}{v^2} (M_{A^0}^2 - 2M_{H^\pm}^2 + M^2), \quad (82)$$

$$\lambda_5 = \frac{1}{v^2} (M^2 - M_{A^0}^2). \quad (83)$$

Where the  $M^2$  parameter is given by  $M^2 = \frac{m_{12}^2}{s_\beta c_\beta}$ . The shorten notation  $\lambda_{ijk} = \lambda_i + \lambda_j + \lambda_k$ .

Furthermore, we derive the couplings relating to Goldstone bosons as follows:

$$\mathcal{L}_K = (D_\mu \Phi_1)^\dagger (D^\mu \Phi_1) + (D_\mu \Phi_2)^\dagger (D^\mu \Phi_2) \quad (84)$$

$$\begin{aligned} \supset & \frac{2M_W^2 s_W}{v} A_\mu W^{\pm, \mu} G^\mp + \frac{4M_W^2 s_W^2}{v^2} A_\mu A^\mu G^\pm G^\mp \\ & + i \frac{2M_W s_W}{v} A^\mu (G^\mp i \partial_\mu G^\pm - G^\pm i \partial_\mu G^\mp) + \dots \end{aligned} \quad (85)$$

From scalar potential, we have

$$-\mathcal{V}(\Phi_1, \Phi_2) \supset -\lambda_{hH^\pm G^\mp} h H^\pm G^\mp - \lambda_{HH^\pm G^\mp} H H^\pm G^\mp + \dots \quad (86)$$

where all coefficient couplings are presented explicitly in terms of bare parameters as well as physical parameters as follows:

$$-\lambda_{hH^\pm G^\mp} = \frac{e c_{\alpha-\beta}}{2M_W s_W} (M_{H^\pm}^2 - M_h^2), \quad (87)$$

$$-\lambda_{HH^\pm G^\mp} = \frac{e s_{\alpha-\beta}}{2M_W s_W} (M_{H^\pm}^2 - M_H^2). \quad (88)$$

For all couplings of CP-even Higgses with fermion-pair, we expand the Yukawa Lagrangian for each type of THDM as follows:

### Type I

$$\begin{aligned} -\mathcal{L}_Y^I &= -\bar{Q}_L \frac{M_u}{v_2} \tilde{\Phi}_2 u_R - \bar{Q}'_L \frac{M_d}{v_2} \Phi_2 d_R - \bar{L}_L \frac{M_l}{v_2} \Phi_2 l_R + h.c \\ \supset & \frac{M_l}{\sqrt{2}v} \frac{s_\alpha}{s_\beta} H \bar{e}_i e_i + \frac{M_l}{\sqrt{2}v} \frac{c_\alpha}{s_\beta} h \bar{e}_i e_i + i \frac{M_l \cot \beta \gamma^5}{\sqrt{2}v} A \bar{e}^i e^i \\ & + \frac{M_u}{\sqrt{2}v} \frac{s_\alpha}{s_\beta} H \bar{u}^i u^i + \frac{M_u}{\sqrt{2}v} \frac{c_\alpha}{s_\beta} h \bar{u}^i u^i - i \frac{M_u \cot \beta \gamma^5}{\sqrt{2}v} A \bar{u}^i u^i \\ & + \frac{M_d}{\sqrt{2}v} \frac{s_\alpha}{s_\beta} H \bar{d}^i d^i + \frac{M_d}{\sqrt{2}v} \frac{c_\alpha}{s_\beta} h \bar{d}^i d^i + i \frac{M_d \cot \beta \gamma^5}{\sqrt{2}v} A \bar{d}^i d^i \end{aligned} \quad (89)$$

### Type II

$$\begin{aligned} -\mathcal{L}_Y^{II} &= -\bar{Q}_L \frac{M_u}{v_2} \tilde{\Phi}_2 u_R - \bar{Q}'_L \frac{M_d}{v_1} \Phi_1 d_R - \bar{L}_L \frac{M_l}{v_1} \Phi_1 l_R + h.c \\ \supset & \frac{M_l}{\sqrt{2}v} \frac{c_\alpha}{c_\beta} H \bar{e}^i e^i - \frac{M_l}{\sqrt{2}v} \frac{s_\alpha}{c_\beta} h \bar{e}^i e^i - i \frac{M_l \gamma^5 \tan \beta}{\sqrt{2}v} A \bar{e}^i e^i \end{aligned}$$

$$\begin{aligned}
& + \frac{M_d c_\alpha}{\sqrt{2v} c_\beta} H \bar{d}^i d^i - \frac{M_d s_\alpha}{\sqrt{2v} c_\beta} h \bar{d}^i d^i - i \frac{M_d \gamma^5 \tan \beta}{\sqrt{2v}} A \bar{d}^i d^i \\
& + \frac{M_u s_\alpha}{\sqrt{2v} s_\beta} H \bar{u}^i u^i + \frac{M_u c_\alpha}{\sqrt{2v} s_\beta} h \bar{u}^i u^i - i \frac{M_u \gamma^5 \cot \beta}{\sqrt{2v}} A \bar{u}^i u^i
\end{aligned} \tag{90}$$

### Type X

$$\begin{aligned}
-\mathcal{L}_Y^X &= -\bar{Q}_L \frac{M_u}{v_2} \tilde{\Phi}_2 u_R - \bar{Q}'_L \frac{M_d}{v_2} \Phi_2 d_R - \bar{L}_L \frac{M_l}{v_1} \Phi_1 l_R + h.c \\
&\supset \frac{M_l c_\alpha}{\sqrt{2v} c_\beta} H \bar{e}^i e^i - \frac{M_l s_\alpha}{\sqrt{2v} c_\beta} h \bar{e}^i e^i - i \frac{M_l \gamma^5 \tan \beta}{\sqrt{2v}} A \bar{e}^i e^i \\
&+ \frac{M_d s_\alpha}{\sqrt{2v} s_\beta} H \bar{d}^i d^i + \frac{M_d c_\alpha}{\sqrt{2v} s_\beta} h \bar{d}^i d^i + i \frac{M_d \gamma^5 \cot \beta}{\sqrt{2v}} A \bar{d}^i d^i \\
&+ \frac{M_u s_\alpha}{\sqrt{2v} s_\beta} H \bar{u}^i u^i + \frac{M_u c_\alpha}{\sqrt{2v} s_\beta} h \bar{u}^i u^i - i \frac{M_u \gamma^5 \cot \beta}{\sqrt{2v}} A \bar{u}^i u^i
\end{aligned} \tag{91}$$

### Type Y

$$\begin{aligned}
-\mathcal{L}_Y^Y &= -\bar{Q}_L \frac{M_u}{v_2} \tilde{\Phi}_2 u_R - \bar{Q}'_L \frac{M_d}{v_1} \Phi_1 d_R - \bar{L}_L \frac{M_l}{v_2} \Phi_2 l_R + h.c \\
&\supset \frac{M_l s_\alpha}{\sqrt{2v} s_\beta} H \bar{e}_i e_i + \frac{M_l c_\alpha}{\sqrt{2v} s_\beta} h \bar{e}_i e_i + i \frac{M_l \gamma^5 \cot \beta}{\sqrt{2v}} A \bar{e}^i e^i \\
&+ \frac{M_u s_\alpha}{\sqrt{2v} s_\beta} H \bar{u}^i u^i + \frac{M_u c_\alpha}{\sqrt{2v} s_\beta} h \bar{u}^i u^i - i \frac{M_u \gamma^5 \cot \beta}{\sqrt{2v}} A \bar{u}^i u^i \\
&+ \frac{M_d c_\alpha}{\sqrt{2v} c_\beta} H \bar{d}^i d^i - \frac{M_d s_\alpha}{\sqrt{2v} c_\beta} h \bar{d}^i d^i - i \frac{M_d \gamma^5 \tan \beta}{\sqrt{2v}} A \bar{d}^i d^i
\end{aligned} \tag{92}$$

### References

- [1] A. Liss *et al.* [ATLAS], [[arXiv:1307.7292](#) [hep-ex]].
- [2] [CMS], [[arXiv:1307.7135](#) [hep-ex]].
- [3] H. Baer *et al.* [ILC], [[arXiv:1306.6352](#) [hep-ph]].
- [4] V. Shiltsev and F. Zimmermann, Rev. Mod. Phys. **93** (2021), 015006 doi:10.1103/RevModPhys.93.015006 [[arXiv:2003.09084](#) [physics.acc-ph]].
- [5] G. Aad *et al.* [ATLAS], Phys. Rev. D **106** (2022) no.5, 052001 doi:10.1103/PhysRevD.106.052001 [[arXiv:2112.11876](#) [hep-ex]].
- [6] G. Aad *et al.* [ATLAS], Phys. Rev. Lett. **114** (2015) no.8, 081802 doi:10.1103/PhysRevLett.114.081802 [[arXiv:1406.5053](#) [hep-ex]].
- [7] G. Aad *et al.* [ATLAS], Eur. Phys. J. C **75** (2015) no.9, 412 doi:10.1140/epjc/s10052-015-3628-x [[arXiv:1506.00285](#) [hep-ex]].
- [8] G. Aad *et al.* [ATLAS], Phys. Rev. D **92** (2015), 092004 doi:10.1103/PhysRevD.92.092004 [[arXiv:1509.04670](#) [hep-ex]].

- [9] A. M. Sirunyan *et al.* [CMS], JHEP **01** (2018), 054 doi:10.1007/JHEP01(2018)054 [[arXiv:1708.04188](#) [hep-ex]].
- [10] M. Aaboud *et al.* [ATLAS], JHEP **11** (2018), 040 doi:10.1007/JHEP11(2018)040 [[arXiv:1807.04873](#) [hep-ex]].
- [11] A. M. Sirunyan *et al.* [CMS], Phys. Lett. B **788** (2019), 7-36 doi:10.1016/j.physletb.2018.10.056 [[arXiv:1806.00408](#) [hep-ex]].
- [12] A. M. Sirunyan *et al.* [CMS], JHEP **03** (2021), 257 doi:10.1007/JHEP03(2021)257 [[arXiv:2011.12373](#) [hep-ex]].
- [13] A. Tumasyan *et al.* [CMS], Phys. Rev. Lett. **129** (2022) no.8, 081802 doi:10.1103/PhysRevLett.129.081802 [[arXiv:2202.09617](#) [hep-ex]].
- [14] G. Aad *et al.* [ATLAS], JHEP **07** (2023), 040 doi:10.1007/JHEP07(2023)040 [[arXiv:2209.10910](#) [hep-ex]].
- [15] G. Aad *et al.* [ATLAS], Phys. Rev. D **108** (2023) no.5, 052003 doi:10.1103/PhysRevD.108.052003 [[arXiv:2301.03212](#) [hep-ex]].
- [16] G. Aad *et al.* [ATLAS], [[arXiv:2406.09971](#) [hep-ex]].
- [17] U. Baur, T. Plehn and D. L. Rainwater, Phys. Rev. Lett. **89** (2002), 151801 doi:10.1103/PhysRevLett.89.151801 [[arXiv:hep-ph/0206024](#) [hep-ph]].
- [18] U. Baur, T. Plehn and D. L. Rainwater, Phys. Rev. D **67** (2003), 033003 doi:10.1103/PhysRevD.67.033003 [[arXiv:hep-ph/0211224](#) [hep-ph]].
- [19] G. Weiglein *et al.* [LHC/LC Study Group], Phys. Rept. **426** (2006), 47-358 doi:10.1016/j.physrep.2005.12.003 [[arXiv:hep-ph/0410364](#) [hep-ph]].
- [20] A. Arhrib, R. Benbrik, C. H. Chen, R. Guedes and R. Santos, JHEP **08** (2009), 035 doi:10.1088/1126-6708/2009/08/035 [[arXiv:0906.0387](#) [hep-ph]].
- [21] J. Grigo, J. Hoff, K. Melnikov and M. Steinhauser, Nucl. Phys. B **875** (2013), 1-17 doi:10.1016/j.nuclphysb.2013.06.024 [[arXiv:1305.7340](#) [hep-ph]].
- [22] D. Y. Shao, C. S. Li, H. T. Li and J. Wang, JHEP **07** (2013), 169 doi:10.1007/JHEP07(2013)169 [[arXiv:1301.1245](#) [hep-ph]].
- [23] U. Ellwanger, JHEP **08** (2013), 077 doi:10.1007/JHEP08(2013)077 [[arXiv:1306.5541](#) [hep-ph]].
- [24] C. Han, X. Ji, L. Wu, P. Wu and J. M. Yang, JHEP **04** (2014), 003 doi:10.1007/JHEP04(2014)003 [[arXiv:1307.3790](#) [hep-ph]].
- [25] A. J. Barr, M. J. Dolan, C. Englert and M. Spannowsky, Phys. Lett. B **728** (2014), 308-313 doi:10.1016/j.physletb.2013.12.011 [[arXiv:1309.6318](#) [hep-ph]].
- [26] D. de Florian and J. Mazzitelli, Phys. Rev. Lett. **111** (2013), 201801 doi:10.1103/PhysRevLett.111.201801 [[arXiv:1309.6594](#) [hep-ph]].
- [27] N. Haba, K. Kaneta, Y. Mimura and E. Tsedenbaljir, Phys. Rev. D **89** (2014) no.1, 015018 doi:10.1103/PhysRevD.89.015018 [[arXiv:1311.0067](#) [hep-ph]].

- [28] J. Cao, D. Li, L. Shang, P. Wu and Y. Zhang, JHEP **12** (2014), 026 doi:10.1007/JHEP12(2014)026 [[arXiv:1409.8431](#) [hep-ph]].
- [29] T. Enkhbat, JHEP **01** (2014), 158 doi:10.1007/JHEP01(2014)158 [[arXiv:1311.4445](#) [hep-ph]].
- [30] Q. Li, Q. S. Yan and X. Zhao, Phys. Rev. D **89** (2014) no.3, 033015 doi:10.1103/PhysRevD.89.033015 [[arXiv:1312.3830](#) [hep-ph]].
- [31] R. Frederix, S. Frixione, V. Hirschi, F. Maltoni, O. Mattelaer, P. Torrielli, E. Vryonidou and M. Zaro, Phys. Lett. B **732** (2014), 142-149 doi:10.1016/j.physletb.2014.03.026 [[arXiv:1401.7340](#) [hep-ph]].
- [32] J. Baglio, O. Eberhardt, U. Nierste and M. Wiebusch, Phys. Rev. D **90** (2014) no.1, 015008 doi:10.1103/PhysRevD.90.015008 [[arXiv:1403.1264](#) [hep-ph]].
- [33] D. E. Ferreira de Lima, A. Papaefstathiou and M. Spannowsky, JHEP **08** (2014), 030 doi:10.1007/JHEP08(2014)030 [[arXiv:1404.7139](#) [hep-ph]].
- [34] B. Hespel, D. Lopez-Val and E. Vryonidou, JHEP **09** (2014), 124 doi:10.1007/JHEP09(2014)124 [[arXiv:1407.0281](#) [hep-ph]].
- [35] V. Barger, L. L. Everett, C. B. Jackson, A. D. Peterson and G. Shaughnessy, Phys. Rev. Lett. **114** (2015) no.1, 011801 doi:10.1103/PhysRevLett.114.011801 [[arXiv:1408.0003](#) [hep-ph]].
- [36] J. Grigo, K. Melnikov and M. Steinhauser, Nucl. Phys. B **888** (2014), 17-29 doi:10.1016/j.nuclphysb.2014.09.003 [[arXiv:1408.2422](#) [hep-ph]].
- [37] F. Maltoni, E. Vryonidou and M. Zaro, JHEP **11** (2014), 079 doi:10.1007/JHEP11(2014)079 [[arXiv:1408.6542](#) [hep-ph]].
- [38] F. Goertz, A. Papaefstathiou, L. L. Yang and J. Zurita, JHEP **04** (2015), 167 doi:10.1007/JHEP04(2015)167 [[arXiv:1410.3471](#) [hep-ph]].
- [39] A. Azatov, R. Contino, G. Panico and M. Son, Phys. Rev. D **92** (2015) no.3, 035001 doi:10.1103/PhysRevD.92.035001 [[arXiv:1502.00539](#) [hep-ph]].
- [40] A. Papaefstathiou, Phys. Rev. D **91** (2015) no.11, 113016 doi:10.1103/PhysRevD.91.113016 [[arXiv:1504.04621](#) [hep-ph]].
- [41] R. Grober, M. Muhlleitner, M. Spira and J. Streicher, JHEP **09** (2015), 092 doi:10.1007/JHEP09(2015)092 [[arXiv:1504.06577](#) [hep-ph]].
- [42] D. de Florian and J. Mazzitelli, JHEP **09** (2015), 053 doi:10.1007/JHEP09(2015)053 [[arXiv:1505.07122](#) [hep-ph]].
- [43] H. J. He, J. Ren and W. Yao, Phys. Rev. D **93** (2016) no.1, 015003 doi:10.1103/PhysRevD.93.015003 [[arXiv:1506.03302](#) [hep-ph]].
- [44] J. Grigo, J. Hoff and M. Steinhauser, Nucl. Phys. B **900** (2015), 412-430 doi:10.1016/j.nuclphysb.2015.09.012 [[arXiv:1508.00909](#) [hep-ph]].

- [45] W. J. Zhang, W. G. Ma, R. Y. Zhang, X. Z. Li, L. Guo and C. Chen, Phys. Rev. D **92** (2015), 116005 doi:10.1103/PhysRevD.92.116005 [arXiv:1512.01766 [hep-ph]].
- [46] A. Agostini, G. Degrassi, R. Gröber and P. Slavich, JHEP **04** (2016), 106 doi:10.1007/JHEP04(2016)106 [arXiv:1601.03671 [hep-ph]].
- [47] R. Grober, M. Muhlleitner and M. Spira, JHEP **06** (2016), 080 doi:10.1007/JHEP06(2016)080 [arXiv:1602.05851 [hep-ph]].
- [48] G. Degrassi, P. P. Giardino and R. Gröber, Eur. Phys. J. C **76** (2016) no.7, 411 doi:10.1140/epjc/s10052-016-4256-9 [arXiv:1603.00385 [hep-ph]].
- [49] S. Kanemura, K. Kaneta, N. Machida, S. Odori and T. Shindou, Phys. Rev. D **94** (2016) no.1, 015028 doi:10.1103/PhysRevD.94.015028 [arXiv:1603.05588 [hep-ph]].
- [50] D. de Florian, M. Grazzini, C. Hanga, S. Kallweit, J. M. Lindert, P. Maierhöfer, J. Mazzitelli and D. Rathlev, JHEP **09** (2016), 151 doi:10.1007/JHEP09(2016)151 [arXiv:1606.09519 [hep-ph]].
- [51] S. Borowka, N. Greiner, G. Heinrich, S. P. Jones, M. Kerner, J. Schlenk and T. Zirke, JHEP **10** (2016), 107 doi:10.1007/JHEP10(2016)107 [arXiv:1608.04798 [hep-ph]].
- [52] F. Bishara, R. Contino and J. Rojo, Eur. Phys. J. C **77** (2017) no.7, 481 doi:10.1140/epjc/s10052-017-5037-9 [arXiv:1611.03860 [hep-ph]].
- [53] Q. H. Cao, G. Li, B. Yan, D. M. Zhang and H. Zhang, Phys. Rev. D **96** (2017) no.9, 095031 doi:10.1103/PhysRevD.96.095031 [arXiv:1611.09336 [hep-ph]].
- [54] K. Nakamura, K. Nishiwaki, K. y. Oda, S. C. Park and Y. Yamamoto, Eur. Phys. J. C **77** (2017) no.5, 273 doi:10.1140/epjc/s10052-017-4835-4 [arXiv:1701.06137 [hep-ph]].
- [55] R. Grober, M. Muhlleitner and M. Spira, Nucl. Phys. B **925** (2017), 1-27 doi:10.1016/j.nuclphysb.2017.10.002 [arXiv:1705.05314 [hep-ph]].
- [56] G. Heinrich, S. P. Jones, M. Kerner, G. Luisoni and E. Vryonidou, JHEP **08** (2017), 088 doi:10.1007/JHEP08(2017)088 [arXiv:1703.09252 [hep-ph]].
- [57] S. Jones and S. Kuttimalai, JHEP **02** (2018), 176 doi:10.1007/JHEP02(2018)176 [arXiv:1711.03319 [hep-ph]].
- [58] J. Davies, G. Mishima, M. Steinhauser and D. Wellmann, JHEP **03** (2018), 048 doi:10.1007/JHEP03(2018)048 [arXiv:1801.09696 [hep-ph]].
- [59] D. Gonçalves, T. Han, F. Kling, T. Plehn and M. Takeuchi, Phys. Rev. D **97** (2018) no.11, 113004 doi:10.1103/PhysRevD.97.113004 [arXiv:1802.04319 [hep-ph]].
- [60] J. Chang, K. Cheung, J. S. Lee, C. T. Lu and J. Park, Phys. Rev. D **100** (2019) no.9, 096001 doi:10.1103/PhysRevD.100.096001 [arXiv:1804.07130 [hep-ph]].
- [61] G. Buchalla, M. Capozzi, A. Celis, G. Heinrich and L. Scyboz, JHEP **09** (2018), 057 doi:10.1007/JHEP09(2018)057 [arXiv:1806.05162 [hep-ph]].
- [62] R. Bonciani, G. Degrassi, P. P. Giardino and R. Gröber, Phys. Rev. Lett. **121** (2018) no.16, 162003 doi:10.1103/PhysRevLett.121.162003 [arXiv:1806.11564 [hep-ph]].

- [63] P. Banerjee, S. Borowka, P. K. Dhani, T. Gehrmann and V. Ravindran, *JHEP* **11** (2018), 130 doi:10.1007/JHEP11(2018)130 [[arXiv:1809.05388](#) [hep-ph]].
- [64] A. A H, P. Banerjee, A. Chakraborty, P. K. Dhani, P. Mukherjee, N. Rana and V. Ravindran, *JHEP* **05** (2019), 030 doi:10.1007/JHEP05(2019)030 [[arXiv:1811.01853](#) [hep-ph]].
- [65] J. Baglio, F. Campanario, S. Glaus, M. Mühlleitner, M. Spira and J. Streicher, *Eur. Phys. J. C* **79** (2019) no.6, 459 doi:10.1140/epjc/s10052-019-6973-3 [[arXiv:1811.05692](#) [hep-ph]].
- [66] J. Davies, F. Herren, G. Mishima and M. Steinhauser, *JHEP* **05** (2019), 157 doi:10.1007/JHEP05(2019)157 [[arXiv:1904.11998](#) [hep-ph]].
- [67] J. Davies, G. Heinrich, S. P. Jones, M. Kerner, G. Mishima, M. Steinhauser and D. Wellmann, *JHEP* **11** (2019), 024 doi:10.1007/JHEP11(2019)024 [[arXiv:1907.06408](#) [hep-ph]].
- [68] L. B. Chen, H. T. Li, H. S. Shao and J. Wang, *Phys. Lett. B* **803** (2020), 135292 doi:10.1016/j.physletb.2020.135292 [[arXiv:1909.06808](#) [hep-ph]].
- [69] L. B. Chen, H. T. Li, H. S. Shao and J. Wang, *JHEP* **03** (2020), 072 doi:10.1007/JHEP03(2020)072 [[arXiv:1912.13001](#) [hep-ph]].
- [70] J. Baglio, F. Campanario, S. Glaus, M. Mühlleitner, J. Ronca, M. Spira and J. Streicher, *JHEP* **04** (2020), 181 doi:10.1007/JHEP04(2020)181 [[arXiv:2003.03227](#) [hep-ph]].
- [71] G. Wang, Y. Wang, X. Xu, Y. Xu and L. L. Yang, *Phys. Rev. D* **104** (2021) no.5, L051901 doi:10.1103/PhysRevD.104.L051901 [[arXiv:2010.15649](#) [hep-ph]].
- [72] H. Abouabid, A. Arhrib, D. Azevedo, J. E. Falaki, P. M. Ferreira, M. Mühlleitner and R. Santos, *JHEP* **09** (2022), 011 doi:10.1007/JHEP09(2022)011 [[arXiv:2112.12515](#) [hep-ph]].
- [73] J. Davies, G. Mishima, K. Schönwald, M. Steinhauser and H. Zhang, *JHEP* **08** (2022), 259 doi:10.1007/JHEP08(2022)259 [[arXiv:2207.02587](#) [hep-ph]].
- [74] D. He, T. F. Feng, J. L. Yang, G. Z. Ning, H. B. Zhang and X. X. Dong, *J. Phys. G* **49** (2022) no.8, 085002 doi:10.1088/1361-6471/ac77a8 [[arXiv:2206.04450](#) [hep-ph]].
- [75] A. A H and H. S. Shao, *JHEP* **02** (2023), 067 doi:10.1007/JHEP02(2023)067 [[arXiv:2209.03914](#) [hep-ph]].
- [76] S. Iguro, T. Kitahara, Y. Omura and H. Zhang, *Phys. Rev. D* **107** (2023) no.7, 075017 doi:10.1103/PhysRevD.107.075017 [[arXiv:2211.00011](#) [hep-ph]].
- [77] S. Alioli, G. Billis, A. Broggio, A. Gavardi, S. Kallweit, M. A. Lim, G. Marinelli, R. Nagar and D. Napoletano, *JHEP* **06** (2023), 205 doi:10.1007/JHEP06(2023)205 [[arXiv:2212.10489](#) [hep-ph]].
- [78] J. Davies, K. Schönwald, M. Steinhauser and H. Zhang, *JHEP* **10** (2023), 033 doi:10.1007/JHEP10(2023)033 [[arXiv:2308.01355](#) [hep-ph]].
- [79] E. Bagnaschi, G. Degrossi and R. Gröber, *Eur. Phys. J. C* **83** (2023) no.11, 1054 doi:10.1140/epjc/s10052-023-12238-8 [[arXiv:2309.10525](#) [hep-ph]].
- [80] J. Davies, K. Schönwald, M. Steinhauser and M. Vitti, [[arXiv:2405.20372](#) [hep-ph]].

- [81] V. Brigljevic, D. Ferencek, G. Landsberg, T. Robens, M. Stamenkovic, T. Susa, H. Abouabid, A. Arhrib, H. Arnold and D. Azevedo, *et al.* [[arXiv:2407.03015](#)] [hep-ph].
- [82] G. V. Jikia, Nucl. Phys. B **412** (1994), 57-78 doi:10.1016/0550-3213(94)90494-4.
- [83] L. Z. Sun and Y. Y. Liu, Phys. Rev. D **54** (1996), 3563-3569 doi:10.1103/PhysRevD.54.3563.
- [84] S. H. Zhu, C. S. Li and C. S. Gao, Phys. Rev. D **58** (1998), 015006 doi:10.1103/PhysRevD.58.015006 [[arXiv:hep-ph/9710424](#)] [hep-ph].
- [85] S. H. Zhu, J. Phys. G **24** (1998), 1703-1721 doi:10.1088/0954-3899/24/9/005.
- [86] G. J. Gounaris and P. I. Porfyriadis, Eur. Phys. J. C **18** (2000), 181-193 doi:10.1007/s100520000520 [[arXiv:hep-ph/0007110](#)] [hep-ph].
- [87] Y. J. Zhou, W. G. Ma, H. S. Hou, R. Y. Zhang, P. J. Zhou and Y. B. Sun, Phys. Rev. D **68** (2003), 093004 doi:10.1103/PhysRevD.68.093004 [[arXiv:hep-ph/0308226](#)] [hep-ph].
- [88] F. Cornet and W. Hollik, Phys. Lett. B **669** (2008), 58-61 doi:10.1016/j.physletb.2008.09.035 [[arXiv:0808.0719](#)] [hep-ph].
- [89] E. Asakawa, D. Harada, S. Kanemura, Y. Okada and K. Tsumura, Phys. Lett. B **672** (2009), 354-360 doi:10.1016/j.physletb.2009.01.050 [[arXiv:0809.0094](#)] [hep-ph].
- [90] E. Asakawa, D. Harada, S. Kanemura, Y. Okada and K. Tsumura, [[arXiv:0902.2458](#)] [hep-ph].
- [91] T. Takahashi, N. Maeda, K. Ikematsu, K. Fujii, E. Asakawa, D. Harada, S. Kanemura, Y. Kurihara and Y. Okada, [[arXiv:0902.3377](#)] [hep-ex].
- [92] R. N. Hodgkinson, D. Lopez-Val and J. Sola, Phys. Lett. B **673** (2009), 47-56 doi:10.1016/j.physletb.2009.02.009 [[arXiv:0901.2257](#)] [hep-ph].
- [93] A. Arhrib, R. Benbrik, C. H. Chen and R. Santos, Phys. Rev. D **80** (2009), 015010 doi:10.1103/PhysRevD.80.015010 [[arXiv:0901.3380](#)] [hep-ph].
- [94] E. Asakawa, D. Harada, S. Kanemura, Y. Okada and K. Tsumura, Phys. Rev. D **82** (2010), 115002 doi:10.1103/PhysRevD.82.115002 [[arXiv:1009.4670](#)] [hep-ph].
- [95] J. Hernandez-Sanchez, C. G. Honorato, M. A. Perez and J. J. Toscano, Phys. Rev. D **85** (2012), 015020 doi:10.1103/PhysRevD.85.015020 [[arXiv:1108.4074](#)] [hep-ph].
- [96] W. Ma, C. X. Yue and T. T. Zhang, Chin. Phys. C **35** (2011), 333-338 doi:10.1088/1674-1137/35/4/003.
- [97] J. Sola and D. Lopez-Val, Nuovo Cim. C **34S1** (2011), 57-67 doi:10.1393/ncc/i2011-11002-1 [[arXiv:1107.1305](#)] [hep-ph].
- [98] Z. Heng, L. Shang and P. Wan, JHEP **10** (2013), 047 doi:10.1007/JHEP10(2013)047 [[arXiv:1306.0279](#)] [hep-ph].
- [99] M. Chiesa, B. Mele and F. Piccinini, Eur. Phys. J. C **84** (2024) no.5, 543 doi:10.1140/epjc/s10052-024-12882-8 [[arXiv:2109.10109](#)] [hep-ph].

- [100] B. Samarakoon and T. M. Figy, Phys. Rev. D **109** (2024) no.7, 075015 doi:10.1103/PhysRevD.109.075015 [[arXiv:2312.12594](#) [hep-ph]].
- [101] M. Demirci, Turk. J. Phys. **43** (2019) no.5, 442-458 doi:10.3906/fiz-1903-15 [[arXiv:1902.07236](#) [hep-ph]].
- [102] T. Hahn and M. Perez-Victoria, Comput. Phys. Commun. **118** (1999), 153-165.
- [103] A. Denner, S. Dittmaier and L. Hofer, Comput. Phys. Commun. **212** (2017), 220-238 doi:10.1016/j.cpc.2016.10.013 [[arXiv:1604.06792](#) [hep-ph]].
- [104] T. Hahn, Comput. Phys. Commun. **140** (2001), 418-431 doi:10.1016/S0010-4655(01)00290-9 [[arXiv:hep-ph/0012260](#) [hep-ph]].
- [105] T. Hahn, [[arXiv:hep-ph/9905354](#) [hep-ph]].
- [106] D. Borah and J. M. Cline, Phys. Rev. D **86** (2012), 055001 doi:10.1103/PhysRevD.86.055001 [[arXiv:1204.4722](#) [hep-ph]].
- [107] M. Gustafsson, S. Rydbeck, L. Lopez-Honorez and E. Lundstrom, Phys. Rev. D **86** (2012), 075019 doi:10.1103/PhysRevD.86.075019 [[arXiv:1206.6316](#) [hep-ph]].
- [108] A. Arhrib, R. Benbrik and N. Gaur, Phys. Rev. D **85** (2012), 095021 doi:10.1103/PhysRevD.85.095021 [[arXiv:1201.2644](#) [hep-ph]].
- [109] M. Klasen, C. E. Yaguna and J. D. Ruiz-Alvarez, Phys. Rev. D **87** (2013), 075025 doi:10.1103/PhysRevD.87.075025 [[arXiv:1302.1657](#) [hep-ph]].
- [110] M. Krawczyk, D. Sokolowska, P. Swaczyna and B. Swiezewska, JHEP **09** (2013), 055 doi:10.1007/JHEP09(2013)055 [[arXiv:1305.6266](#) [hep-ph]].
- [111] A. Arhrib, R. Benbrik and T. C. Yuan, Eur. Phys. J. C **74** (2014), 2892 doi:10.1140/epjc/s10052-014-2892-5 [[arXiv:1401.6698](#) [hep-ph]].
- [112] N. Chakrabarty, D. K. Ghosh, B. Mukhopadhyaya and I. Saha, Phys. Rev. D **92** (2015) no.1, 015002 doi:10.1103/PhysRevD.92.015002 [[arXiv:1501.03700](#) [hep-ph]].
- [113] A. Ilnicka, M. Krawczyk and T. Robens, Phys. Rev. D **93** (2016) no.5, 055026 doi:10.1103/PhysRevD.93.055026 [[arXiv:1508.01671](#) [hep-ph]].
- [114] A. Datta, N. Ganguly, N. Khan and S. Rakshit, Phys. Rev. D **95** (2017) no.1, 015017 doi:10.1103/PhysRevD.95.015017 [[arXiv:1610.00648](#) [hep-ph]].
- [115] J. Kalinowski, W. Kotlarski, T. Robens, D. Sokolowska and A. F. Zarnecki, JHEP **12** (2018), 081 doi:10.1007/JHEP12(2018)081 [[arXiv:1809.07712](#) [hep-ph]].
- [116] D. Dercks and T. Robens, Eur. Phys. J. C **79** (2019) no.11, 924 doi:10.1140/epjc/s10052-019-7436-6 [[arXiv:1812.07913](#) [hep-ph]].
- [117] C. W. Chiang and K. Yagyu, Phys. Rev. D **87** (2013) no.3, 033003 doi:10.1103/PhysRevD.87.033003 [[arXiv:1207.1065](#) [hep-ph]].
- [118] R. Benbrik, M. Boukidi, M. Ouchemhou, L. Rahili and O. Tibssirte, Nucl. Phys. B **990** (2023), 116154 doi:10.1016/j.nuclphysb.2023.116154 [[arXiv:2211.12546](#) [hep-ph]].

- [119] G. C. Branco, P. M. Ferreira, L. Lavoura, M. N. Rebelo, M. Sher and J. P. Silva, Phys. Rept. **516** (2012), 1-102 doi:10.1016/j.physrep.2012.02.002 [[arXiv:1106.0034](#) [hep-ph]].
- [120] M. Aoki, S. Kanemura, K. Tsumura and K. Yagyu, Phys. Rev. D **80** (2009), 015017 doi:10.1103/PhysRevD.80.015017 [[arXiv:0902.4665](#) [hep-ph]].
- [121] S. Nie and M. Sher, Phys. Lett. B **449** (1999), 89-92 doi:10.1016/S0370-2693(99)00019-2 [[arXiv:hep-ph/9811234](#) [hep-ph]].
- [122] S. Kanemura, T. Kasai and Y. Okada, Phys. Lett. B **471** (1999), 182-190 doi:10.1016/S0370-2693(99)01351-9 [[arXiv:hep-ph/9903289](#) [hep-ph]].
- [123] A. G. Akeroyd, A. Arhrib and E. M. Naimi, Phys. Lett. B **490** (2000), 119-124 doi:10.1016/S0370-2693(00)00962-X [[arXiv:hep-ph/0006035](#) [hep-ph]].
- [124] I. F. Ginzburg and I. P. Ivanov, Phys. Rev. D **72** (2005), 115010 doi:10.1103/PhysRevD.72.115010 [[arXiv:hep-ph/0508020](#) [hep-ph]].
- [125] S. Kanemura, Y. Okada, H. Taniguchi and K. Tsumura, Phys. Lett. B **704** (2011), 303-307 doi:10.1016/j.physletb.2011.09.035 [[arXiv:1108.3297](#) [hep-ph]].
- [126] S. Kanemura and K. Yagyu, Phys. Lett. B **751** (2015), 289-296 doi:10.1016/j.physletb.2015.10.047 [[arXiv:1509.06060](#) [hep-ph]].
- [127] L. Bian and N. Chen, JHEP **09** (2016), 069 doi:10.1007/JHEP09(2016)069 [[arXiv:1607.02703](#) [hep-ph]].
- [128] W. Xie, R. Benbrik, A. Habjia, S. Taj, B. Gong and Q. S. Yan, Phys. Rev. D **103** (2021) no.9, 095030 doi:10.1103/PhysRevD.103.095030 [[arXiv:1812.02597](#) [hep-ph]].
- [129] J. Haller, A. Hoecker, R. Kogler, K. Mönig, T. Peiffer and J. Stelzer, Eur. Phys. J. C **78** (2018) no.8, 675 doi:10.1140/epjc/s10052-018-6131-3 [[arXiv:1803.01853](#) [hep-ph]].
- [130] Khiem Hong Phan, Dzung Tri Tran and Thanh Huy Nguyen, *in preparation*.